OKO GUIDE TO ADAPTIVE OPTICS

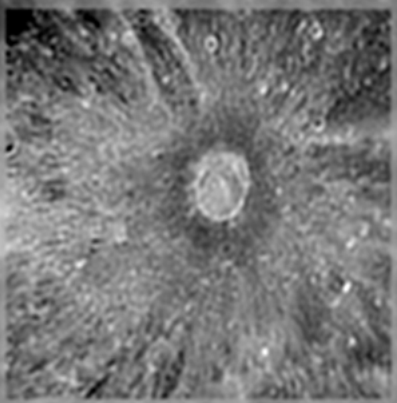

FLEXIBLE OKO OPTICAL

OKO GUIDE TO ADAPTIVE OPTICS

OKO Technologies

Polakweg 10-11, 2288 GG, Rijswijk ZH,
The Netherlands

Fourth edition, May 2013

http://www.okotech.com

Polakweg 10-11, 2288 GG Rijswijk ZH, the Netherlands
PO Box 581, 2600AN Delft, the Netherlands

Authors: G. Vdovin, O. Soloviev, M. Loktev, V. Patlan
E-mail: oko@okotech.com

Front cover: image of the Moon surface processed in real time with OKO StillI software

Contents

1 Introduction 1
- 1.1 Adaptive optics 1
- 1.2 Wavefronts 2
- 1.3 Deformable mirrors 4
- 1.4 Closed-loop wavefront control 6
- 1.5 Quality of AO correction 8
- 1.6 Wavefront measurement 10
  - 1.6.1 Interferometric analysis 10
  - 1.6.2 Hartmann test 11

2 Deformable mirrors 13
- 2.1 MMDM and PDM 13
- 2.2 MMDM 16
- 2.3 PDM model 18
- 2.4 Optimal design of a DM 21
- 2.5 Correction performance 23
- 2.6 DM and atmospheric correction 25
- 2.7 Print-through 27
- 2.8 PDM under laser load 27
- 2.9 MMDM under laser load 28
- 2.10 MMDM temporal stability 29
- 2.11 MMDM temperature stability 31
- 2.12 MMDM nonlinearity 32

2.13 MrFit: DM simulation package 33
2.14 Publications based on OKO DM 34

Bibliography **34**
2.15 Acceptable DM defects 42
2.15.1 Surface defects 42
2.15.2 Scratches on PDM 43
2.15.3 DM aging 43

3 Wavefront sensors **45**
3.1 "FrontSurfer" software 46
3.1.1 Basic features 46
3.1.2 Version for deformable mirrors 48
3.2 "FrontSurfer" hardware 50
3.2.1 Typical configuration 50
3.2.2 Supported camera types and interfaces 50
3.2.3 Microlens arrays 51
3.2.4 Hartmann masks 53
3.2.5 Choice of the proper array 54
3.3 Wavefront measurements 54
3.3.1 The sensing mode 55
3.3.2 Hartmanngram capture 56
3.3.3 How to obtain a good hartmanngram 56
3.3.4 How "FrontSurfer" works 57
3.3.5 Further information 59
3.4 Shop testing setups 59
3.4.1 Testing of transmission optics 60
3.4.2 Testing of reflective optics 61
3.4.3 Testing of microlenses 62
3.5 Optical conjugation 63
3.5.1 Compensation of the curvature 65

4 AO systems **67**
4.1 Design of an adaptive optical system 67
4.2 "FrontSurfer" in the AO mode 69
4.2.1 Calibration of the AO 69
4.3 Breadboard system 71
4.4 AOS test data 72
4.4.1 37-channel MMDM system 72

4.4.2 37-channel PDM system 76
4.4.3 Optimization-based operation 80
4.4.4 Feedforward tip-tilt correction 80
4.4.5 Feedforward Zernike modes 81
4.5 LighPipes software package 84

5 Imaging through turbulence 87
5.1 Approach 87
5.2 StillI software package 90

6 Consulting 93

7 Deformable mirrors, technical data 95
7.1 DM model codes 95
7.2 MMDM10-1-focus 96
7.3 OKO MMDM15-37 98
7.4 MMDM15-17-TT 103
7.5 MMDM30-39/59/79 107
7.6 MMDM40-59/79 112
7.7 MMDM50-79 116
7.8 MMDM11x39-19/38 linear 119
7.9 PDM30-19 123
7.10 PDM30-37 128
7.11 PDM50-19/37/79/109 132
7.12 PDM11x55-20 139
7.13 PDM-2-TT fast steering platform 143
7.14 General remarks 144

8 HV amplifiers and interface 145
8.1 High-voltage amplifier units 145
8.1.1 Unipolar HV amplifiers for OKO DM 145
8.1.2 Bipolar HV amplifiers 146
8.1.3 A4MEMS prototyping HV amplifier 147
8.2 20-ch HV amplifier board 149
8.3 EDAC-40 driver module 150
8.3.1 Specifications 150
8.3.2 General design and principle of operation 152
8.4 DAC-40-USB driver module 153
8.4.1 General design 153

8.4.2 Programming interface 154
8.5 24-channel PCI DAC board 155
8.5.1 Programming interface 155
8.6 Four-channel USB DAC 157
8.7 Four-channel high voltage driver 157

9 Frequently asked questions 159
9.1 Deformable mirrors 159
9.2 Wavefront sensors 163
9.3 Adaptive optical systems 166

10 Warranty and Export Disclaimers 169
10.1 Warranty 169
10.2 Export 170

Bibliography 171

1

INTRODUCTION

Flexible Optical B.V. (OKO Tech) is a small Dutch business operating in the field of application-oriented development of laser and high resolution imaging adaptive optics. From its foundation in 1997, OKO offers high-quality deformable mirrors featuring extremely smooth surface with HR metal and dielectric coatings, suitable for the most demanding imaging and (high energy and high power) laser applications.

This document describes basic principles of Adaptive Optics (AO), wavefront (WF) correction and measurement, using the products of OKO Technologies (Flexible Optical BV), including Micromachined Membrane Deformable Mirrors (MMDM), Piezoelectric Deformable Mirrors (PDM), Shack-Hartmann wavefront sensors, optimization, and feedforward control.

1.1 Adaptive optics

Aberrations are some deviations from the ideal that lead to reduced resolution or power efficiency of the optical system. Static aberrations are inherent to optical systems, and correction of static aberrations is achieved by complex optical designs. In this way, lithographic lenses providing almost aberration-free imaging, are designed with tens of extremely precise components. However, even ideal systems suffer from external conditions, such as the at-

mospheric turbulence or thermal effects. In these cases, adaptive compensation of aberrations is crucially important, and the term *"adaptive optics"* is used.

Defocus is the simplest example of dynamic aberration. Even the human eyes need to change focus, when the distance to the subject is changed. Focus in the photographic cameras serves the same purpose. To provide accommodation and focusing, optical systems need to have adjustable design. Most frequently, the adjustment is done mechanically, by moving one, or a group of components.

Adaptive optics (AO) is a rapidly developing branch of applied optics [1], aimed to active compensation of phase aberrations that are far more complex than focus.

1.2 Wavefronts

"Wavefront" is a key term in adaptive optics. We shall use the following definition. The electric field vector of a monochromatic light wave can be represented in the form

$$\mathbf{E}(\mathbf{r},t) = \mathbf{E}(\mathbf{r})e^{i(\mathbf{kr}+\varepsilon(\mathbf{r}))}e^{-i\omega t}, \tag{1.1}$$

where k is the wave vector, which is perpendicular to both **E** and **H** vectors of the electromagnetic field and has a modulus related to the wavelength λ as $k = 2\pi/\lambda$; ω is the angular frequency related to the temporal frequency ν as $\omega = 2\pi\nu$; $\mathbf{E}(\mathbf{r})$ describes the amplitude, and $\varphi(\mathbf{r}) = \mathbf{kr} + \varepsilon(\mathbf{r})$ the phase of the oscillating field **E**. The surfaces of equal phase are known as *wavefronts*.

Wavefront can be also defined in terms of geometrical optics, as a continuous surface that is orthogonal to all rays in the light beam.

The distribution of the optical phase in a certain plane, such as the pupil plane of an optical system, provides a good approximation of the wavefront in many cases. This is the reason why the measurement of the optical phase distribution is often referred to as *"wavefront measurement"* or *"wavefront sensing"*. However, this does not apply for strong aberrations, especially if these are accompanied by significant amplitude modulation and wavefront

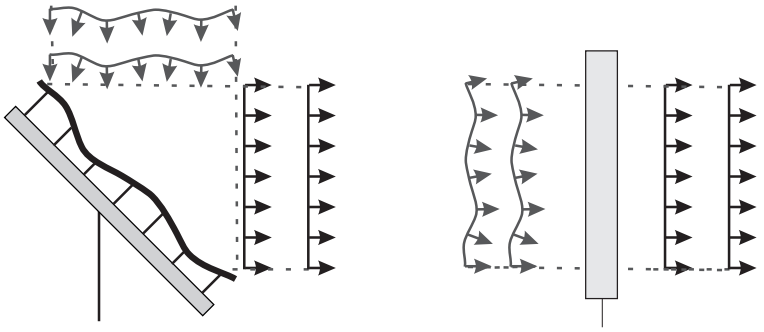

Figure 1.1: *Principle of wavefront correction in deformable mirrors (on the left) and LC phase modulators (on the right).*

dislocations; in this situation both the amplitude and phase distributions should be analyzed.

A short overview of the most popular wavefront measurement methods (interferometric methods and Shack-Hartmann test) is given below.

The wavefront shape can be corrected by modifying the optical phase profile. The core principle used in the *wavefront correction* is *phase conjugation*. For wavefront correction the correcting phase profile should be optically conjugated to the measured phase aberration. Correction with the conjugated phase profile results in an ideal flat wavefront. However, if the wavefront cannot be precisely determined or precisely replicated by the relay optics, or if diffraction effects dominate, the phase conjugation cannot be precisely employed.

Operation of phase modulation devices is based on control of the optical path difference (OPD), which can be written as $\mathrm{OPD} = n\Delta z$, where n is the refractive index, and Δz is the path travelled by the wave. OPD is related to the phase φ as $\varphi = 2\pi \cdot \mathrm{OPD}/\lambda$.

Deformable mirrors, which is the primary technology for wavefront correctors, modulate Δz, operating in the reflective mode — see Figure 1.1 on the left.

Liquid crystal (LC) phase modulators represent a low-cost alternative to mechanically driven mirrors; their operation is based on modulation of refraction index n of the LC layer under the

applied electric field in transparent or reflective mode (Figure 1.1 on the right). LC devices are easy to integrate with transmissive lens systems, however they also have some inherent drawbacks such as slow response, dispersion, relatively high optical losses, pixelated response and polarization sensitivity.

1.3 Deformable mirrors

Deformable mirror (DM) is the most frequently used wavefront corrector. Literally it means a mirror with deformable surface. DMs have many inherent advantages, such as they do not introduce chromatic aberrations, they can be coated with extremely highly reflective coatings so that they cause no power loss in the optical system, and - from the control perspective - they can be represented as linear systems, so that the adaptive optical system can be controlled within the framework of traditional linear control theory.

There are several DM types::

- Membrane DM [2, 3] are formed by a thin membrane, deformed by an array of electrostatic or magnetic actuators.
- Bimorph DM [4] is formed by two or more layers of different materials. The deformation is achieved by local lateral actuation of one of the layers. Mathematically the bimorph DMs are very close to the membrane DM, but have very different design and engineering features.
- Continuous facesheet DM with push-pull actuators.
- Deformable mirrors based on the reflection from liquid surface [5].

Deformable mirrors are characterized by the number of degrees of freedom. Quite frequently the degrees of freedom are chosen in the form of Zernike polynomials. These polynomials form ideal set of functions orthogonal inside a circle. Also Zernike polynomials have been traditionally used to describe the low-order aberrations of optical systems, long before the term “adaptive optics” was introduced.

The response functions of the majority of DMs are quite different from Zernike polynomials, however, in most cases, Zernike polynomials can be approximately formed by the DM as a combination of its natural responses. The quality of reproduction of low-order Zernike polynomials characterizes the DM ability to compensate the random optical aberrations.

However, in general, the correction quality in adaptive optical system depends on many factors, such as:

- Amplitude of the aberration.
- Spatial spectrum of the aberration. It can be expressed as the statistical weight of different Zernike terms, or in the form of a decomposition over any other orthogonal set of functions.
- Temporal spectrum of the aberration.
- Influence functions of the deformable mirror and the statistical match between the influence functions and the spatial spectrum of the aberration.
- Response time of the DM and statistical match between the mirror bandwidth and the temporal spectrum of the aberration.

Wavefront correctors are traditionally subdivided into two classes according to the implemented compensation technique — *zonal* and *modal* . Zonal correctors such as segmented mirrors with piston and/or tip-tilt actuators allow individual control of a phase over a set of subapertures providing step-wise phase compensation, whereas modal ones such as deformable mirrors use a set of smooth functions (modes, or influence functions) to approximate the required phase function.

Modal-type deformable mirrors are presented in a series of modifications: membrane, bimorph and continuous faceplate mirrors with different geometries of actuators and boundary conditions. OKO Technologies produces membrane mirrors based on micromachining technology and continuous faceplate mirrors with piezoelectric actuators. These mirrors shall be further referred to as micromachined membrane deformable mirrors (*MMDMs*) and piezoelectric deformable mirrors (*PDMs*), respectively.

1.4 Closed-loop wavefront control

The majority of adaptive optical systems are based on the traditional phase-conjugate scheme [1]. Its operation can be explained using a simplified example from astronomy. A light wave coming from a distant star forms an image of this star in a telescope. Passing through the atmosphere, the light wave is affected by fluctuations in density of the atmosphere due to turbulence, distorting the front of the wave (Fig. 1.2(a)) and producing a blurred image. Two elements compensate for this effect: *wavefront sensor*, which measures the wavefront distortion, and *wavefront corrector*, which produces the phase function conjugated to the aberrated wavefront, thus correcting the distortion of an initial wavefront. The processing unit (computer) coordinates operation of these two elements (Fig. 1.2(b)). As the atmospheric distortions evolve over time, the system should perform several hundred measurements and corrections per second. In some systems, an additional tip-tilt mirror is used to reduce the large stroke requirements for the wavefront corrector. For compensation of aberrations produced by "thick" layers of highly aberrated media, multi-conjugate adaptive systems must be used. Volume aberrations are described satisfactorily by layered models [6], and several "wavefront sensor — wavefront corrector" pairs need to be used to compensate them.

In the past, until the 90s the applications were restricted to high-budget observatories and military projects on the delivery of high-energy laser beams for missile defense and secure communications, due to the extremely high cost of AO systems.

Recently, the advances in sensors and electronics brought down the cost of adaptive optics, leading to many new applications in scientific, industrial and medical fields [7, 8]. The most important applications include retinal imaging in ophthalmology [9], confocal microscopy [10], ultra-short laser pulse shaping [11] and machine vision.

OKO Technologies not only produces high-quality components for imaging and laser AO systems, but also provides integrated solutions for closed-loop control of a deformable mirror using the measurement data obtained from a (Shack-) Hartmann wavefront sensor, optimization of a certain beam parameter or function, or open-loop control of the deformable mirror. For these purpose we

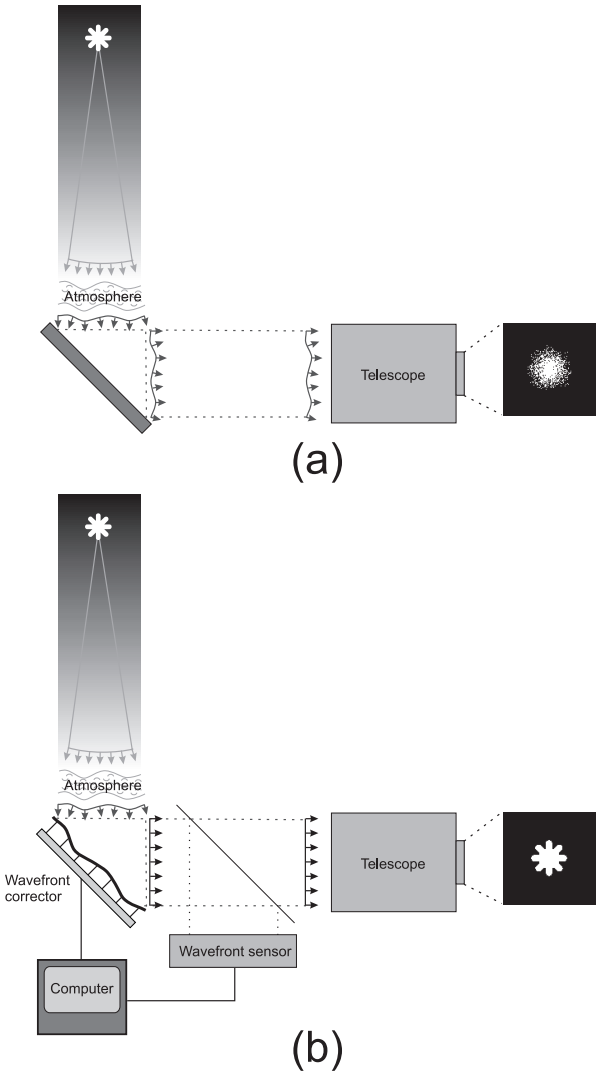

Figure 1.2: *Image blurring induced by atmospheric wavefront distortions in astronomy (a); operation of the adaptive optical system (b).*

have developed software suites:

- "FrontSurfer" Hartmann-Shack WF sensor for closed-loop phase conjugation AO and optical shop testing
- "Mizer" software for open-loop control of Zernike terms, using OKO deformable mirrors
- "BeamTuner": software for the optimization of the beam parameters such as the beam brightness, focal spot, shape and the image sharpness.

These software tools and packages can be custom integrated with the AO components produced by OKO Technologies and other vendors to build a wide variety of AO systems satisfying very strict requirements for the beam quality, stability and power.

1.5 Quality of AO correction

In the imaging setup, the optical system builds an image of the object. Each object point serves as individual point source, emitting (or reflecting) the light independently of its neighbors. The rays emitted by the object point propagate to all directions, and the wavefront, which is a surface, orthogonal to these rays, is a sphere. To form an image, the optical system (ideal lens) converts the divergent spherical wavefront into a convergent spherical wavefront. All rays, orthogonal to this convergent wavefront intersect in a single point, forming a sharp image. Since an object can be formed by many points, the optical system should form a separate non-distorted convergent spherical wave for each object point.

Any aberration in the path between the object and the image, distorts the convergent spherical wave. The more the wavefront deviates from the ideal sphere, the less sharp the formed image will be. Strehl parameter SP is one of the basic metrics, characterizing the optical quality:

$$\mathrm{SP} = e^{-\sigma^2}, \qquad \sigma \ll 1, \tag{1.2}$$

where σ is the angular *rms* WF deviation from the ideal sphere. The physical meaning of the SP is very simple — it shows the

axial intensity in the focus of aberrated optical system, related to the intensity I_0 produced by an ideal unaberrated beam in the far field, which is given by the expression:

$$I_0 = \frac{\pi^2 (D/2)^4}{\lambda^2 L^2} I_{\mathrm{Ap}}, \tag{1.3}$$

where D is the aperture diameter, L is the distance and I_{Ap} is the intensity in the aperture.

The expression 1.2 does not produce any reliable result for large σ - for instance if we deal with thermal aberrations in a single mode laser: due to the speckle pattern in the focal spot, the on-axis intensity takes a random value for each realization.

However, for the particular case of atmospheric turbulence following Kolmogorov statistics, the following expression gives a good approximation to the average value of Strehl in the far field:

$$\mathrm{SP} \approx \frac{1}{(1+\sigma^2)^{6/5}} \tag{1.4}$$

It follows from the equations 1.2 and 1.4 that to achieve a good optical quality, the *rms* deviation from the best fit sphere should not exceed 1 radian, or $\lambda/(2\pi)$, while $\lambda/(4\pi)$ already provides almost diffraction limited quality. Assuming the wavelength of visible light is 633 nm (red light), we can conclude that 200 nm *rms* deviation from the best fit sphere deviation will deliver unacceptable optical quality with $\mathrm{SP} \sim 0.02$, the 100 nm deviation is sufficient for moderate (not good yet) optical quality, while the deviation of 50 nm will deliver a good quality with $\mathrm{SP} \sim 0.75$. The transition from very bad, to good is really sharp: 4-times change in the WF error corresponds to about 40-times change in the axial intensity!

For "diffraction quality" efficiency, the residual aberration after the AO correction should satisfy to the criterium of at least $\lambda/10$ or better. If this condition is not met, then the AO system — although correctly designed and working as expected — can be considered inefficient.

Let us consider a situation when the AO system reduces the *rms* aberration by a factor of 10. If the initial aberration is 30 radians, then the Strehl will remain close to zero in both cases:

without AO correction (e^{-900}) and with AO correction (e^{-81}). But if the initial aberration is 5 radians, then the Strehl will be almost zero without AO correction (e^{-25}), but will be improved to a value close to one: ($e^{-0.25}$) by the application of AO correction.

Both systems — with 30 rad *rms* and with 5 rad rad *rms* — are optically bad. But in the first case, the AO system is inefficient, and in the second — very efficient.

This simple example illustrates that the AO technology can be very useful, but only if the AO is properly designed and matched to the expected aberration. Random application of "general adaptive optics" to a "generally bad optical system", in many cases, will result in little or no improvement.

The rule of thumb should be: **the optical system should be designed as good as possible without the AO. If the optical quality is still not satisfactory, or if dynamic correction is needed, then further analysis should be applied to determine whether the AO can improve the situation.**

1.6 Wavefront measurement

1.6.1 Interferometric analysis

Interferometric methods are widely used in optical shop testing. Standard interferometric optical setup uses two (or more) coherent light beams. The first one (main beam) contains information about the object being analyzed; the object is either reflective or transparent. The second beam, which has a flat or spherical wavefront, is used as a reference. Let us suppose that the electric fields of these light beams are identically oriented and have equal magnitudes E_0 but different phases in the measurement plane,

$$\begin{aligned} \mathbf{E}_1(\mathbf{r},t) &= \mathbf{E}_0(\mathbf{r})e^{-i\omega t}, \\ \mathbf{E}_2(\mathbf{r},t) &= \mathbf{E}_0(\mathbf{r})e^{i\varphi(\mathbf{r})}e^{-i\omega t}. \end{aligned} \tag{1.5}$$

The phase difference φ results from the path-length difference ΔL between the waves and can be written as

$$\varphi = 2\pi\frac{\Delta L}{\lambda}, \tag{1.6}$$

where λ is the wavelength of light. Now, the net electric field has magnitude

$$\mathbf{E}_{\text{net}}(\mathbf{r},t) = |\mathbf{E}_1 + \mathbf{E}_2| = 2E_0 \cos\left(\frac{\varphi(\mathbf{r})}{2}\right) e^{i\varphi(\mathbf{r})/2} e^{-i\omega t}. \tag{1.7}$$

Photo-detectors, such as photodiodes and CCD cameras, can detect only intensity of the light field, which is the time average of E^2. If we write individual intensities as $I_0 = E_0^2/2$ then the net intensity from the two light waves can be expressed as

$$I_{\text{net}}(\mathbf{r}) = 4I_0 \cos^2\left(\frac{\varphi(\mathbf{r})}{2}\right) = 4I_0 \cos^2\left(\frac{\pi \Delta L(\mathbf{r})}{\lambda}\right). \tag{1.8}$$

The intensity distribution $I_{\text{net}}(\mathbf{r})$ can be used to obtain information about the phase distribution $\varphi(\mathbf{r})$ or the wavefront difference $\Delta L(\mathbf{r})$. Extraction of phase from this intensity distribution is usually meant under wavefront reconstruction in interferometry. In general case the problem of phase reconstruction is ill-posed, and there are numerous techniques to get rid of ambiguity in the reconstruction.

Interferometric methods cover a wide range of measurement problems from shape to roughness measurements and may provide accuracy up to subnanometer range. However, as the most reliable methods are either calculation intensive or require multiple measurements, they are difficult to use for the real-time wavefront analysis.

1.6.2 Hartmann test

Among many approaches to test the quality of optical components in the industry and to get the real time wavefront information in adaptive optics, *Hartmann test* has its own distinct place. Hartmann (and *Shack-Hartmann*) tests are simple and can be explained in terms of pure geometrical optics.

The wavefront to be reconstructed is sampled by a screen with many sub-apertures (in Hartmann test) or by a dense array of lenslets (Shack-Hartmann test) — see Figure 1.3. Each sub-aperture (lenslet) produces a light spot on the screen or position sensitive detector. Position of the light spot is associated with

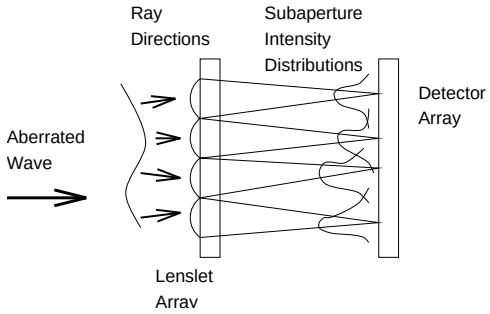

Figure 1.3: *Principle of Shack-Hartmann test*

the local slope of the incoming wavefront, averaged over the subaperture (lenslet) area. After all local slopes of the wavefront are registered, one can reconstruct the shape of the wavefront. Shack-Hartmann method has the advantages of gathering more light power per spot and covering the whole sensing area.

The results of the test are very robust and easy to interpret. This advantage made the Shack-Hartmann sensor the most popular tool for real-time wavefront measurements in adaptive optics. It is also suitable for shape measurements in optical shop testing. OKO Technologies offers both Shack and Shack-Hartmann sensors and *"FrontSurfer"* software for wavefront reconstruction. The sensor consist of a custom-made Hartmann mask or lenslet array coupled to a high-resolution CCD or CMOS camera.

2

DEFORMABLE MIRRORS

OKO Technologies produces two types of deformable mirrors — Micromachined Membrane Deformable Mirrors (MMDM) and Piezoelectric Deformable Mirrors (PDM). They are discussed further in this chapter. The test results of MMDM and PDM in an AO setup can be found in Chapter 4.

2.1 MMDM and PDM

MMDM in its essence is a membrane DM. The membrane is fabricated using the technology of bulk micromachining. The membrane is very thin, 0.5 to 10 μm thick, depending on the technology used, and can be fabricated with diameters from 5 to to 50 mm. The membrane is mounted over a two-dimensional array of electrodes. Any potential applied between the membrane and the individual electrode, results in deformation of the membrane caused by electrostatic attraction. Combinations of voltages applied to different electrodes can form certain shapes on the membrane surface.

The MMDM membrane can be only attracted to the electrode structure, producing a concave optical shapes, with reference to a flat surface. However, if we choose a slightly concave reference, then a bi-directional operation is possible. To achieve it, the membrane should be initially deflected towards the actuators and

made perfectly spherical by adjusting the actuator voltages. From this state the membrane can be moved to both positive — from the electrode structure and negative — towards the actuator structure — see Fig. 2.1.

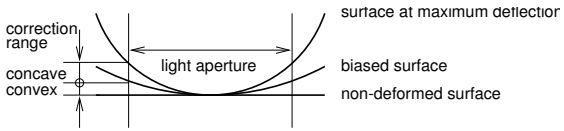

Figure 2.1: *Biased operation of MMDM.*

The membrane is fixed at the edges. When a constant potential is applied to all actuators, the DM will take a concave shape. If the membrane is round, the deformation will form a good approximation to a sphere. In general, the biased shape depends on the geometry of the membrane and the geometry of the actuators. Since the edges of MMDM membrane are fixed, the light aperture of MMDM is usually ∼1.4 times smaller than the full membrane size. This ratio provides the best compromise for the correction of all low-order aberrations, with respect to the amplitude and quality of correction. Full membrane aperture can be used only for correction of defocus.

MMDM is controlled by inexpensive electrostatic electrodes. It is possible to fabricate these electrode with very high density. However, small electrodes cause small deflections of the membrane. Therefore the maximum number of electrodes in a MMDM is limited by the amplitude of response of a single individual electrode at the maximum voltage.

There are two parameters that are important when the amplitude of MMDM response is described:

- maximum stroke when all actuators are at maximum (for a round DM it corresponds to the sag of spherical surface);
- maximum difference between the neighbor actuators.

At present (May 2013) OKO Technologies produces 15 mm DMs with 37 channels, 30 mm DMs with 39, 59, and 79 channels, 40 mm DMs with 59 and 79 channels, and 50 mm DMs with 79

channels. All of them are optimized to achieve at least 1000 to 1300 nm maximum deflection per actuator, with 1.8 mm minimum actuator pitch.

MMDMs feature zero hysteresis and can be used in feedforward control systems after preliminary calibration. Very low power consumption allows building of small and efficient power supplies for multichannel DMs. We have experience in building 40-channel MMDM controllers with total consumption not exceeding 1 W in active mode.

Piezoelectric DM is formed by a thin solid plate, made of glass, fuzed silica or silicon, depending on application. The plate is coated with appropriate optical coating and bonded to a two-dimensional array of piezoelectric actuators. Elongation of individual actuators cause global deformation of the reflective plate.

Unlike MMDM, the piezoelectric DMs (PDM) have actuators that can push and pull the reflective plate. When they push, the plate is deformed and the neighbor actuators are also slightly deformed. The stroke per actuator is therefore defined not only by the force applied, but also by the stiffness of the actuator relative to the stiffness of the reflective plate.

PDM deformable plate is bonded only to actuators and has a free edge. When all actuators move together, the plate is translated, without any deformation. The range of translation is equal to the maximum stroke of a free actuator.

At present (May 2013), OKO PDM can be fabricated with minimum pitch of about 4.3 mm, free actuator stroke of 6 μm and, depending on the stiffness of the reflective plate, the inter-actuator stroke can be in the range 1 to 3 μm.

Piezoelectric DMs demonstrate hysteresis of 7 to 15%. This property limits their applicability for feedforward control.

Since the amplitude of local response of a piezoelectric DM depends only on the stiffness of the plate and the actuators, these DMs can be scaled to very large numbers of control channels.

Piezoelectric DMs are suitable for fast feedback-based correction of low and high-order aberrations with large amplitude.

2.2 MMDM

The membrane model is applicable to simulation of the response of a MMDM when the thickness of the reflective substrate is so small that its cylindrical stiffness [12]

$$D = Eh^3/12(1-\nu) \tag{2.1}$$

can be neglected. Here E is the Young's modulus, h is the thickness of the substrate and ν is the Poisson ratio. We assume that the membrane is absolutely stretchable and preserves its shape due to its lateral tension. The shape of the stretched membrane depends mainly on the shape of its contour and on the amount of the surface tension. In the case of a relatively large membrane with ~10 mm diameter and a thickness of only 0.5 μm, this model gives excellent approximation for the static DM behavior. Let us consider the simplified diagram of the micro-fabricated DM shown in Fig. 2.2.

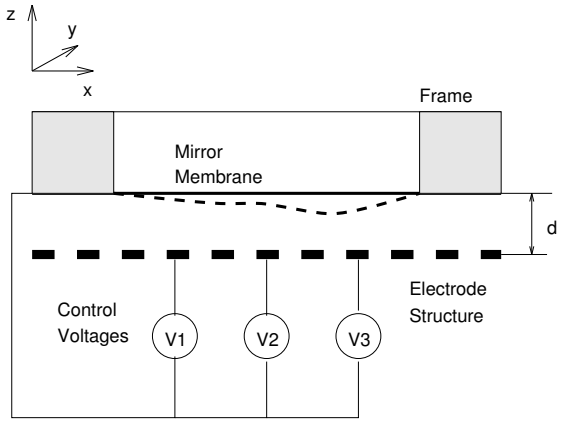

Figure 2.2: *Simplified diagram of a membrane DM.*

Suppose the DM surface is deformed by applying voltages $V_1 \ldots V_N$ to the two-dimensional grid of N actuators positioned at a distance D under the membrane. Let the membrane, having a uniform thickness, be stretched by a uniform surface tension T [N/m]. In this model we shall also suppose that the distance d

is much larger than the maximum membrane deflection, so that the electrostatic pressure P does not depend on the membrane deformation. A nonlinear case of large membrane deflections will be considered later.

The Z-component of the membrane deflection $S(x, y)$ in the linear case is described by the Poisson equation (where Δ denotes Laplace operator):

$$\Delta S(x, y) = P/T \tag{2.2}$$

where the electrostatic pressure P is given by:

$$P = \frac{\varepsilon\varepsilon_o V(x, y)^2}{d(x, y)^2} \tag{2.3}$$

Equations (2.2, 2.3) must be supplied with a set of boundary conditions, describing the shape of the membrane contour: $S_c = F(x, y)$.

Analytical solution of equations (2.2, 2.3) for arbitrary geometries of membrane contour and pressure distributions is complicated. For technical estimations the finite difference numerical model of the membrane DM, allowing for arbitrary boundary conditions and pressure distributions, was developed.

To solve the Poisson equation numerically, the functions S and P are determined on a square grid with equal steps δ_{XY} in the X and Y directions. The grid nodes are indexed as i and j for X and Y directions correspondingly. The grid approximation of the Laplace operator has the form:

$$\Delta S \approx \frac{S_{i+1,j} + S_{i-1,j} + S_{i,j+1} + S_{i,j-1} - 4S_{i,j}}{\delta_{XY}^2}.$$

Using this form we can write a finite-differential version of the Poisson equation (2.2) as:

$$\frac{S_{i+1,j} + S_{i-1,j} + S_{i,j+1} + S_{i,j-1} - 4S_{i,j}}{\delta_{XY}^2} = \frac{P_{i,j}}{T}. \tag{2.4}$$

This system of linear equations (2.4) can be solved by a direct method of Gauss elimination. This leads to a very large matrix of coefficients, which is frequently not acceptable, because storage requirements for such a matrix in many cases exceed the memory

possibilities of modern computers. The open form of the expression for the membrane deformation $S_{i,j}$ follows immediately from (2.4):

$$S_{i,j} = -\frac{1}{4}\left(\delta_{XY}^2 \frac{P_{i,j}}{T} - S_{i-1,j} - S_{i+1,j} - S_{i,j+1} - S_{i,j-1}\right) \qquad (2.5)$$

The expression (2.5) can be used for solving the Poisson equation by iterations when the right-hand side of (2.4) $P_{i,j}/T$ is known and the boundary conditions $S_{i,j}$ are explicitly given. C-code for solving the problem for arbitrary actuator and membrane shapes is available free from OKO Technologies.

2.3 PDM model

The continuous faceplate DM model is applicable to simulation of the response of a PDM. The mechanical design of such a DM is very simple in its essence: discrete actuators are fixed to a stable DM base and bonded to a thin flexible DM plate. The edge of the plate is left free. The geometry of the flexible plate is made circular for the majority of applications, but square and rectangular DMs are used for beam control in high-power lasers and for ultrafast pulse shaping.

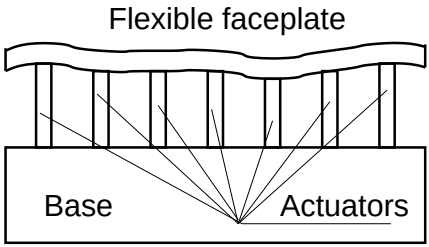

Figure 2.3: *Simplified scheme of a faceplate DM.*

Implementation of PDM is more complicated than the simple model described above. Stress-free assembly of the deformable plate with actuator stack, minimization of the coating stress, good initial figure, implementing of cooling system for a high-power operation — this is an incomplete list of challenges. Nevertheless,

a simple mechanical model of continuous faceplate DM is very useful for preliminary estimations of the amplitude and shape of the DM influence functions and the correction performance.

Analysis that follows is based on a thin-plate model. Rigorous theory of thin plate bending can be found in [12].

A small-deflection thin-plate model will be used to derive the expressions for DM response. In the framework of this model, the thickness of the plate is considered to be small in comparison with the plate size and the plate deformations are small in comparison to the plate thickness. These assumptions are satisfactory in many practical cases.

The deflection S of a thin plate is described by the biharmonic equation

$$\Delta\Delta S = \frac{P}{D} \tag{2.6}$$

where D is the cylindrical stiffness described by equation (2.1), and P is the load applied to the plate.

Let us consider a circular plate with a free edge. As shown in [13], its deformation is caused by a set of point-like forces P_i, which act in points ζ_i and can be presented as a superposition of functions, accurate to within the term $S_0 + S_1 r\cos\varphi + S_2 r\sin\varphi$. This term governs the translation and rotation of the plate as a whole:

$$S(z,\bar{z}) = \frac{1}{16\pi R}\sum_{i=1}^{N} P_i S(z,\bar{z},\zeta_i,\bar{\zeta}_i) + S_0 + S_1 \mathrm{Re}\, z + S_2 \mathrm{Im}\, z, \tag{2.7}$$

where

$$\begin{aligned} S(z,\bar{z},\zeta,\bar{\zeta}) &= (z-\zeta)(\bar{z}-\bar{\zeta})\left\{\ln(z-\zeta)+\ln(\bar{z}-\bar{\zeta})+\frac{1-\mu}{3+\mu}\right. \\ &\times \left.[\ln(1-z\bar{\zeta})+\ln(1-\bar{z}\zeta)]\right\}+\frac{(1-\mu)^2}{(1+\mu)(3+\mu)} z\bar{z}\zeta\bar{\zeta} \\ &+ \frac{8(1+\mu)}{(1-\mu)(3+\mu)}[(1-z\bar{\zeta})\ln(1-z\bar{\zeta})+k(z\bar{\zeta}) \\ &+ (1-\bar{z}\zeta)\ln(1-\bar{z}\zeta)+k(\bar{z}\zeta)], \end{aligned} \tag{2.8}$$

$z = r\cos\varphi + ir\sin\varphi$, $\zeta = \rho\cos\psi + i\rho\sin\psi$ are coordinates expressed

in the complex-valued form, and k is the logarithmic integral

$$k(x) = \int_0^x \frac{\ln(1-\alpha)}{\alpha} d\alpha. \tag{2.9}$$

Equations (2.7)-(2.9) can be used for simulation of the influence functions of PDM and evaluation of its correction quality. For instance, to calculate the best approximation of an arbitrary wavefront $\phi(x, y)$ by a continuous faceplate DM with a free edge and N actuators, it is necessary to find N unknown forces P_i and 3 coefficients S_0, S_1 and S_2. They can all be found from a system of $N + 3$ linear equations. The first N equations are obtained by minimization of the *rms* error using the least-squares method; the 3 supplementary equations from statics represent conditions of mechanical equilibrium of the plate:

$$\begin{cases} \sum_{j=1}^{N} P_j \int\int_\Omega S(z,\bar{z},z_i,\bar{z}_i)S(z,\bar{z},z_j,\bar{z}_j)dxdy \\ +S_0 \int\int_\Omega S(z,\bar{z},z_i,\bar{z}_i)dxdy + S_1 \int\int_\Omega S(z,\bar{z},z_i,\bar{z}_i)xdxdy \\ +S_2 \int\int_\Omega S(z,\bar{z},z_i,\bar{z}_i)ydxdy \\ = \int\int_\Omega S(z,\bar{z},z_i,\bar{z}_i)\phi(x,y)dxdy, \qquad i = 1 \dots N, \\ \sum_{j=1}^{N} P_j = 0, \\ \sum_{j=1}^{N} P_j x_j = 0, \\ \sum_{j=1}^{N} P_j y_j = 0. \end{cases} \tag{2.10}$$

This system can be easily solved using standard Gauss elimination.

2.4 Optimal design of a DM

The shape of a MMDMDM is described by the Poisson equation:

$$\Delta\varphi(x,y) = p(x,y)/T, \tag{2.11}$$

where p is the pressure caused by the actuators and T is the membrane tension. A similar equation (2.11) describes the shape of a bimorph DM formed with two active layers, with the term p/T describing the distribution of bending moments applied to the plate [4] and the function φ satisfying to some additional boundary conditions.

The shape of a PDM, in the thin plate approximation is described by the biharmonic equation [12]:

$$\Delta^2\varphi(x,y) = p(x,y)/D, \tag{2.12}$$

where the source p describing the action of actuators satisfies the conditions of static equilibrum, D is the cylindrical stiffness and $\varphi(x,y)$ satisfies to some additional boundary conditions. Equation (2.12) assumes the plate have tip-tilt degrees of freedom in the points of attachment to the actuators.

To find the DM controls p corresponding to the phase error $\varphi(x,y)$ we need to apply the differential operator Δ (Δ^2 for the continuous facesheet DM) to the phase function φ.

It is a common practice to decompose aberrated wavefronts in series over the Zernike polynomials. Substituting $\varphi = Z_n^m$ where Z_n^m is a Zernike polynomial with the radial order n and azimutal order $\pm m$ as defined in [14], we find [15] that

$$\Delta\varphi(x,y) = 0, \tag{2.13}$$

for all Zernike polynomials Z_n^m with $n = |m|$ including piston, tip, tilt, astigmatism, trefoil, etc.; and

$$\Delta^2\varphi(x,y) = 0, \tag{2.14}$$

for all Zernike polynomials Z_n^m with $n = |m|$ and also with $n-2 = |m|$, including piston, tip, tilt, defocus, astigmatism, trefoil, coma and some higher order aberrations.

This result can be explained by the fact that the equations (2.11, 2.12) describe the DM shape in terms of actions p defined only within the correction aperture, while some modes can be exactly defined only by actuators positioned outside the correction aperture. These modes can not in principle be found as an exact solution of eq. (2.11) or (2.12) in terms of correction actions p inside the correction aperture.

Practical correction of any aberration satisfying to (2.13) for a membrane and bimorph DM, or (2.14) for a thin-plate DM, performed only by the actuators positioned within the aperture, results in a "bumpy" approximation to the desired shape. To obtain a high quality correction, a certain number of actuators should be positioned outside of the DM aperture so that the conditions (2.13, 2.14) are satisfied inside the aperture, while the external actuators produce the required correction. The number of these external actuators should be large enough to produce a sufficient number of independent modes. Considering all low-order Zernike polynomials up to the 4th order, we see that out of all 15 modes, 14 satisfy to the condition (2.14), and 9 satisfy to both (2.13) and (2.14). Counting very roughly that each actuator corrects one mode, we conclude that to correct the low-order terms described by (2.14), the continuous faceplate DM should have at least 14 actuators and a bimorph or a membrane DM should have at least 9 actuators placed outside its correction aperture.

Also, from very basic considerations, it follows that any DM described by the Poisson equation requires at least two actuators to be placed outside the working aperture per period of the azimuthal aberration of the highest expected order.

Any DM described by the biharmonic equation, such as a continuous facesheet DM with push-pull actuators, requires at least four actuators to be placed outside the working aperture per period of the azimuthal aberration of the highest expected order, and these actuators should not be positioned on a single circle.

These rules assume the actuators of the DM are linear and can produce any force. In practice, the design of the DM should take into account the actuator clipping and saturation, therefore practical DM designs can deviate from these recipes.

It also follows from the analysis that any response of the continuous facesheet DM is described by a 4-th order function. Any

attempt to correct the focus of a laser beam with such a DM will result in a print-through, causing hot (black) spots in the beam in the places where the actuators are positioned. This property is inherent to the design of the continuous faceplate DM. **OKO fabricates special edge-actuated continuous facesheet deformable mirrors that are free from any print-through and can be operated with CW laser loads of up to tens of kW.**

2.5 Correction performance

Computer models described in sections 2.2 and 2.3 were used for calculation of the influence functions of the 15-mm 37-channel MMDM ("OKO DM"), 37-ch OKO PDM and 109-ch OKO PDM.

The *rms* correction for the Zernike polynomials up to the 8-th order is shown in Fig. 2.4 for three different values of the correction aperture $R = 0.8;\ 0.6;\ 0.4$ of a 37-ch MMDM. The case $R = 1$ is not considered due to the fixed edge. The graph clearly shows that the correction quality improves significantly with the decrease of R for all modes Z_n^m with $n = m$, which can be explained by the increase in the number of actuators positioned outside the aperture. Correction of aberrations Z_7^1, Z_7^3 and Z_8^0 is strongly dependent on the number of internal actuators, resulting in optimal correction with $R = 0.8$ when the maximum number of actuators is positioned inside the correction aperture. All other modes require simultaneous correction with internal and external actuators, therefore the optimum correction is reached in the vicinity of $R = 0.6 \ldots 0.7$.

Figure 2.5 (top) shows the residual *rms* correction error for a 37-ch DM for low order Zernike polynomials Z_n^m for three different values of the correction aperture $R = 1;\ 0.8;\ 0.65$. The correction quality of low-order aberrations is poor when the full aperture $R = 1$ is used and all actuators are positioned within the correction aperture. The quality improves significantly for smaller R practically for all low-order aberrations, as the number of actuators inside the correction aperture decreases, while the external actuators form the otherwise impossible correction modes. Polynomials Z_7^3 and Z_7^5 do not satisfy to (2.14), therefore the correction of these terms requires at least some actuators to

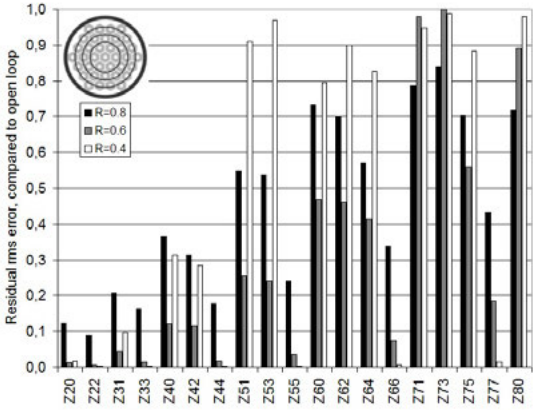

Figure 2.4: *Calculated quality of correction the Zernike modes Z_n^m up to $n = 8$ for the 15-mm MMDM controlled by 37 actuators, for different sizes of the correction aperture.*

be positioned within correction aperture. For these modes, the correction quality is better for the full aperture $R = 1$ and the error increases for smaller correction apertures such as $R = 0.8$ and $R = 0.65$.

The Fig. 2.5 (bottom) shows the correction quality calculated for a 109-ch PDM for Zernike terms up to the 10-th order. As in all previous cases, the correction quality reaches its maximum when a significant number of actuators is positioned outside the correction aperture. The aperture of $R = 0.65 \ldots 0.8$ is optimal for this DM. For example, if the DM diameter is 5cm, the optimal aperture would be in the range between 3.25 to 4 cm.

In practice, to achieve the optimal quality of correction, a MMDM should be used with correction apertures in the range $R = 0.6 \ldots 0.7$ of the full membrane aperture, while a PDM should be used with working apertures in the range $R = 0.65 \ldots 0.8$ of the full DM aperture.

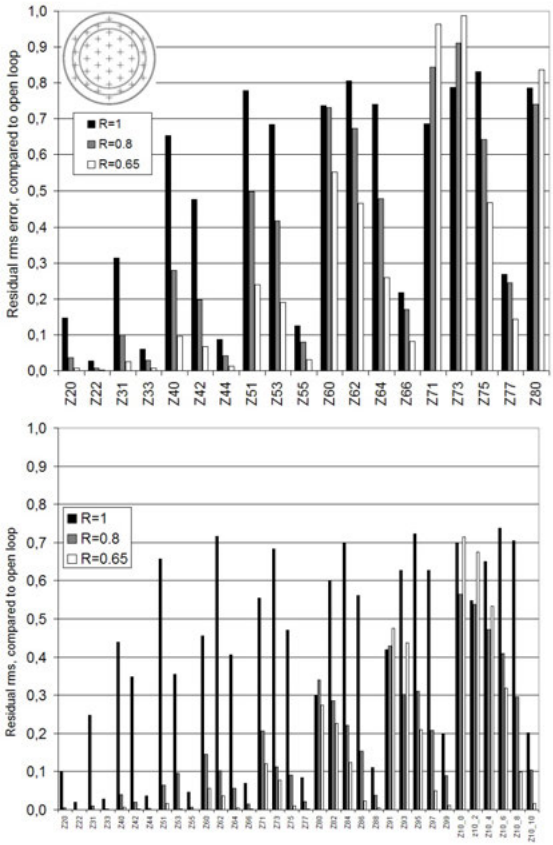

Figure 2.5: *Calculated quality of correction the Zernike modes Z_n^m up to $n = 8$ for a PDM controlled by 37 actuators (top) and for Zernike modes up to the 10-th order for a PDM controlled by 109 actuators, for different sizes of the correction aperture.*

2.6 DM and atmospheric correction

To evaluate optical performance of a wavefront corrector, we need to apply it to a whole class of optical fields. As the main practical application of adaptive optics for many years was high-resolution imaging through the turbulent atmosphere, we shall use the

statistics of random wavefronts induced by atmospheric turbulence. The Kolmogorov model is the most frequently used for turbulence description because of its relative mathematical simplicity and good agreement with experiment [16].

Modal wavefront correction is usually described in terms of complete orthogonal sets of functions, such as Zernike polynomials or Karhunen-Loéve functions. The last one is a special set of functions, best fit for representation of random wavefronts with statistics described by the Kolmogorov theory. For these sets the *rms* wavefront aberrations were evaluated in [17] for the generalized case of modal correctors with Karhunen-Loéve basis.

The comparison study of different types of modal correctors was presented in [18].

The results of comparison of optical performances of the 37-channel piston, continuous faceplate and membrane mirrors are shown in Table 2.1. All the mirrors have the same hexagonal structure of actuators. Maximum values of the turbulence parameter D_p/r_0 in the third column correspond to the Strehl parameter of 0.5.

In the model framework (linear response, no actuator clipping), the PDM is more advantageous: it provides better fitting, faster response and larger actuator stroke, compared to MMDM.

Table 2.1: *Comparison of the correction performances of 37-channel piston, continuous faceplate and membrane DM with hexagonal structure of actuators. Efficiency corresponds to the equivalent number of Zernike modes.*

DM type	**Residual aberrations, %**	$(D_\mathrm{p}/R_0)_\mathrm{max}$	**Efficiency**
Piston	22.7	4.69	5
Membrane	9.68	10.9	22
Continuous faceplate, free edge	9.02	14.2	33

2.7 Print-through

The PDM response satisfying to the bi-harmonic equation, is described by at least a 4-th order function. Most of the statistically important low-order aberrations, have lower order. This mismatch causes “bumpy” correction, when the high-order DM response approaches the aberration in average, but introduces an undesirable high spatial frequency term. This high-frequency aberration is named “print-through”. Print-through is inherent to the continuous faceplate DM.

The print-through has little effect and can be tolerated in incoherent imaging systems. However, it may have negative effects in very high contrast systems, sensitive to scattered light, such as planet finders and coronographs.

In laser AO, the print-through causes hot and black spots in the beam. It requires some additional attention, especially in high-power systems working with high thermal loads, or with very high light intensities, on the boundary of self-focusing. In these situations, additional intensity non-uniformity may have drastic negative effects and even cause destruction of optical components.

The print-through can be eliminated by:

- Using membrane mirrors (second order response)
- Placing part of the total number of actuators outside the light aperture of the continuous faceplate DM.

OKO fabricates special high-power laser PDM, featuring zero print-through within the light aperture.

2.8 PDM under laser load

OKO fabricates PDM with high-reflective multilayer dielectric coatings for high power and high intensity applications. In principle, PDM technology allows us to use the same types of coatings, that are used for solid optical components and laser mirrors. In addition, the 50 mm PDM has a built-in fan to facilitate dissipation of excessive heat from the DM package.

OKO PDM reported to work with total CW power load of up to 30 kW.

Also we can supply custom-coated PDM with multi-wavelength coatings, low-dispersion coatings and special coatings for femtosecond applications.

2.9 MMDM under laser load

This section presents the results of investigation of a MMDM under continuous laser load and in an optimization setup. Its temporal response and tip-tilt correction possibilities are also investigated. More technical details can be found in [19, 20].

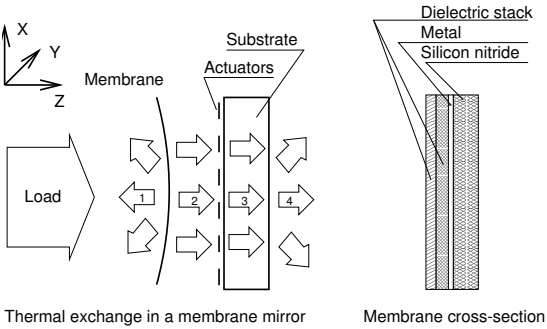

Figure 2.6: *A biased micromachined deformable mirror under laser load.*

Laser load causes change of the membrane temperature t, reducing the tension T due to the thermal expansion of the membrane material. Behavior of micromachined membrane deformable mirrors under continuous laser load has been investigated experimentally and theoretically in [19]. It was shown that load-induced variation of the membrane temperature and mechanical tension result in additional thermal deformation of the deformable mirror figure. Modeling the membrane tension and thermal deformation as functions of beam diameter, optical power and DM design parameters, the authors found that the thermal resistance of the DM substrate is critical for high-power operation. According to the estimations made, an optimally designed membrane DM with 99.8% reflectivity can be safely loaded with up to 500 W of optical power in a 10 mm diameter beam. This model was compared with experimental data obtained for micro-machined

membrane deformable mirrors with five different types of reflective coatings loaded with up to 70 W beam with power density of up to 20 W/mm^2. Operation of a multilayer membrane DM was demonstrated in a stable resonator of a diode-pumped YAG:Nd laser with output power of up to 4.5 W.

In [21] a 10 mm 19-channel MMDM coated with silver and a 12-layer dielectric stack was tested inside the resonator of a CV YAG laser with output power of 200 W. The optical load on the DM reached 600 W in a 6 mm beam. The DM operated continuously without any signs of degradation.

MMDMs can be used for CW laser applications with beam powers of up to 500 W with power density of the order of 2 kW/cm^2. The optimization of the package design can increase the loads, making the DMs applicable for high-power CW applications. OKO DMs for high-power applications satisfy the following requirements:

- High reflectivity is achieved by coating the membrane with a highly-reflective metal (silver) further enhanced by a multilayer dielectric stack.
- Low thermal resistance of the gap between the membrane and the electrode structure.
- Low thermal resistance of the electrode structure and between the DM substrate and the ambient, essential for heat evacuation.

2.10 MMDM temporal stability

Since MMDM has negligible hysteresis, it can be used as a quasi-static correction element. Such a corrector should possess certain stability over time, to avoid frequent re-calibration of the system.

For the long term stability the deformable mirror has been first set to the biased shape by setting the bias voltage to all actuators. After that the DM has been run in a closed-loop adaptive optics, to achieve the best fit to the spherical reference.

Fig. 2.7 illustrates the DM behavior during a 16-day stability test. In both cases (self referenced and with a reference to the spherical surface) the rms error did not exceed $\lambda/10$.

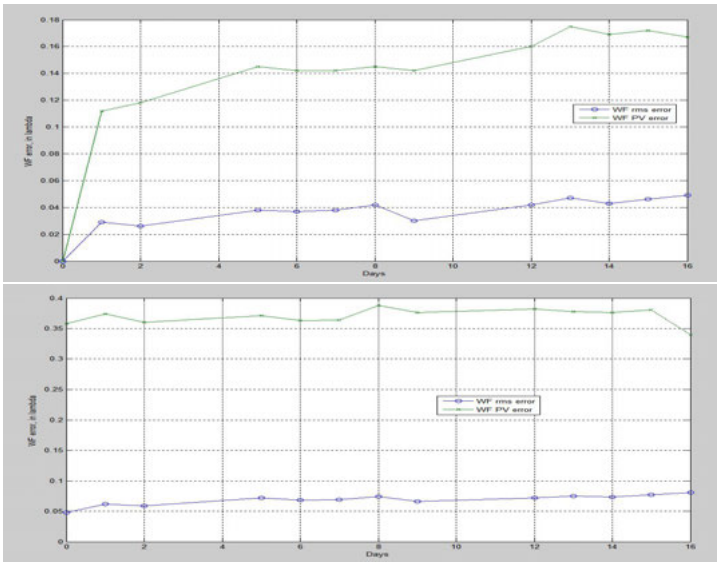

Figure 2.7: *MMDM aberration, in lambda, with respect to the initial DM figure (top) and to the ideal sphere (bottom), as a function of time during 16-day stability test*

Although the DM instability is small, it is measurable. The main sources of the instability would be:

- thermal deformations of the DM structure;
- instability of the control electrical signals;
- relaxation of mechanical stress in the DM structure.

MMDM with a reduced influence of these factors can be fabricated on a special order.

The off the shelf 15-mm OKO MMDM instability in the reflected WF reaches rms $\lambda/20$ in 16 days. The error with respect to the nearest sphere changes from $\lambda/20$ in the first day, to about $\lambda/10$ in the 16th day.

2.11 MMDM temperature stability

The aberration of the off-the-shelf OKO MMDM15-37 increases with the temperature change - see Fig. 2.8. The focus term is caused by the temperature dependence of the membrane tension. It is inherent to the mirror design, very predictable, and can be pre-calibrated. However, the main aberration was caused by the astigmatism, which strongly depends on the thermal compensation in the mechanical design of the mirror, which also can be optimized.

In [22] off-the-shelf MMDM15-37 has being operated at cryogenic temperatures, $T = 78$K. The magnitude of the surface deflection was reduced by around 20%, compared with the room temperature value, however the DM remained operational.

OKO can deliver temperature-compensated designs of MMDM, featuring reduced temperature drift, operable in the range from cryogenic, to up to $+120°$C.

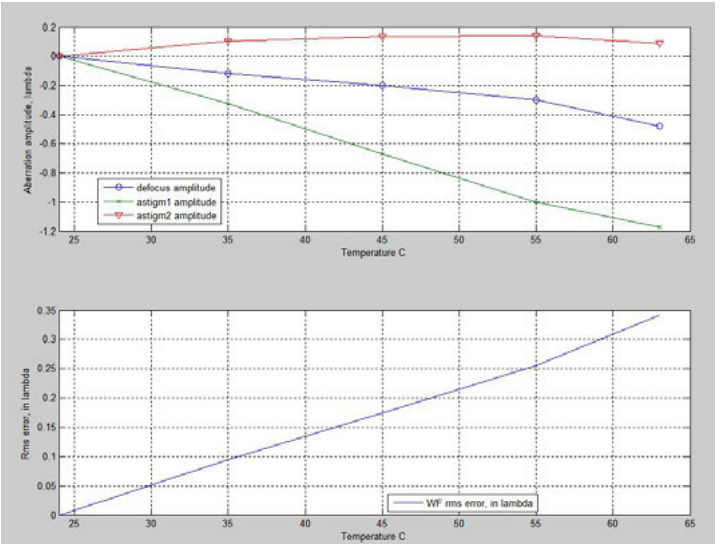

Figure 2.8: *Temperature dependance of MMDM15-37 aberrations in the range* $24°$ *to* $63°C$

2.12 MMDM nonlinearity

The test consisted in application of the same increasing voltage to all actuators of the 15mm OKO MMDM. The increasing DM response was monitored till the membrane catastrophically collapsed to the electrode structure. The DM response as a function of bias voltage is shown in Fig. 2.9. The DM response versus bias voltage has demonstrated a satisfactory fit to a parabola, for deflections of up to 20μm. Higher deflections vs voltage are described by a polynomial of a higher order. The DM deflection is quite sensitive and unstable in the vicinity of the collapse point. The maximum (collapse) voltage can differ from one device to another and from batch to batch.

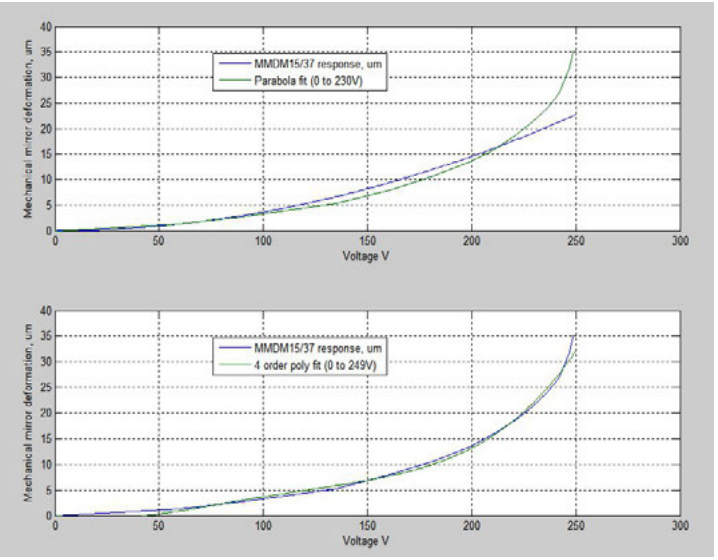

Figure 2.9: *MMDM maximum deflection, as a function of bias voltage. The DM membrane collapsed to the electrode structure at 250 V.*

Although non-linear, the response of MMDM features zero hysteresis. MMDM can be operated in a pre-calibrated feedforward mode with a very high optical precision and low temporal drift.

2.13 MrFit: DM simulation package

MrFit is a MS Windows program to simulate the static behavior of membrane and continuous facesheet DM. It calculates the voltages to be applied to the actuators, to achieve the best possible compensation of a specified aberration, defined as a combination of Zernike terms. The program shows — see for instance Fig. 2.10 and 2.11 — the surfaces of the wavefront, the best fit with a specified DM, and the approximation error. The output can be obtained as a gray scale plot, interferogram, or a 3D surface. The software can take into account the effects caused by the clipping of the actuator voltages, providing realistic output accounting for the limited stroke of the DM actuators.

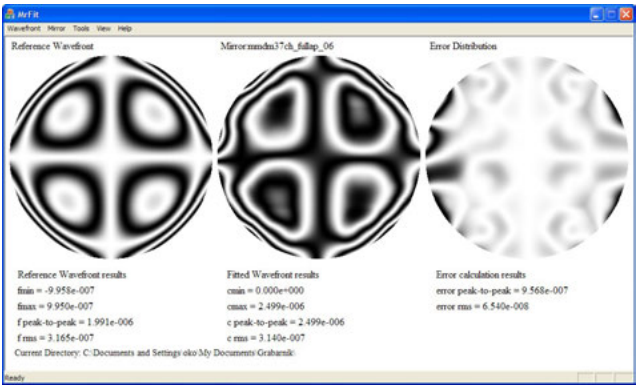

Figure 2.10: *MrFit main window with interferometric visualization.*

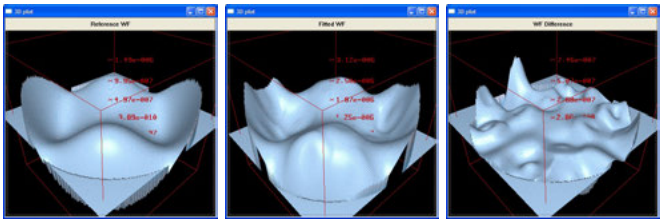

Figure 2.11: *3D plots of an aberration, the best fit obtained with a membrane DM, and the approximation error.*

The full commercial version of the program simulates any circular membrane or a continuous facesheet DM, with any number and geometry of actuators.

A free version of the software is available from the OKO Technologies website. It simulates only the deformable mirrors produced by OKO Technologies.

Please contact OKO Technologies for any further information about the commercial and the free version of the software.

2.14 Publications based on OKO DM

In addition to the testing results presented in this chapter, there are numerous publications containing useful technical information on OKO DMs and their applications. An uncomplete list of these publications is given below.

[1] Gleb Vdovin and P. M. Sarro. Flexible mirror micromachined in silicon. *Appl. Opt.*, 34(16):2968–2972, Jun 1995.

[2] Gleb Vdovin. Reconstruction of an object shape from the near-field intensity of areflected paraxial beam. *Appl. Opt.*, 36(22):5508–5513, Aug 1997.

[3] G.V. Vdovin, Simon Middelhoek, and Pasqualina M. Sarro. Technology and applications of micromachined silicon adaptive mirrors. *Optical Engineering*, 36:1382, 1997.

[4] F. Druon, G. Cheraux, J. Faure, J. Nees, A. Maksimchuk M. Nantel, G. Mourou, J.C. Chanteloup, and G. Vdovin. Wavefrontcorrection of femtosecond terawatt lasers by deformable mirrors. *Optics Letters*, 23:1043, 1998.

[5] A. F. Naumov, M. Yu. Loktev, I. R. Guralnik, and G. Vdovin. Liquid-crystal adaptive lenses with modal control. *Opt. Lett.*, 23(13):992–994, Jul 1998.

[6] Alexander F. Naumov and Gleb Vdovin. Multichannel liquid-crystal-based wave-front corrector with modal influence functions. *Opt. Lett.*, 23(19):1550–1552, Oct 1998.

[7] Gleb V. Vdovin, Nicolas Kugler, and Martin Schacht. Membrane deformable mirrors under CW laser load. In *Adaptive Optics Systems and Technology*, volume 3762 of *Proc. SPIE*, pages 58–66, September 27 1999.

[8] Erik Zeek, Kira Maginnis, Sterling Backus, Ulrich Russek, Margaret Murnane, Gérard Mourou, Henry Kapteyn, and Gleb Vdovin. Pulse compression by use of deformable mirrors. *Opt. Lett.*, 24(7):493–495, Apr 1999.

[9] Lijun Zhu, Pang-Chen Sun, Dirk-Uwe Bartsch, William R. Freeman, and Yeshaiahu Fainman. Adaptive control of a micromachined continuous-membrane deformable mirror for aberration compensation. *Appl. Opt.*, 38(1):168–176, Jan 1999.

[10] Lijun Zhu, Pang-Chen Sun, Dirk-Uwe Bartsch, William R. Freeman, and Yeshaiahu Fainman. Wave-front generation of zernike polynomial modes with a micromachined membrane deformable mirror. *Appl. Opt.*, 38(28):6019–6026, Oct 1999.

[11] Lijun Zhu, Pang-Chen Sun, and Yeshaiahu Fainman. Aberration-free dynamic focusing with a multichannel micromachined membrane deformable mirror. *Appl. Opt.*, 38(25):5350–5354, Sep 1999.

[12] O. Albert, L. Sherman, G. Mourou, T. B. Norris, and G. Vdovin. Smart microscope: an adaptive optics learning system for aberration correction in multiphoton confocal microscopy. *Opt. Lett.*, 25(1):52–54, Jan 2000.

[13] R. Bartels, S. Backus, E. Zeek, L. Misoguti, G. Vdovin, I. P. Christov, M. M. Murnane, and H. C. Kapteyn. Shaped-pulse optimization of coherent emission of high-harmonic soft x-rays. *Nature*, 406(6792):164–166, 2000.

[14] M. Yu. Loktev, V. N. Belopukhov, F. L. Vladimirov, G. V. Vdovin, G. D. Love, and A. F. Naumov. Wave front control systems based on modal liquid crystal lenses. *Review of Scientific Instruments*, 71(9):3290–3297, 2000.

[15] C. Paterson and J. C. Dainty. Hybrid curvature and gradient wave-front sensor. *Opt. Lett.*, 25(23):1687–1689, Dec 2000.

[16] Carl Paterson, I. Munro, and J. Dainty. A low cost adaptive optics system using a membrane mirror. *Opt. Express*, 6(9):175–185, Apr 2000.

[17] E. Zeek, R. Bartels, M. M. Murnane, H. C. Kapteyn, S. Backus, and G. Vdovin. Adaptive pulse compression for transform-limited 15-fs high-energy pulse generation. *Opt. Lett.*, 25(8):587–589, Apr 2000.

[18] Michael R. Armstrong, Peter Plachta, Evgueni A. Ponomarev, and R. J. D. Miller. Versatile 7-fs optical parametric pulse generation and compression by use of adaptive optics. *Opt. Lett.*, 26(15):1152–1154, Aug 2001.

[19] Harold Dyson, Ray Sharples, N. Dipper, and Gleb Vdovin. Cryogenic wavefront correction using membrane deformable mirrors. *Opt. Express*, 8(1):17–26, Jan 2001.

[20] Enrique J. Fernández, Ignacio Iglesias, and Pablo Artal. Closed-loop adaptive optics in the human eye. *Opt. Lett.*, 26(10):746–748, May 2001.

[21] Mikhail Loktev, Davies William De Lima Monteiro, and Gleb Vdovin. Comparison study of the performance of piston, thin plate and membrane mirrors for correction of turbulence-induced phase distortions. *Optics Communications*, 192(12):91 – 99, 2001.

[22] Robert K. Tyson and Benjamin West Frazier. Microelectromechanical system programmable aberration generator for adaptive optics. *Appl. Opt.*, 40(13):2063–2067, May 2001.

[23] Gleb Vdovin and Vadim Kiyko. Intracavity control of a 200-w continuous-wave nd:yag laser by a micromachined deformable mirror. *Opt. Lett.*, 26(11):798–800, Jun 2001.

[24] S. Kotova, M. Kvashnin, M. Rakhmatulin, O. Zayakin, I. Guralnik, N. Klimov, P. Clark, Gordon Love, A. Naumov, C. Saunter, M. Loktev, G. Vdovin, and L. Toporkova. Modal

liquid crystal wavefront corrector. *Opt. Express*, 10(22):1258–1272, Nov 2002.

[25] Walter Lubeigt, Gareth Valentine, John Girkin, Erwin Bente, and David Burns. Active transverse mode control and optimization of an all-solid-state laser using an intracavity adaptive-optic mirror. *Opt. Express*, 10(13):550–555, Jul 2002.

[26] S. C. McQuaide. Three-dimensional virtual retinal display using a deformable membrane mirror. Master's thesis, University of Washington, 2002.

[27] Sarah C. McQuaide, Eric J. Seibel, Robert Burstein, and Thomas A. Furness. Three-dimensional virtual retinal display system using a deformable membrane mirror. *SID Symposium Digest of Technical Papers*, 33(1):1324–1327, 2002.

[28] Gleb Vdovin and Mikhail Loktev. Deformable mirror with thermal actuators. *Opt. Lett.*, 27(9):677–679, May 2002.

[29] D. C. L. Cheung, T. H. Barnes, and T. G. Haskell. Feedback interferometry with membrane mirror for adaptive optics. *Optics Communications*, 218:33–41, March 2003.

[30] Enrique Fernandez and Pablo Artal. Membrane deformable mirror for adaptive optics: performance limits in visual optics. *Opt. Express*, 11(9):1056–1069, May 2003.

[31] J. Garduño-Mejía, A. Greenaway, and D. Reid. Designer femtosecond pulses using adaptive optics. *Opt. Express*, 11(17):2030–2040, Aug 2003.

[32] Christoph U. Keller, Claude Plymate, and S. M. Ammons. Low-cost solar adaptive optics in the infrared. In *Innovative Telescopes and Instrumentation for Solar Astrophysics*, volume 4853 of *Proc. SPIE*, pages 351–359, 2003.

[33] Gleb Vdovin, Mikhail Loktev, and Alexander Naumov. On the possibility of intraocular adaptive optics. *Opt. Express*, 11(7):810–817, Apr 2003.

[34] Jesus Garduño-Mejía, Alan H. Greenaway, and Derryck T. Reid. Programmable spectral phase control of femtosecond pulses by use of adaptive optics and real-time pulse measurement. *J. Opt. Soc. Am. B*, 21(4):833–843, Apr 2004.

[35] Eirini Theofanidou, Laurence Wilson, William J. Hossack, and Jochen Arlt. Spherical aberration correction for optical tweezers. *Optics Communications*, 236(13):145 – 150, 2004.

[36] Eugenie Dalimier and Chris Dainty. Comparative analysis of deformable mirrors for ocular adaptive optics. *Opt. Express*, 13(11):4275–4285, May 2005.

[37] R. El-Agmy, H. Bulte, A. H. Greenaway, and D. Reid. Adaptive beam profile control using a simulated annealing algorithm. *Opt. Express*, 13(16):6085–6091, Aug 2005.

[38] M.Y. Loktev. *Modal wavefront correctors based on nematic liquid crystals*. PhD thesis, TU Delft, 2005.

[39] Oleg Soloviev and Gleb Vdovin. Hartmann-shack test with random masks for modal wavefront reconstruction. *Opt. Express*, 13(23):9570–9584, Nov 2005.

[40] G. Vdovin, M. Loktev, A. Simonov, V. Kijko, and S. Volkov. Adaptive correction of human-eye aberrations in a subjective feedback loop. *Opt. Lett.*, 30(7):795–797, Apr 2005.

[41] Stéphane R. Chamot, Chris Dainty, and Simone Esposito. Adaptive optics for ophthalmic applications using a pyramid wavefront sensor. *Opt. Express*, 14(2):518–526, Jan 2006.

[42] David Merino, Chris Dainty, Adrian Bradu, and Adrian Gh. Podoleanu. Adaptive optics enhanced simultaneous en-face optical coherence tomography and scanning laser ophthalmoscopy. *Opt. Express*, 14(8):3345–3353, Apr 2006.

[43] Markus Rueckel, Julia A. Mack-Bucher, and Winfried Denk. Adaptive wavefront correction in two-photon microscopy using coherence-gated wavefront sensing. *Proceedings of the National Academy of Sciences*, 103(46):17137–17142, 2006.

[44] Amanda J. Wright, Brett A. Patterson, Simon P. Poland, John M. Girkin, Graham M. Gibson, and Miles J. Padgett. Dynamic closed-loop system for focus tracking using a spatial light modulator and a deformable membrane mirror. *Opt. Express*, 14(1):222–228, Jan 2006.

[45] S Campbell, S M F Triphan, R El-Agmy, A H Greenaway, and D T Reid. Direct optimization of femtosecond laser ablation using adaptive wavefront shaping. *Journal of Optics A: Pure and Applied Optics*, 9(11):1100, 2007.

[46] N A Klimov, S P Kotova, S A Samagin, M Yu Kvashnin, G V Vdovin, and M Yu Loktev. Modal liquid-crystal wavefront corrector on a ceramic substrate: the single-contact approximation. *Quantum Electronics*, 37(12):1169, 2007.

[47] Mikhail Loktev, Gleb Vdovin, Nikolai Klimov, and Svetlana Kotova. Liquid crystal wavefront corrector with modal response based on spreading of the electric field in a dielectric material. *Opt. Express*, 15(6):2770–2778, Mar 2007.

[48] A. J. Wright, S. P. Poland, J. M. Girkin, C. W. Freudiger, C. L. Evans, and X. S. Xie. Adaptive optics for enhanced signal in cars microscopy. *Opt. Express*, 15(26):18209–18219, Dec 2007.

[49] Gleb Vdovin, Oleg Soloviev, Alexander Samokhin, and Mikhail Loktev. Correction of low order aberrations using continuous deformable mirrors. *Opt. Express*, 16(5):2859–2866, Mar 2008.

[50] Sem Sem Chin, Karen M. Hampson, and Edward A. H. Mallen. Effect of correction of ocular aberration dynamics on the accommodation response to a sinusoidally moving stimulus. *Opt. Lett.*, 34(21):3274–3276, Nov 2009.

[51] Karen M. Hampson, Sem Sem Chin, and Edward A. Mallen. Dual wavefront sensing channel monocular adaptive optics system for accommodation studies. *Opt. Express*, 17(20):18229–18240, Sep 2009.

[52] Yanan Huang, Jingfang Wan, Ming-Chieh Cheng, Zhipeng Zhang, Sissy M. Jhiang, and Chia-Hsiang Menq. Three-axis rapid steering of optically propelled micro/nanoparticles. *Review of Scientific Instruments*, 80(6):063107, 2009.

[53] Jörgen Thaung, Per Knutsson, Zoran Popovic, and Mette Owner-Petersen. Dual-conjugate adaptive optics for wide-field high-resolution retinal imaging. *Opt. Express*, 17(6):4454–4467, Mar 2009.

[54] C.M.S. Corley, Masaki Nagashima, and B.N. Agrawal. Beam control and a new laboratory testbed for adaptive optics in a maritime environment. In *Aerospace Conference, 2010 IEEE*, pages 1–13, 2010.

[55] H. Song, R. Fraanje, G. Schitter, H. Kroese, G. Vdovin, and M. Verhaegen. Model-based aberration correction in a closed-loop wavefront-sensor-less adaptive optics system. *Opt. Express*, 18(23):24070–24084, Nov 2010.

[56] Xiaodong Tao, Hyungsuck Cho, and Farrokh Janabi-Sharifi. Optical design of a variable view imaging system with the combination of a telecentric scanner and double wedge prisms. *Appl. Opt.*, 49(2):239–246, Jan 2010.

[57] Dominik Walter, Helge Bürsing, and Reinhard Ebert. Emission of spiral patterns from filaments in the infrared. *Opt. Express*, 18(23):24258–24263, Nov 2010.

[58] Favio Bortoletto, Carlotta Bonoli, Paolo Panizzolo, Catalin D. Ciubotaru, and Fabio Mammano. Multiphoton fluorescence microscopy with grin objective aberration correction by low order adaptive optics. *PLoS ONE*, 6(7):e22321, 07 2011.

[59] M. Loktev, G. Vdovin, O. Soloviev, and S. Savenko. Experiments on speckle imaging using projection methods. In *Unconventional Imaging, Wavefront Sensing, and Adaptive Coded Aperture Imaging and Non-Imaging Sensor Systems*, volume 8165 of *Proc. SPIE*, pages 81650M–81650M–10, September 13 2011.

[60] Mikhail Loktev, Oleg Soloviev, Svyatoslav Savenko, and Gleb Vdovin. Speckle imaging through turbulent atmosphere based on adaptable pupil segmentation. *Opt. Lett.*, 36(14):2656–2658, Jul 2011.

[61] Saisai Niu, Jianxin Shen, Chun Liang, Yunhai Zhang, and Bangming Li. High-resolution retinal imaging with micro adaptive optics system. *Appl. Opt.*, 50(22):4365–4375, Aug 2011.

[62] Kotaro Okamura and Takayoshi Kobayashi. Octave-spanning carrier-envelope phase stabilized visible pulse with sub-3-fs pulse duration. *Opt. Lett.*, 36(2):226–228, Jan 2011.

[63] Gleb Vdovin, Oleg Soloviev, Mikhail Loktev, and Slava Savenko. Imaging through turbulence with temporally and spatially multiplexed systems. In *Optics in Atmospheric Propagation and Adaptive Systems XIV*, volume 8178 of *Proc. SPIE*, pages 81780F–81780F–8, October 14 2011.

[64] Gleb Vdovin, Oleg Soloviev, Mikhail Loktev, Slava Savenko, and Lukasz Dziechciarczyk. Optimal correction and feed-forward control of low-order aberrations with piezoelectric and membrane deformable mirrors. In *Unconventional Imaging, Wavefront Sensing, and Adaptive Coded Aperture Imaging and Non-Imaging Sensor Systems*, volume 8165 of *Proc. SPIE*, pages 81650W–81650W–10, September 13 2011.

[65] M. Loktev, G. Vdovin, O. Soloviev, S. Kryukov, and S. Savenko. Adaptive optics combined with computer post-processing for horizontal turbulent imaging. In *Real-Time Image and Video Processing*, volume 8437, pages 84370Y–84370Y–9, June 1 2012.

[66] Eric S. ten Have and Gleb Vdovin. Physical and mechanical properties of a tir-based liquid micro deformable mirror. In *Micro-Optics*, volume 8428 of *Proc. SPIE*, pages 84281W–84281W–11, 2012.

2.15 Acceptable DM defects

Deformable mirrors fabricated by OKO Technologies are complex opto-electro-mechanical systems. In many cases we fabricate these mirrors to a customer's specification, which result in an unique product. It is practically impossible to deliver a custom-made DM which is absolutely free of any defects. In all cases we look for the best possible compromise.

This section gives an overview of mirror defects that we do tolerate.

2.15.1 Surface defects

Deformable mirrors are complex opto-electro-mechanical systems, they can have various defects in mechanics, electronics and optics, which are invisible to the human eye. Many of these defects can be real killers to the mirror performance, but since they are invisible, they are not a concern at the first inspection.

The situation is quite different with respect to the surface defects. In vision systems, small surface defects practically do not influence the performance of the optics. They add slightly to the scattering, but these effects are negligible compared to the harm caused by the phase aberrations. We have experience with very badly scratched mirrors that perform perfectly in vision systems. In most cases surface defects are quite harmless. Unfortunately, at the first inspection, they take all the customer's attention, simply because they are clearly visible.

Surface defects can be important in two cases: in AO systems with very low scattering and in high-power laser systems. In both cases we can deliver a mirror that is free of surface defects, or with some minor defects that do not impair the performance.

The majority of DM delivered by OKO Technologies are free of surface defects. However, the process of fabrication of a DM is quite complicated, therefore sometimes we tolerate visible defects on the surface of a DM, if these defects do not impair the performance of the mirror.

2.15.2 Scratches on PDM

DM we deliver are free of major scratches. Some minor scratches may appear but the experience shows that these minor scratches appear most frequently in the imagination of the customer. Attempts to remove these minor scratches, does not matter real or imaginary, almost always result in real major scratches all over the mirror surface.

Contact OKO Technologies if you have any doubt. We do not replace deformable mirrors scratched by customers.

2.15.3 DM aging

MMDM feature very little to negligible temporal drift.

PDM can feature a certain amount of temporal drift, caused by the relaxations of the internal strains, glue shrinkage, actuator aging, etc. These drifts do not exceed the maximum of 0.5μm *rms* surface error during the mirror warranty period, the drifts are expected but not guaranteed to be negligible in mirrors that are older than 1 year.

There is a reason why we quote a long lead time: the PDM mechanics should relax to a stable state. Frequently the customer needs the DM to be delivered in a very short notice after the order is placed. In many cases such a rush leads to unacceptable drift of the mirror parameters in the first months of operation. We do not do rush shipping that may jeopardize the DM quality.

3

WAVEFRONT SENSORS

This chapter describes the wavefront analysis and control system "FrontSurfer", based on Hartmann (Hartmann-Shack) measurement principle. The system can be used for:

- Optical shop testing of transmissive and reflective optics: lenses, mirrors, lens assemblies, collimators, etc.;
- Real-time display of low-order aberrations (tip/tilt, defocus, coma, astigmatism) in so-called "Alignment mode".
- Real-time control and compensation of wavefront aberrations in combination with OKO Technologies deformable mirror system.

"FrontSurfer" includes:

- "FrontSurfer" software that runs under MS Windows 95/98/-2000/NT/XP/7. Linux is not supported for the latest versions of "FrontSurfer", but the Linux version can be supplied by request with a complete system including computer;
- measurement head, including a 1/2" monochromatic CCD or CMOS camera with computer interface and a high-precision Hartmann mask or a lenslet array in a C-mount. The measurement head consisting of UI-2210M camera and C-mounted microlens array is shown in Figure 3.1.

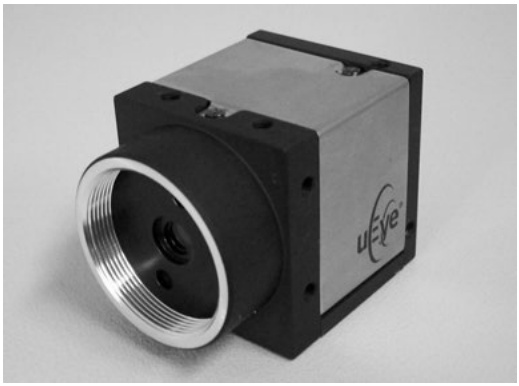

Figure 3.1: *Shack-Hartmann wavefront sensor, measurement head*

The system reconstructs two-dimensional wavefront profiles with *rms* sensitivity of better than $\lambda/100$. The system can be used for measurements in visible (using either monochromatic or white light) and infrared.

A special configuration was developed for volume control of the quality of microlens arrays. The system automatically measures the low-order aberrations of each microlens. As a result, the distribution of low-order aberrations, pitch irregularities and other defects can be plotted over the whole array area. Arrays of up to 30x40 microlenses were measured. The processing time for one array of 1200 microlens did not exceed 10 hours. This configuration is available on request and includes a micro-positioning stage.

3.1 "FrontSurfer" software

"FrontSurfer" is available in two configurations: with and without support for deformable mirrors and adaptive optics feedback.

3.1.1 Basic features

All versions of "FrontSurfer" have the following features:

- Reconstructs the optical wavefront from Hartmann and Shack-Hartmann sensor data.

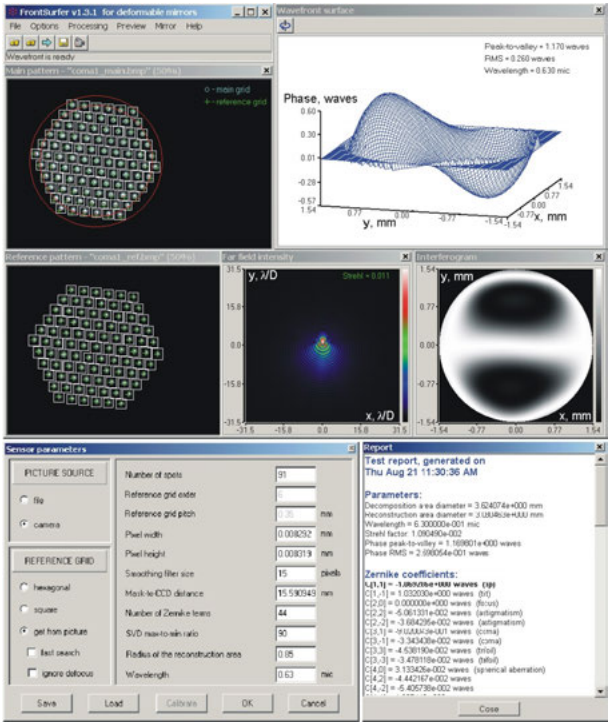

Figure 3.2: *“FrontSurfer” interface*

- Produces wavefront plot, synthetic interferogram, far field intensity and reports on Zernike terms (see Figure 3.2). All measurement data and results can be exported to several popular formats.
- Processes spot patterns obtained with hexagonal, orthogonal or random Hartmann masks and microlens arrays with arbitrary number of apertures.
- Operates with and without reference pattern: in the last case the parameters of the Hartmann mask or microlens array are used as a reference.
- In the reference mode, allows manually defining the area of

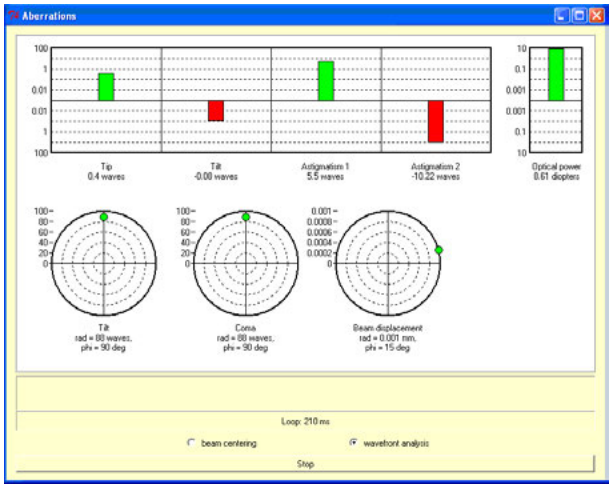

Figure 3.3: *"Aberrations" window in the alignment mode*

interest (aperture), which could be circular, elliptic, square or rectangular with an optional circular obscuration in the center.

- In the alignment mode, real time bar graph display of tip, tilt, defocus, coma and astigmatism; polar display of tilt, coma, astigmatism and position of the intensity maximum (see Figure 3.3).
- Allows to extract any aberration expressed in Zernike polynomials or eliminate any Zernike terms.
- Can be interfaced to third-party cameras by developing a custom video plugin according to provided programming interface specification.

3.1.2 Version for deformable mirrors

The "FrontSurfer" version for deformable mirrors has the following additional features:

- Manual control of voltages applied to the mirror.

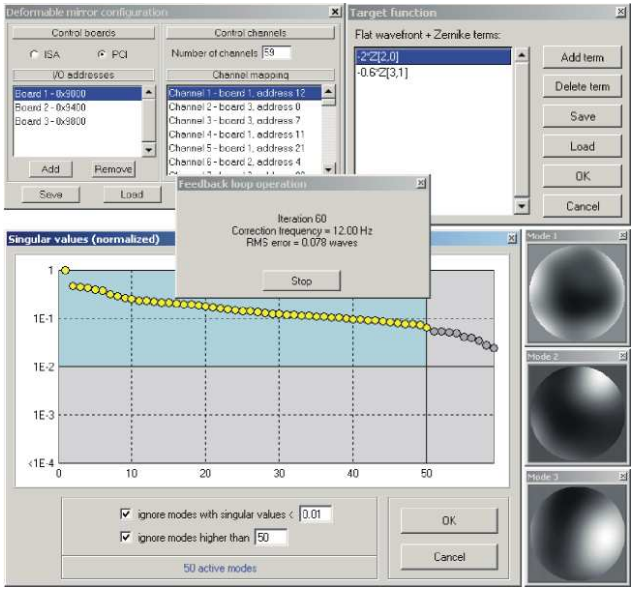

Figure 3.4: *“FrontSurfer”, interface of the version for deformable mirrors*

- Closed-loop correction in real time. Average correction rate depends on the camera type and computer performance and can be in the range 25 to 1500 Hz.
- Singular value decomposition (SVD) algorithm with user-defined number of modes for stable feedback.
- Can generate a given aberration in addition to the reference. The aberration is defined as a combination of Zernike polynomials and can be manually controlled during the closed-loop correction interactively.
- Supports all types of MMDM and PDM devices produced by OKO Technologies.
- Can be configured for a custom-made mirror interfaced to OKO’s PCI boards, USB and ethernet DAC driver modules.

- Can be interfaced to a custom DM driver, with a custom plugin.

3.2 "FrontSurfer" hardware

3.2.1 Typical configuration

Table 3.1: *Characteristics of three typical FrontSurfer Shack-Hartmann wavefront sensor configurations*

Parameter	Config. 1	Config. 2	Config. 3
Camera model	UI-2210M	UI-1540M	UI-2210M
Sensor type	CCD	CMOS	CCD
Camera interface	USB 2.0	USB 2.0	USB 2.0
Array geometry	hexagonal	orthogonal	orthogonal
Array pitch	300 μm	200 μm	150 μm
Array focal distance	$\sim$18 mm	7 mm	10 mm
Clear aperture	3.9 mm	$\leq$4.5 mm	$\leq$4.5 mm
Subapertures	127	$\leq$400	$\leq$700
Maximum tilt, fast mode	0.008 rad	0.014 rad	0.007 rad
Maximum tilt, slow mode	0.066 rad	N/A	N/A
Repeatability, RMS	$\lambda/300^{*}$	$\lambda/150^{*}$	$\lambda/150^{*}$
Repeatability, P-V	$\lambda/60^{*}$	$\lambda/20^{*}$	$\lambda/20^{*}$
Maximum acquisition rate	75 fps	25 fps	75 fps
Processing rate, fast mode	25 fps**	10/20 fps**	10 fps**
Processing rate, slow mode	1 fps**	N/A	N/A
Recommended Zernike terms	$\leq$44	$\leq$150	$\leq$300
Wavelength	400...900 nm	400...1000 nm	400...900 nm
Absolute mode	Yes	No	No
Reference mode	Yes	Yes	Yes

* For λ=0.633 μm
** For low-order aberration analysis on a PC with AMD Athlon XP1800+ processor and 256 MB RAM

Characteristics of three typical configurations of FrontSurfer wavefront sensor are given in Table 3.1. However, the system can be reconfigured according to the customer's requirements by choosing a different camera, Hartmann mask or microlens array. The options currently available are given below.

3.2.2 Supported camera types and interfaces

Using the custom video plugin interface, almost any camera can be interfaced to FrontSurfer. The plugin can be developed either

by OKO Technologies (if requested) or by a customer by oneself according to our specification. We have ready to use plugins for a number of popular cameras, including Basler “Pilot” series Ethernet cameras, uEye CMOS and CCD cameras, a number of IR cameras produced by Xenics, as well for devices providing MS DirectShow interface (including inexpensive web-cameras and analog frame grabbers). Typically, with inexpensive UEye camera, the acquisition performance is 40 to 100 frames per second. In special cases, depending on the computer, camera interface and the area of interest, our plugins have provided acquisition of up to 2000 frames per second.

3.2.3 Microlens arrays

OKO Technologies produces high-quality replicated microlens arrays specially for the use with FrontSurfer wavefront sensors. As one of the standard options, we offer a hexagonal array of 127 microlenses with a focal distance about 18 mm and a pitch of 300 μm, mounted in a C-mount.

Besides, OKO Technologies offers a range of microlens arrays fabricated in glass and fused silica with small numerical aperture and 99% optical fill factor. Microstructures provide for optimum spectral efficiency (UV to far infrared) and for the best mechanical and thermal stability. These arrays work with very high optical loads. To provide a cost-efficient solution, all listed arrays can be replicated in series in plastic. Microlens arrays with orthogonal and hexagonal arrangements are listed in Table 3.2 and Table 3.3, respectively. Recommended options to be used with 1/2-inch cameras are as follows:

- APO-Q-P192-F3.17, provides ~400 subapertures over a 4.5 mm circular area;
- APO-Q-P200-F7.0, ~400 subapertures over 4.5 mm;
- APO-Q-P150-F10, ~700 subapertures over 4.5 mm;
- APO-Q-P150-F3.5, ~700 subapertures over 4.5 mm.

Table 3.2: *Positive orthogonal microlens arrays*

Product type	Material	Pitch, μm	Radius, mm	Focal distance, mm	Maximum size
APO-Q-P2200-F209 (633)	Fused silica	2200	95,52	209	30x30 lenses (70x70mm)
APO-GB-P1500-F24.3 (633)	BK-7	1500	12,5	24,3	6x6 lenses (10x10mm)
APO-GB-P1500-F39.3 (633)	BK-7	1500	20,4	39	6x6 lenses (10x10mm)
APO-Q-P1100-F105 (633)	Fused silica	1100	48.0	105	55x55 lenses (62x62mm)
APO-Q-P1100-F209 (633)	Fused silica	1100	95,52	209	55x55 lenses (62x62mm)
APO-Q-P1061-F158 (633)	Fused silica	1061	72,4	158	55x55 lenses (62x62mm)
APO-Q-P1000-F40 (633)	Fused silica	1000	18.0	40	60x60 lenses (61x61mm)
APO-Q-P1000-F4,64 (633)	Fused silica	1000	2,12	4,64	60x60 lenses (61x61mm)
APO-Q-P500-F19,7 (633)	Fused silica	500	9	19,7	100x100 lenses (50x50mm)
APO-Q-P500-F8,31 (633)	Fused silica	500	3,8	8,31	100x100 lenses (50x50mm)
APO-Q-P300-F40 (633)	Fused silica	300	18.0	40	200x200 lenses (61x61mm)
APO-Q-P300-F118 (633)	Fused silica	300	54	118	200x200 lenses (61x61mm)
APO-Q-P300-F2 (633)	Fused silica	300	0,94	2,0	200x200 lenses (61x61mm)
APO-Q-P384-F5.75 (633)	Fused silica	384	2 627	5,75	5x5 lenses (2,5x2,5mm)
APO-Q-P222-F1,86 (633)	Fused silica	222	0,85	1,86	200x200 lenses (45x45mm)
APO-Q-P222-F0,93 (633)	Fused silica	222	0,43	0,93	200x200 lenses (45x45mm)
APO-Q-P192-F5.75 (633)	Fused silica	192	2 627	5,75	9x9 lenses (2x2mm)
APO-Q-P192-F3.17 (633)	Fused silica	192	1,45	3,17	200x200 lenses (45x45mm)
APO-Q-P200-F7.0 (633)	Fused silica	200	3,2	7.0	300x300 lenses (61x61mm)
APO-Q-P200-F40 (633)	Fused silica	200	18,2	40	300x300 lenses (61x61mm)
APO-Q-P150-F10 (633)	Fused silica	150	4,57	10	400x400 lenses (61x61mm)
APO-Q-P150-F3.5 (633)	Fused silica	150	1,6	3,5	400x400 lenses (61x61mm)
APO-Q-P148-F1,24 (633)	Fused silica	148	0,6	1,24	400x400 lenses (61x61mm)
APO-Q-P100-F0,217 (532)	Fused silica	100	0,1	0,217	500x500 lenses (51x51mm)
APO-GT-P100-F0,143 (633)	StiH-53	100	0,12	0,143	500x500 lenses (51x51mm)
APO-P(GB)-P250-F0,57 (633)	BK-7/NOA-61	250	0,32	0,57	25x25mm
APO-P(GB)-P200-F1,25 (633)	BK-7/NOA-61	200	0,7	1,25	40x40mm
APO-P(GB)-P200-F6,4 (633)	BK-7/NOA-61	200	3,32	6,4	25x25mm
APO-P(GB)-P300-F1,7 (633)	BK-7/NOA-61	300	0,94	1,7	25x25mm
APO-P(GB)-P300-F107 (633)	BK-7/NOA-61	300	60	107	25x25mm

Table 3.3: *Positive hexagonal microlens arrays*

Product type	Material	Pitch, μm	Radius, mm	Focal distance, mm	Maximum size
APH-GT-P1300-F5.2 (633)	StiH-53	1300	4,3	5,2	20x20 lenses (26x26mm)
APH-GT-P1300-F3,26 (633)	StiH-53	1300	2,74	3,26	20x20 lenses (26x26mm)
APH-Q-P1000-F36,7 (633)	Fused silica	1000	16,8	36,7	60x60 lenses (61x61mm)
APH-Q-P480-F10,91 (633)	Fused silica	480	5	10,9	100x100 lenses (51x51mm)
APH-Q-P250-F2 (633)	Fused silica	250	1	2	240x240 lenses (60x60mm)
APH-P(GB)-P250-F0,57 (633)	BK-7/NOA-61	250	0,32	0,57	145x145mm
APH-P(GB)-P30-F0,042 (633)	BK-7/NOA-61	30	0,024	0,042	50x50mm

Table 3.4: *Hartmann masks; size of each mask is* 10×10 *mm*

Material	Geometry	Aperture	Subapertures		
		size, mm	number	type	diameter, μm
Glass	Orthogonal	7	64	Circular	200
Glass	Orthogonal	7	64	Circular	300
Glass	Orthogonal	7	64	Circular	450
Glass	Orthogonal	7	64	Square	200
Glass	Orthogonal	7	64	Square	300
Glass	Orthogonal	7	64	Square	450
Glass	Orthogonal	3.5	36	Circular	200
Glass	Orthogonal	3.5	36	Circular	300
Glass	Orthogonal	3.5	49	Circular	200
Glass	Orthogonal	3.5	49	Circular	300
Glass	Orthogonal	3.5	64	Circular	200
Glass	Orthogonal	3.5	64	Circular	300
Glass	Orthogonal	3.5	81	Circular	200
Glass	Hexagonal	3.5	37	Circular	300
Fused silica	Hexagonal	3.5	37	Circular	200
Fused silica	Hexagonal	3.5	61	Circular	200
Fused silica	Hexagonal	3.5	91	Circular	200
Fused silica	Hexagonal	3.5	127	Circular	100
Fused silica	Hexagonal	3.5	169	Circular	100

3.2.4 Hartmann masks

OKO Technologies offers calibrated Hartmann masks with orthogonal and hexagonal geometries. Masks are fabricated in glass and fused silica and coated with patterned aluminum (glass masks) or chromium (fused silica masks). Since the holes are positioned with very high precision and aberration of the mask is negligible, these masks can be used for absolute wavefront sensing, without

calibration on a reference light beam. Available configurations are listed in Table 3.4.

3.2.5 Choice of the proper array

The choice of a proper microlens array or Hartmann mask, is a trade-off between the measurement range the precision. We advise the following criteria:

1. Sufficient sampling, matching the maximum aberration spatial frequency. If the aberrations can be described by N Zernike terms, we would recommend using at least $2N \ldots 3N$ subapertures. The relay optical scheme should rescale the beam to cover the desired number of sub-apertures.

2. Microlens arrays are more efficient in terms of collecting light, providing smaller and brighter spots, which is especially important for low-light applications. However, Hartmann masks can be manufactured with higher precision and can provide better results in the absolute wavefront measurement mode (see page 55) for smooth wavefronts.

3. The wavefront tilt in the sensor input should not exceed half pitch of the microlens array divided by its focal length.

4. The Strehl ratio of net aberrations over the area of each sub-aperture should be sufficiently high: at least 0.2. It will ensure the good quality of spots.

5. The sensitivity of the wavefront sensor improves proportionally to to the focal length of the microlens array - or, in case of a Hartmann sensor - to the distance between the mask and image sensor).

3.3 Wavefront measurements

The principle of (Shack-)Hartmann test is shortly explained in Section 1.6.2. Here we describe how “FrontSurfer” processes the measurement data to reconstruct the wavefront and give some hints on how to achieve better results.

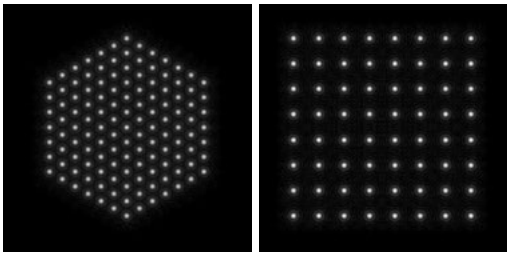

Figure 3.5: *Complete hexagonal (left) and orthogonal (right) spot patterns.*

3.3.1 The sensing mode

"FrontSurfer" can operate with and without a reference pattern. In the latter case, the geometric parameters of the Hartmann mask or microlens array are used as a reference, which allows for absolute wavefront sensing. A complete hexagonal or orthogonal structure of spots (see Figure 3.5) is desirable for this mode, although the program can tolerate up to 5 % missing spots. In the reference mode, the pattern can be neither complete nor regular; one can even use an array with random positioning of sub-apertures.

The choice between the *absolute measurement* and *reference* modes depends on the application. If the wavefront sensor is used for alignment of an optical system (i.e., collimation or astigmatism removal) then the absolute measurement mode would be more useful. If it is used in an optical testing scheme similar to those described in Section 3.4 then the reference mode is preferable, as it allows to neglect aberrations of the relay optics.

The reference mode allows the user to define area of interest (aperture) in the reference pattern manually. This feature is very useful for sensors with a large mask (or lenslet array), whose sub-apertures fill the whole area of the image sensor. The user can choice between circular, elliptic, square and rectangular aperture. Example hartmanngrams with manually defined circular aperture and central obscuration are shown in Figure 3.6.

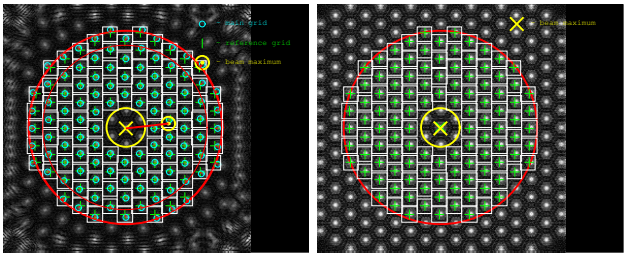

Figure 3.6: *Main (left) and reference (right) Hartmann spot patterns in the reference mode with manually defined aperture and central obscuration.*

3.3.2 Hartmanngram capture

"FrontSurfer" provides interfacing to video capture devices using external plugins. It makes possible to customize "FrontSurfer" for using with almost any camera and any frame grabber.

Besides, "FrontSurfer" has embedded support of "Video for Windows" interface, which allows to work with any TV tuner device using this interface.

In the absolute measurement mode we deal with only one intensity pattern; we refer to it as the *main pattern* as it contains information about the wavefront to be reconstructed. In the reference mode, we also use the second intensity pattern, which contains information about geometry of the Hartmann mask (lenslet array) and aberrations of the relay optics. We refer to it as the *reference pattern*.

3.3.3 How to obtain a good hartmanngram

Each sub-aperture of the Hartmann mask (lenslet array) produces a light spot on the CCD or CMOS image sensor matrix; thus, the reconstruction software should deal with an intensity distribution consisting of a set of spots. For correct processing it is important to minimize the background noise and prevent saturation of spots. Although it may be possible to locate spots in presence of noise and saturation, these factors may affect the precision and repeatability of the results. Examples of a good and bad intensity patterns are

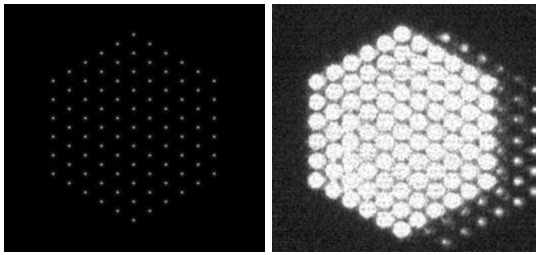

Figure 3.7: *Intensity patterns from the Shack-Hartmann sensor; a good quality one (left), one with noise and saturation (right).*

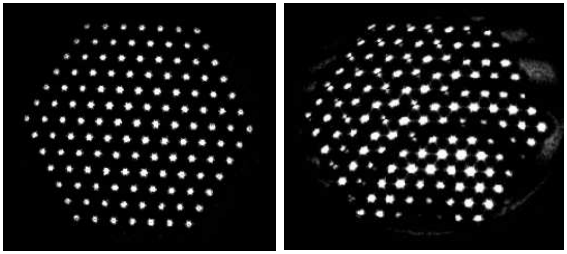

Figure 3.8: *Intensity patterns with inhomogeneous intensity; acceptable (left) and unacceptable quality (right).*

shown in Figure 3.7

It is also important to minimize the variation of intensity between the spots. This variation may be caused by the structure of the illuminating beam, interference with parasitic beams reflected from the components of the optical system, bad optical conjugation between the sensor and the object under test, birefringence of the object and too strong aberrations. Example hartmanngrams with acceptable and unacceptable intensity variation are shown in Figure 3.8.

3.3.4 How "FrontSurfer" works

At the first stage of processing, "FrontSurfer" applies a smoothing filter to the intensity pattern in order to minimize the influence of the intensity noise. Then it tries to locate centroids of the

brightest spots in the smoothed intensity distribution. Not more than a given number of spots with the intensity higher than a specified threshold value is being located. The window size of the smoothing filter, the maximum number of spots to be located and the intensity threshold (with respect to the maximum intensity) can be adjusted by the user.

Centroids of spots of the main pattern form the so-called *main grid*, and ones of the reference pattern form the *reference grid*. In the absolute measurement mode, "FrontSurfer" generates the reference grid as an ideal hexagonal or orthogonal grid with a specified pitch and dimension. "FrontSurfer" optimizes the position and rotation angle of the ideal grid to provide the closest correspondence between the nodes of the two grids.

At the next stage "FrontSurfer" calculates local tilts of the wavefront. This is implemented by finding a correspondence between coordinates of centroids of two grids – the main and reference ones – and calculating displacement of each spot due to aberrations. The minimum permitted displacement can be specified by the user. If no correspondence is found for a certain spot, or its displacement exceeds the specified limit, the spot is discarded. For calculation of the tilts, "FrontSurfer" uses the pixel dimensions and the distance between the Hartmann mask (lenslet array) and the CCD (CMOS) matrix. These parameters can be either set by the user manually or obtained by calibrating the sensor.

Wavefront reconstruction is performed based on the reference grid and the array of the corresponding local tilts. "FrontSurfer" uses *modal reconstruction*, which means that the required wavefront is represented by a series expansion over a system of linearly independent basis functions, and the coefficients of expansion are calculated in terms of this basis. The reconstructed wavefront is then defined continuously throughout the whole aperture of the sensor.

The reconstruction is divided in several stages:

1. **Calculation of the basis responses**. As the basic functions, "FrontSurfer" uses sets of tilts, which correspond to aberrations represented by Zernike polynomials. The number of Zernike terms can be adjusted by the user. As the

reconstruction error tends to grow with the number of terms over a certain limit [23], for each mask there is an optimum number of terms. For our "standard" arrays with 127 microlenses we advise using 44 Zernike terms.

2. **Orthogonalization of the basis responses**. Even for aberrations described by orthogonal Zernike polynomials, the corresponding responses of the wavefront sensor may be non-orthogonal. "FrontSurfer" uses singular value decomposition (SVD) algorithm to construct an orthogonal basis [24]. Discarding of those modes having relatively low singular values allows to make reconstruction more steady, especially if the wavefront is approximated by large number of Zernike terms. The range of "good" SVD values can be adjusted by the user. Normally, taking into account modes with singular values larger than 1/100 of the maximum one provides stable reconstruction.

3. **Decomposition** of the tilts over the orthogonalized basis using SVD algorithm; it results in a set of Zernike coefficients representing the wavefront.

4. **Calculation of the wavefront** as a superposition of Ze-nike polynomials with the coefficients found.

3.3.5 Further information

For further information, please refer to the latest version of the "FrontSurfer" manual, which is available from http://www.okotech.com.

3.4 Shop testing setups

Optical setup for testing of optical components with the Shack-Hartmann wavefront sensor should satisfy the following conditions:

- The relay optics should re-image the plane of the object to the plane of the Hartmann mask (lenslet array).

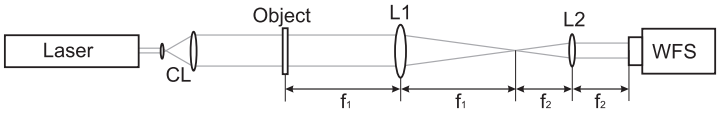

Figure 3.9: *Typical measurement scheme for testing of transparent optics with Shack-Hartmann wavefront sensor. Here CL is a collimator; L_1 and L_2 are lenses with focal distances f_1 and f_2, respectively; WFS is the wavefront sensor.*

- The scheme should scale the beam in such a way that the image of the scaled object (wavefront) is densely filled with Hartmann sub-apertures.

- The optics should allow for calibration. In the general case, it consists of separate measurement of the complete setup aberration with ideal object or a source of ideal wavefront, replacing the one to be tested.

Three typical measurement schemes are considered below.

3.4.1 Testing of transmission optics

A typical optical setup for measurement of transparent optics with Shack-Hartmann wavefront sensor is shown on Figure 3.9. The object under test should be placed in a collimated laser beam. A telescopic system consisting of two lenses, L_1 and L_2, is used to re-image the aperture of the object to the microlens array (or Hartmann mask) of the wavefront sensor. The system should scale the area to be measured to the aperture size of the wavefront sensor; the scaling factor is equal to f_1/f_2, where f_1 and f_2 are focal distances of the lenses L_1 and L_2, respectively.

Although "FrontSurfer" is able to perform "absolute" wavefront measurement without any reference pattern, it is advisable to switch to the reference mode. It allows to get rid of aberrations of the relay optics, which are always present due to imperfection of the components and misalignment in the system. Reference pattern can be measured with the object removed from the setup.

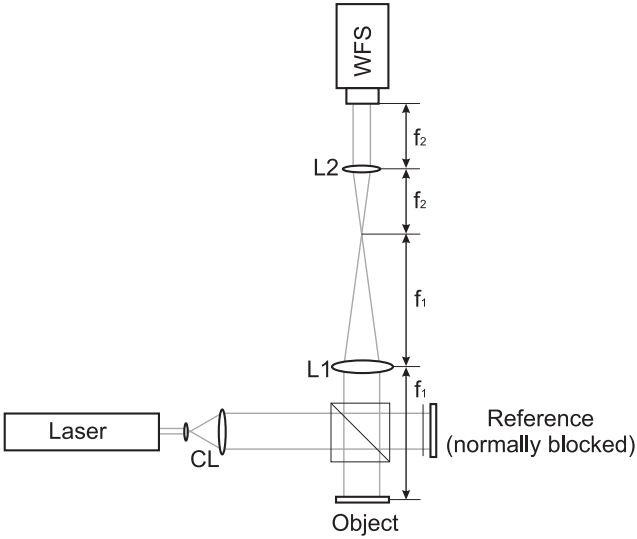

Figure 3.10: *Typical measurement scheme for testing of reflective optics with Shack-Hartmann wavefront sensor. See Figure 3.9 for notations.*

3.4.2 Testing of reflective optics

A typical optical setup for measurement of reflective optics is shown on Figure 3.10. To facilitate calibration, it is convenient to build it in a similar way to the Twyman-Green interferometer, where a beam splitter divides the incoming beam in two branches. The object is placed the in first branch behind the beam splitter, and the reference (normally a high-quality flat or spherical mirror) in the second one. The beams reflected from the object and reference are then directed to the wavefront sensor. A telescopic system similar to the one from the previous scheme (Figure 3.9) is used to provide conjugation between the object and WFS with proper scaling. One of the branches should always be blocked – the first branch for measurement of the reference pattern, and the second one for testing of the object.

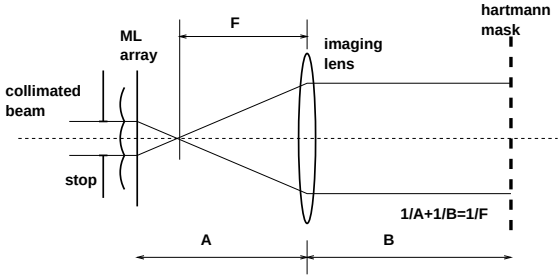

Figure 3.11: *Measurement scheme for testing of a microlens with Shack-Hartmann wavefront sensor.*

3.4.3 Testing of microlenses

An example of a relay system designed to measure the aberrations of a microlens for fiber coupling applications is shown in Figure 3.11. In this case the microlens has a small diameter (1 mm) compared to the Hartmann mask aperture (4 mm). A telescope formed by the microlens itself and the imaging lens is used to couple the microlens aperture to the sensor mask. The Hartmann mask is co-incident with the microlens image.

Calibration of the setup consists of two steps:

1. Obtaining of an ideal reference wavefront.

2. Calibration of the imaging microlens.

In the first step we ensure that the aberration of the illuminating beam is negligible over the aperture of the microlens. In the simplest case this can be achieved by illumination of the microlens with slightly divergent wavefront produced by a remote pinhole source. If there are no optical components between the pinhole and tested microlens, we can be sure the illumination wavefront is close to ideal.

In the second step, we place another pinhole in the focus of the microlens. By doing that we eliminate all aberrations of the setup, except for the aberrations introduced by the imaging lens, to be able to measure the aberration of the relay optics only.

In the last step, we remove the pinhole and measure the total aberration. To obtain the aberration of the microlens, the aberra-

tion of the imaging setup measured at step 2 should be extracted from the measurement result.

In this example we have used slightly divergent wavefront instead of collimated. This does not introduce any significant problem if the radius of curvature of the wavefront is much larger than the focal length of the microlens under test. If the lens has focal length of 4 mm and the point source is placed at 1 m from the lens, spherical aberration introduced by "wrong" illumination is negligible. Nevertheless, it is always advisable to check expected aberrations using ray-tracing code.

3.5 Optical conjugation

The input pupil of the WF sensor should be optically conjugated with the pupil of the optical system. Conjugated is achieved by placing the sensor input in the image of the pupil. If the sensor is positioned outside of the pupil image, any aberrations in the pupil will cause geometrical beam distortions in the sensor input, leading to erroneous measurement. Pupil conjugation is extremely important: wrong conjugation is the cause of numerous disappointments with WF measurement.

Usually the conjugation is achieved with an afocal telescope, formed by two positive lenses with focal lengths F_1 and F_2, respectively.

The coupling telescope reduces the transversal dimension of the light beam by a factor (F_1/F_2), and magnifies all ray angles with the same factor, thus preserving the geometrical amplitude of aberration Δ. For the input aberration represented by a parabola $\Delta(a) = a^2/2R$ where a is the radial coordinate and R is the radius of curvature, the F number FN is defined as R/A, where A is the semi-diameter of the input pupil. Expressing the F number in terms of aberration amplitude, we obtain $FN = A/(2\Delta)$. If the aperture is reduced M times by the coupling telescope, the F number of the beam is also reduced M times.

Scaling of the F number imposes serious practical restrictions on the range of optical powers that can be controlled by the sensor. The practically acceptable range of F numbers is always

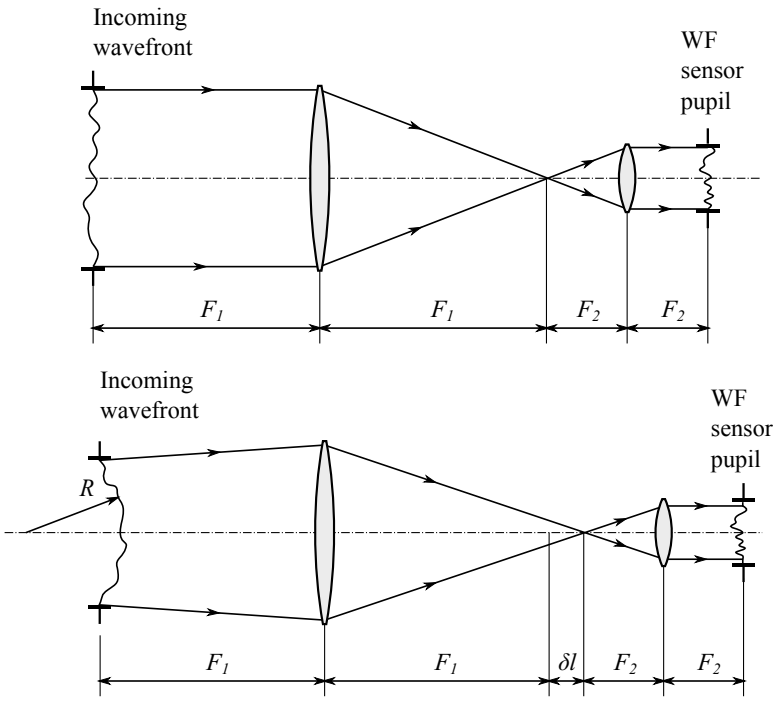

Figure 3.12: *Scaling of the WF in an afocal telescope with zero WF curvature (top), and compensation for a non-zero curvature (bottom). Here* $\delta l = \frac{F_1^2}{R}$.

limited by the complexity and aberrations of the telescope optics. While F numbers in the range between infinity and 10 are easily achievable with single lenses and achromatic doublets, the range between 10 and 3 calls for a somewhat more complicated optics and, finally, the range between 3 and 1 can be very expensive and also very difficult to correct for intrinsic aberrations.

It follows from Fig 3.12 that the F number of the wavefront at the telescope input should be considerably smaller than (FN/M) where FN is the F number of any of two lenses forming the cou-

pling telescope – assuming that both components of the telescope have equal F number – and M is the telescope magnification. Finally, both the wavefront curvature and the wavefront tilts should not exceed the specifications of the sensor at the input pupil of the sensor.

3.5.1 Compensation of the curvature

To secure the maximum measurement range for higher-order aberrations, the input of the wavefront sensor should have zero spherical term. To compensate for the sphericity of incoming wavefront, a calibrated spherical or parabolic phase shift could be added to the wavefront at the input of the telescope. This can be achieved by using a pinhole as a source of diverging spherical wave. The pinhole diameter d_p should produce light beam diverging in the diffraction angle $1/FN$. To satisfy this condition, d_p should satisfy to $d_p \sim FN \cdot 2.44\lambda$.

Also, the WF curvature in the input pupil of the sensor can be compensated by changing the distance between the lenses of the telescope, preserving the position of the input pupil in the front focus of the first lens, and keeping the point of ray convergence in the front focus of the second lens. Under these conditions, the shift of the first lens is given by $\delta l = F_1^2/R$. It is easy to see that such a compensation does not change the pupil magnification (F_1/F_2), however it can result in additional (spherical) aberration introduced into the wavefront.

The easiest practical way to achieve such a compensation consists in mounting of the wavefront sensor, together with the second lens of the telescope, on a moving stage with movement range of at least $(\pm F_1^2/R_{min})$, where R_{min} is the shortest expected radius of curvature of the input WF. In this case, to accommodate for the possible range of the input wavefront curvatures, he physical diameter of the first lens should be increased by at least $((R_{min} + F_1)/R_{min})$.

4

AO SYSTEMS

OKO Technologies not only produces components for AO systems but also provides integrated solutions based on “FrontSurfer” and “BeamTuner” software, for closed-loop control of a deformable mirror using the measurement data obtained from a (Shack-)Hartmann wavefront sensor, or from the optimization feedback.

These software packages and tools can be be integrated not only with the components produced by OKO Technologies, but also with third-party components and systems.

4.1 Design of an adaptive optical system

The optical scheme of a phase-conjugated AO system should satisfy the following conditions.

1. The optics should re-image the plane of the mirror to the plane of the Hartmann mask (or microlens array) with proper scaling. An example of such an optical conjugation scheme is shown in Figure 3.10.

2. In a similar way, optical conjugation should be provided between the DM and the source of aberrations.

3. In a similar way, optical conjugation should be provided between the system pupil, and the tip-tilt corrector, if any.

In general, phase-conjugated AO contains three planes conjugated to the pupil: the DM, the WF sensor and the tip-tilt corrector. Each conjugation requires a telescope, and each telescope introduces additional static aberration and scattering. **To reduce the number of conjugated planes, OKO fabricates MMDM15-17-tip-tilt - special deformable mirror mounted on a tip-tilt stage.**

An important remark should be done regarding the use of micromachined membrane deformable mirrors (MMDM). As the membrane can only be pulled by electrostatic forces but cannot be pushed, it should be biased to provide deformation in both directions (see Figure 2.1). It means that one will get much better results when optimizing the mirror with respect to a sphere, than when optimizing it with respect to a flat surface. This sphere should be taken into account when the mirror is incorporated into the optical setup. The optimum radius of the bias curvature can be evaluated assuming the mirror flexure to be in the middle of the range.

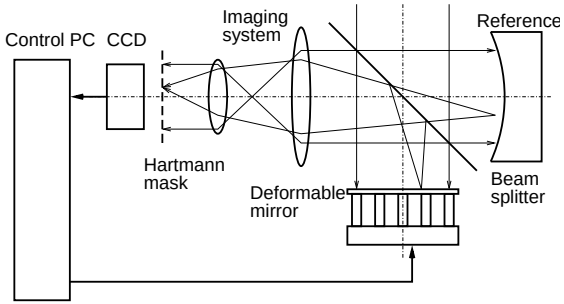

Figure 4.1: *Scheme of typical adaptive optics setup.*

The typical setup for functional feedback loop is shown in the Figure 4.1. A high-quality flat or spherical mirror can be used as a reference. A concave spherical mirror is preferable for the use with MMDM due to its biased operation, and a flat mirror for PDM systems.

4.2 “FrontSurfer” in the AO mode

Closed-loop correction mode is implemented in the version of “FrontSurfer” for deformable mirrors. Overview of the features of this version is described on page 48.

Before starting closed-loop correction with a deformable mirror (DM), the mirror should be properly configured. “FrontSurfer” supports standard OKO’s ISA, PCI, USB and ethernet interface modules for deformable mirrors. Configuration files can be supplied for standard OKO’s DM types. It is possible to integrate “FrontSurfer” with a non-OKO DM interface by developing a custom plugin according to our specification.

4.2.1 Calibration of the AO

After the mirror is coupled with the wavefront sensor, it should be calibrated.

The calibration consists in the measurement of all Shack-Hartmann sensor responses (displacements of spots) corresponding to the actions of the actuators. These responses form the *influence matrix* of the mirror; we shall denote it as **A**. Calibration should be performed after any change in the optical setup.

Before calibration, one needs to make sure that:

- **The DM is optically conjugated to the WF sensor.**
- **The pupil of the system is optically conjugated to the DM.**

The first condition is extremely important for the stability of the feedback. Bad alignment of conjugated planes causes geometrical distortions and movement of the beam on the WF sensor, resulting in an unstable behavior of the AO system. The second condition is important, as it defines the final quality of the AO correction. Conjugation between the DM and the WF sensor can be checked by introducing tilts in the mirror plane. These tilts should not cause any movement of the beam in the sensor input. In the HS response one should observe only movement of spots. If the conjugation is correct, no new spots, caused by the beam movement on the sensor input, should appear with the DM tilts.

After the pupil images are aligned and conjugated, the reference spot pattern, corresponding to the ideal performance of the AO system, should be obtained. The method of obtaining such an image depends on the AO system structure. Usually it is registered by injecting a diffraction limited reference beam into the the AO system in such a way, that all internal aberrations of the system are accounted for in the reference image. In the Fig. 4.1 it is achieved by blocking the DM arm and registering the spot pattern obtained by reflection on the reference mirror. In practice, **obtaining the reference image that takes into account all the internal aberrations of the AO system can happen to be one of the most important and cumbersome operations in the whole process of the AO system alignment and calibration.**

After calibration, the influence matrix $\mathbf{A}$ is subjected to singular value decomposition (SVD) $\mathbf{A} = \mathbf{USV}^T$ [24]. The columns of the matrix $\mathbf{U}$ make up an orthonormal set of the mirror deformations (modes), and the values of the diagonal matrix $\mathbf{S}$ represent the gains of these modes. Discarding modes with small singular values improves controllability of the system [25], however can lead to the accumulation of errors that are correctable by the mirror, but excluded from the set of SVD modes.

The "FrontSurfer" software allows to visualize the modes and singular values, and to limit the number of modes employed for the WF correction. Example singular values and SVD modes for MMDM and PDM can be found in Section 4.4.

"FrontSurfer" perform wavefront correction in a series of iterations. If the residual aberration ϕ_n at the n-th iteration corresponds to the set of actuator signals $\mathbf{X}_n$ then the actuator signals at the next step $\mathbf{X}_{n+1}$ will be given by

$$\mathbf{X}_{n+1} = \mathbf{X}_n - g\mathbf{A}^{-1}\phi_n,$$

where g is the feedback coefficient with value in the range (0..1], $\mathbf{A}^{-1}$ is the pseudo-inverse of $\mathbf{A}$ given by $\mathbf{A}^{-1} = \mathbf{VS}^{-1}\mathbf{U}^T$.

The target wavefront is defined as a combination of Zernike polynomials, and can be manually controlled during the correction using arrow keys of the computer keyboard."Left" and "Right" switch between Zernike modes while "Up" and "Down" control

the amplitude of the chosen Zernica mode. Examples of Zernike aberrations generated in this way by the MMDM and PDM, are given in Section 4.4.

4.3 Breadboard system

OKO Technologies supplies breadboard systems, which can be used as a basis for building of applied adaptive optics systems. Applications include scientific instrumentation, astronomy, ophthalmology, laser optics and optical alignment systems.

Our system includes the following components[1]:

- Deformable mirror (MMDM with up to 79 channels or PDM with up to 109 channels).
- PC interface for the deformable mirror (a set of 24-channel PCI DAC boards or 40-channel USB driver modules).
- High-voltage amplifier units for the deformable mirror.
- "FrontSurfer" WF sensor with AO loop enabled, see section 3.2 for available configurations.
- All necessary cables and documentation.
- Laptop or desktop PC (optional).

Figure 4.2: *Complete adaptive optical system with a 37-channel PDM.*

[1]The configuration can be customized according to the customer's request

OKO Technologies also offers a complete closed-loop adaptive optical system (AOS), which includes all necessary optical and mechanical components (see Figure 4.2). It can be used for real-time correction of optical aberrations and generation of precision wavefronts. The speed of control depends on the camera and computer; up to 90 frames per second is achieved with inexpensive Ueye camera and a laptop computer.

4.4 AOS test data

4.4.1 37-channel MMDM system

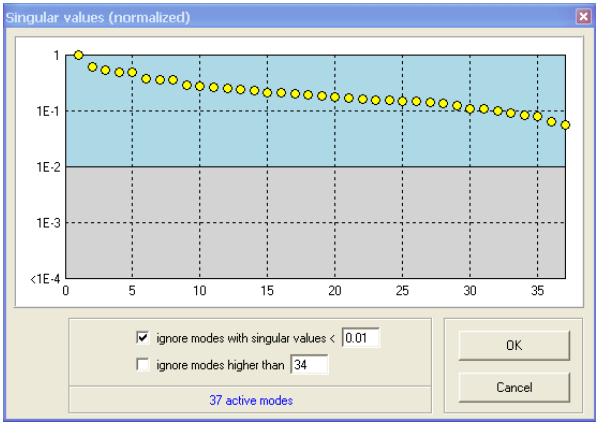

Figure 4.3: *Singular values of a 37-channel MMDM.*

Experimental singular values for a 37-channel micromachined membrane deformable mirror are given in Figure 4.3; first 20 SVD modes are shown in Figure 4.4.

Flat mirror has been used as a reference. Control started from the initial shape of the mirror, with all control voltages set to zero; this shape is shown in Figure 4.5. As the mirror can be operated only in a biased mode, a bias curvature relative to the reference was introduced by adding the Zernike term Z[2,0] with -1 μm amplitude to the target function.

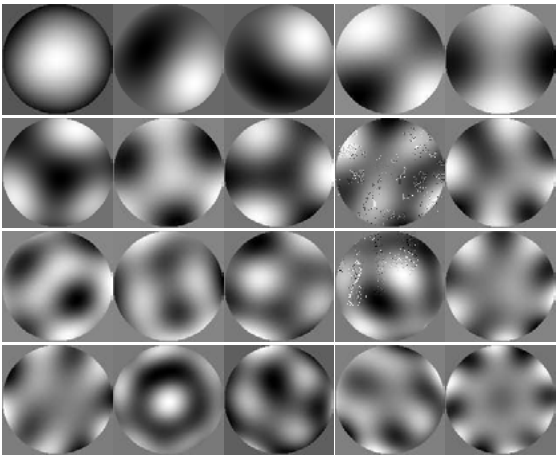

Figure 4.4: *First 20 SVD modes of a 37-channel MMDM.*

Spherical wavefront corresponding to the bias curvature was generated in the first test - see Figure 4.6. The residual aberrations are shown in Figure 4.7. In the following tests various Zernike aberrations were generated, in addition to the bias curvature; the results are shown in Figures 4.8-4.11.

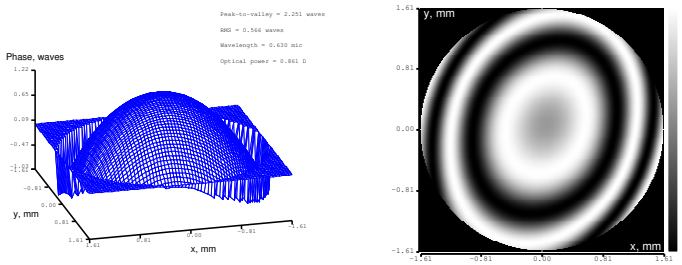

Figure 4.5: *Initial shape of a 37-channel MMDM, which was produced by setting all mirror values to 0.*

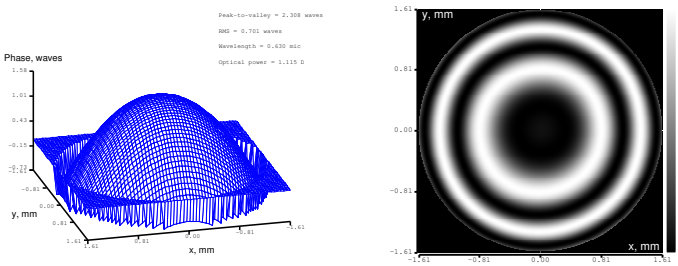

Figure 4.6: *37-channel MMDM; optimization with respect to the reference curvature (Zernike term Z[2,0]=-1 μm).*

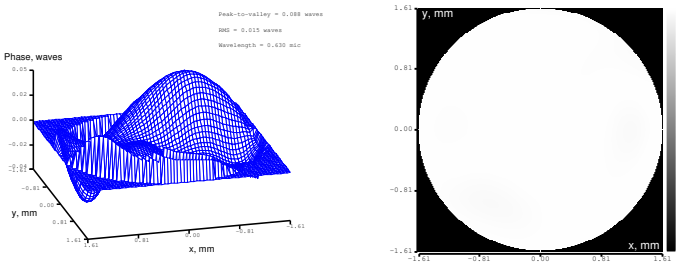

Figure 4.7: *37-channel MMDM, optimization with respect to the reference curvature (Zernike term Z[2,0]=-1 μm); residual aberrations.*

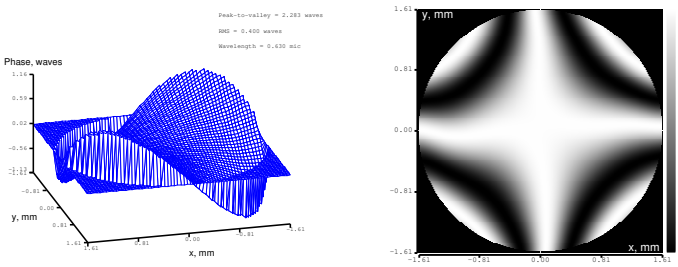

Figure 4.8: *Astigmatism generated by a 37-channel MMDM with respect to the reference curvature, Zernike term Z[2,2], amplitude 1 μm.*

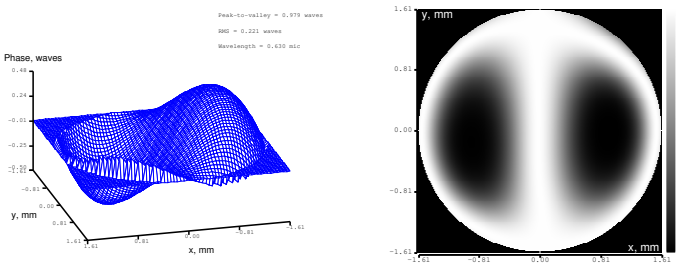

Figure 4.9: *Coma generated by a 37-channel MMDM with respect to the reference curvature, Zernike term Z[3,1], amplitude 0.5 μm.*

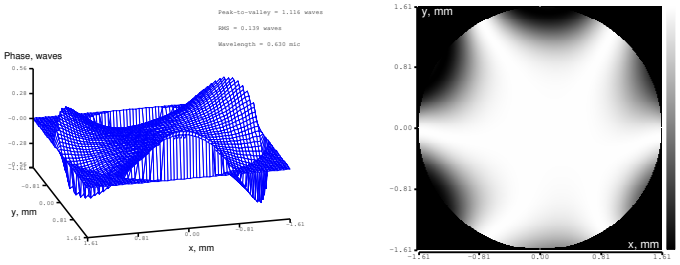

Figure 4.10: *Trifoil generated by a 37-channel MMDM with respect to the reference curvature, Zernike term Z[3,3], amplitude 0.5 μm.*

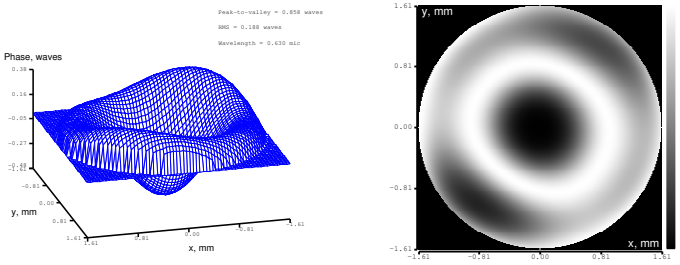

Figure 4.11: *Spherical aberration generated by a 37-channel MMDM with respect to the reference curvature, Zernike term Z[4,0], amplitude 0.3 μm.*

4.4.2 37-channel PDM system

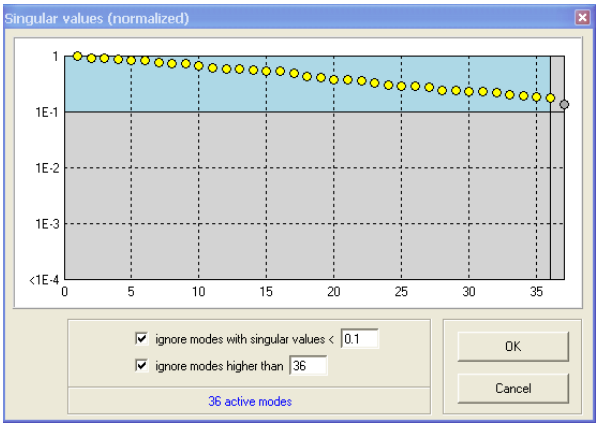

Figure 4.12: *Singular values of a 37-channel PDM.*

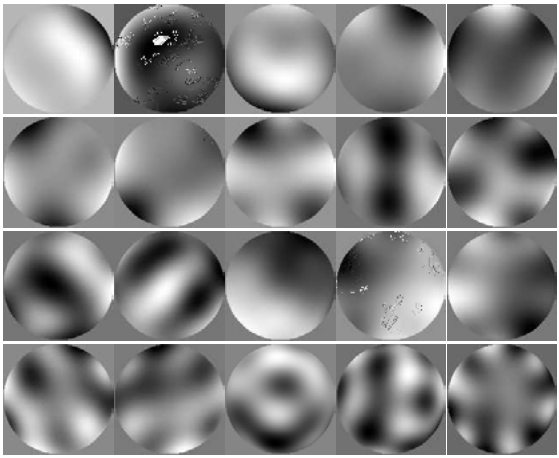

Figure 4.13: *First 20 SVD modes of a 37-channel PDM.*

Experimental singular values for a 37-channel piezoelectric deformable mirror are given in Figure 4.12; first 20 SVD modes are shown in Figure 4.13.

Flat mirror was used as a reference. Optimization started from the initial shape of the mirror, which was produced by setting all mirror values to zero; this shape is shown in Figure 4.14.

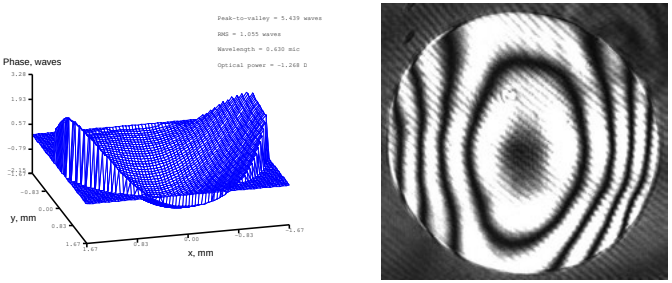

Figure 4.14: *Initial shape of a 37-channel PDM, which was produced by setting all mirror values to 0, with respect to the reference mirror.*

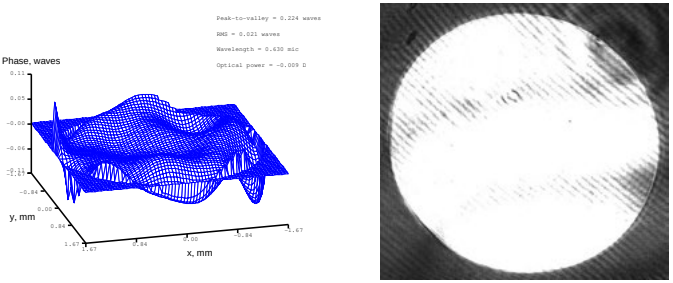

Figure 4.15: *37-channel PDM; optimization with respect to the reference mirror; residual aberrations.*

In the first test the mirror was flattened; residual aberrations are shown in Figure 4.15.

In the following tests, various Zernike aberrations were generated in addition to the bias curvature; results are presented in Figures 4.16-4.21.

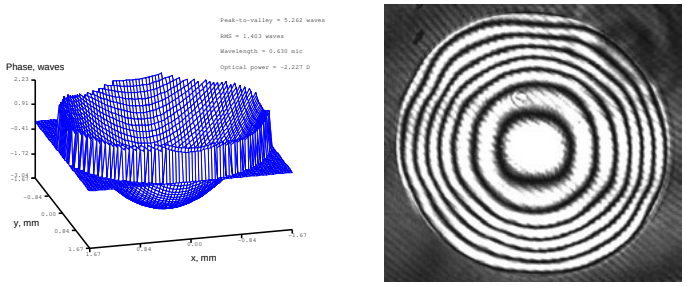

Figure 4.16: *Defocus generated by a 37-channel PDM, Zernike term Z[2,0], amplitude 2 μm.*

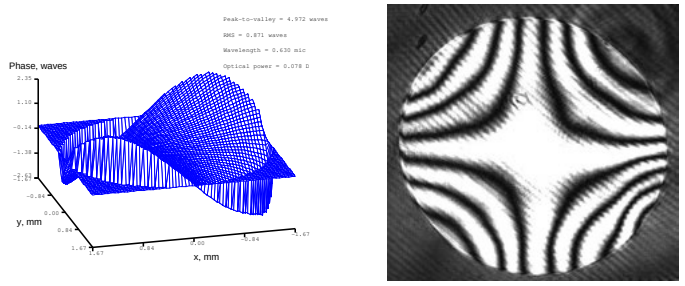

Figure 4.17: *Astigmatism generated by a 37-channel PDM, Zernike term Z[2,2], amplitude 2 μm.*

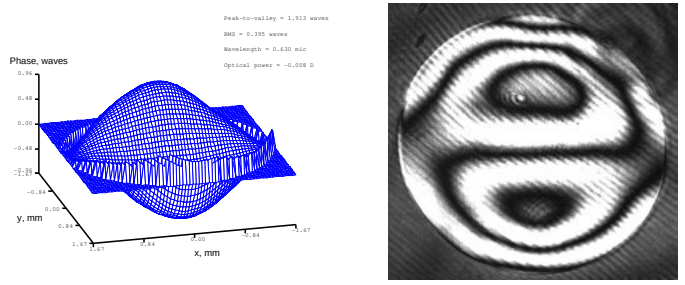

Figure 4.18: *Coma generated by a 37-channel PDM, Zernike term Z[3,1], amplitude 1 μm.*

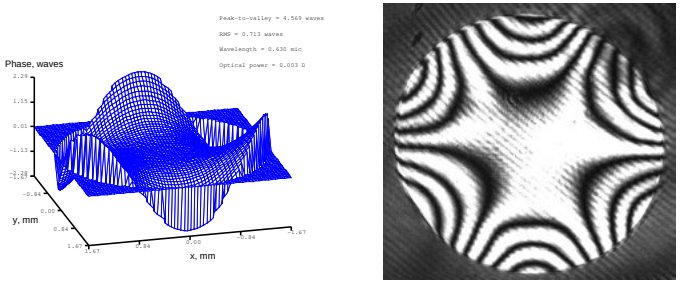

Figure 4.19: *Trifoil generated by a 37-channel PDM, Zernike term Z[3,3], amplitude 2 μm.*

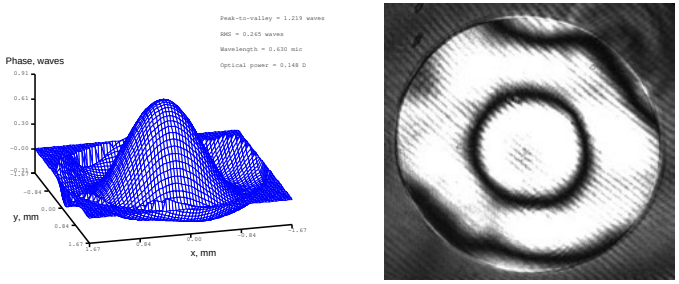

Figure 4.20: *Spherical aberration generated by a 37-channel PDM, Zernike term Z[4,0], amplitude 0.5 μm.*

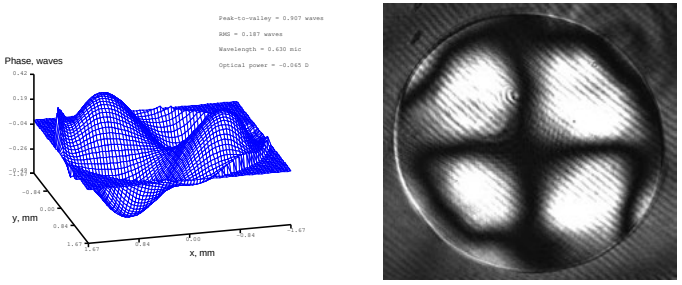

Figure 4.21: *Zernike term Z[4,2] generated by a 37-channel PDM, amplitude 0.5 μm.*

4.4.3 Optimization-based operation

The optimization of the DM figure can be used to maximize a certain quality metric, such as brightness, wavefront, focal spot shape, laser output power, fiber coupling efficiency, image sharpness, etc.

For instance, the optimization of OKO DM shape was used in [26] to manyfold increase the efficiency of harmonic generation.

OKO "BeamTuner" optimization software - see Fig. 4.22 uses CCD for registering the focal image. It can use different optimization algorithms and criteria, such as beam brightness, image sharpness, etc., for image-based feedback optimization.

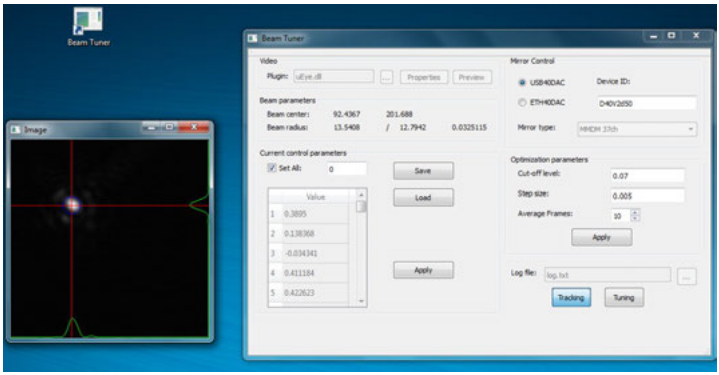

Figure 4.22: *BeamTuner software and the focal spot, resulted from the beam optimization*

4.4.4 Feedforward tip-tilt correction

Although the MMDM is not designed for scanning applications, small amount of tip and tilt can be introduced by appropriate combination of the actuator voltages. Negligible hysteresis permits for quick and precise one-step program control of the surface tip and tilt. To calibrate the MMDM for the tip tilt, we found four sets of actuator voltages, corresponding to the positions of the focused beam in four corner of a small square, in the focal plane. Then, the actuator voltages for any position of the focused beam, inside

the square, can be found by linear interpolation of the "corner" voltage sets. Scanning the beam between the image pixels was implemented with a speed of 500 pixels per second (see Fig. 4.23).

Tip-tilt correction with the MMDM membrane reduces the DM range for correction of higher-order aberrations. Therefore it is recommended to use a separate tip-tilt stage for jitter correction. **OKO produces a special 17-ch MMDM mounted on a piezoelectric tip-tilt stage, integrated in the DM package.**

Figure 4.23: *Examples of a diffraction-limited focal spot scanning, demonstrating the tip-tilt correction performance. These images were obtained by scanning 6-mm laser beam using 19-ch adaptive mirror having 1 cm clear aperture.*

4.4.5 Feedforward Zernike modes

In many applications deformable mirrors can be used as programmable wavefront correctors, without feedback. Such a control has been used in Ref. [27], to control the aberration corrector in a smart microscope, by use of a pre-calibrated lookup table.

Another important area is the correction of Zernike polynomials. Unfortunately, the influence functions of a DM are very different from the Zernike polynomials, while direct control of Zernike polynomials brings serious advantages, such as quicker convergence of optimization algorithms- see Ref. [28].

The control in terms of Zernike polynomials can be easily realized by transformation of the coordinate system in the N-dimensional space of the actuator controls:

$$C_i = \sum_{1}^{N} a_{i,j} U_j \tag{4.1}$$

where $a_{i,j}$ is the calibration matrix representing each Zernike polynomial as a combination of actuator voltages U_j. **OKO offers MiZer: a software tool for feedforward control of the**

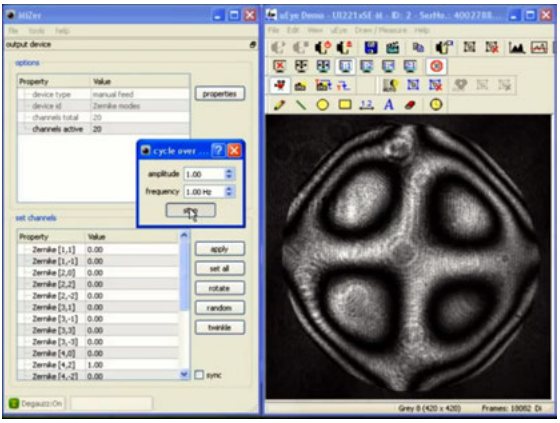

Figure 4.24: *Screen shot of MiZer: the software tool for feedforward control of the deformable mirror in terms of Zernike polynomials. The nterferogram corresponds to Z_4^2 formed with a 37-ch piezoelectric deformable mirror in a feedforward mode.*

deformable mirror in terms of Zernike polynomials – see Fig. 4.24.

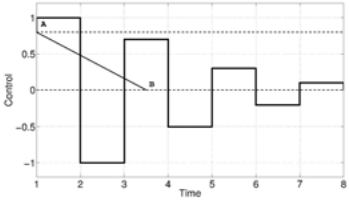

Figure 4.25: *Actuator control by fading AC voltage, "degaussing". To go from A to B, the voltage follows a more complicated pattern, represented by fading meander. We found that this control method reduces the hysteresis error by a factor of ≈5, however requires a longer time for actuator settling.*

Since the piezoelectric actuators feature up to 10% hysteresis, the precision of feedforward control is limited. The well known methods of hysteresis compensation are: the feedback (which is not applicable for an obvious reason), and pre-compensation

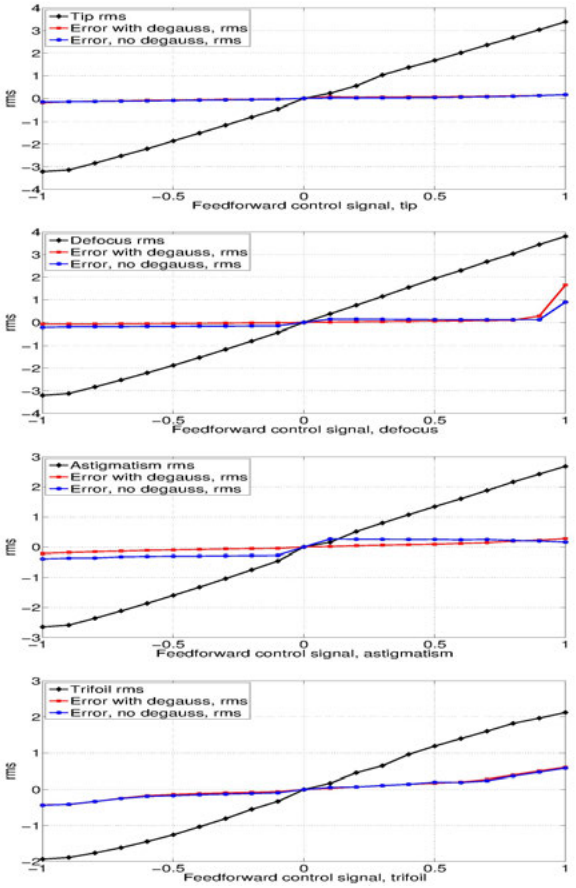

Figure 4.26: *Wavefront error in waves, $\lambda = 0.63\mu m$ as a function of aberration amplitude, for feedforward control of an optimized 18-ch piezoelectric deformable mirror. This error includes both the error due to hysteresis, and approximation error defined by the mirror geometry*

based on the calibrated hysteresis model and control history tracking [29]. However, we have chosen a simpler approach, consisting in the application of fading alternate voltage to the actuator, as

shown in Fig. 4.25. We call it "degauss" for its similarity with degaussing of magnetic objects.

We found that the precision of feedforward control of a PDM does not depend on the mirror initial position, but strongly depends on whether the "degauss" has been applied to the actuators: the *rms* wavefront error was equal to $\sim 0.3\lambda$ and P-V error equal to $\sim 1.5\lambda$ without "degauss", versus *rms* of $\sim 0.05\lambda$ and P-V of $\sim 0.2\lambda$ with "degauss". So, simple hysteresis compensation by fading AC control voltage reduces the hysteresis error by a factor of ≈ 5. Note that the error due to hysteresis is independent of the approximation error, which depends on the geometry and mechanics of the mirror.

Figure 4.26 shows the wavefront error as a function of the amplitude of low-order Zernike term, formed by a feedforward control, with and without hysteresis compensation by means of fading AC control applied at each control step.

4.5 LighPipes software package

LightPipes is a set of software tools for simulation of propagation, diffraction and interference of coherent light, based on the scalar theory of diffraction. The toolbox includes spectral, FFT-based and finite-difference based light propagation models. Special tools have been developed for the propagation through lenses with coordinate transforms, simulation of any combination of Zernike aberrations, mode analysis in laser resonators, interferometers, inverse problems, waveguides and propagation in media with non-uniform distribution of refraction index and turbulence.

The following versions of the package are available:

- In April 1999, OKO released the source code of LightPipes for Linux/Unix under GNU GPL.
- The MatLab and MathCAD versions have a number of advantages:
  - Enhanced readability of the document with text added to the commands.
  - The graphics-, animation- and other features of MathCAD can be combined with the LightPipes commands.

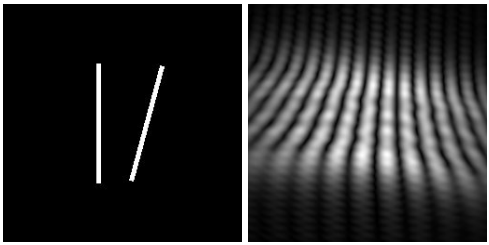

Figure 4.27: *LightPipes model of the Young interferometer with tilted slit: the slit pattern (left) and the far field interference pattern (right)*

- You can use variable arguments in the function calls and handle complex data structures in a very simple way.
- Enhanced flexibility and fast execution.

Contact oko@okotech.com for the pricing and availability of the MatLab and MathCAD versions of the software. Software manuals and examples are available at http://www.okotech.com/lightpipes.

5

IMAGING THROUGH TURBULENCE

5.1 Approach

There are numerous military, security and navigation applications for long-term surveillance. For instance, it is critically important to tell a machine gun from a paddle in the hands of a suspected pirate, while the potential danger is still far away. However, the imaging resolution is limited by the air turbulence.

It is quite common to characterize the turbulent seeing with a single parameter r_0, having the meaning of the largest aperture size that still provides near-diffraction limited imaging in the turbulent conditions. In astronomy, when observation is conducted from the surface, up through the atmosphere, the usual value of r_0 is in the range from 5 ... 50 cm. However, the horizontal imaging in a sunny day can easily result in r_0 of several mm, even for relatively short observation distances of the order of 1 km.

A typical horizontal imaging situation is illustrated in Fig. 5.1. Both the aperture and the object are usually much larger than the r_0. The light bundles from different object points go through different areas of turbulence, resulting in uncorrelated phase distortions for object points. The distortions are correlated within a small isoplanatic angle, that has the order of magnitude of r_0/L

where L. In the close vicinity to the aperture all ray bundles pass through the same turbulence and the wavefront distortions introduced in this volume can be considered isoplanatic. To complicate the situation even further, not all wavefront distortions created by the turbulence, reach the aperture. In the far field, the isoplanatic patch is not resolved by the optic, and the turbulence introduces geometric distortions and warps in the otherwise sharp image.

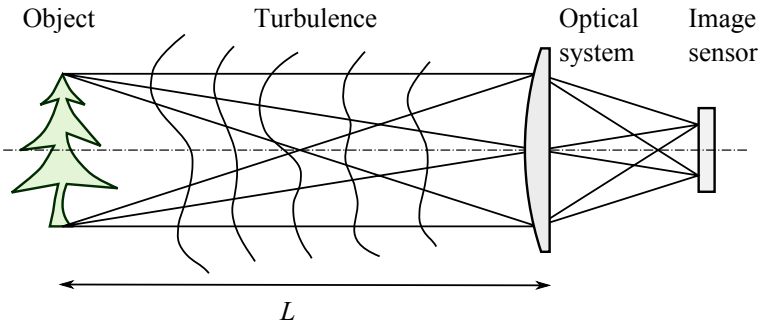

Figure 5.1: *Horizontal turbulent imaging*

Adaptive optics (AO) is the first choice technology for correction of dynamic optical aberrations. It can be directly applied to the isoplanatic aberrations, introduced in the optical system itself and in the close vicinity to the aperture, where the turbulence is still isoplanatic.

If the object size is large and the turbulence is strong, the weight of the isoplanatic correctable component will be close to negligible, and the performance of AO can be found insufficient to justify its extra complexity. The AO performance can be improved by correcting only the wavefronts emitted by a single point of the object, realizing so-called ”foveated” imaging (fovea is the small part of the human eye’s retina that provides the sharpest image). Generally speaking, foveated AO correction amplifies the aberration and fuzziness of the remaining image outside the isoplanatic patch. Further, the size of the isoplanatic patch can happen to be smaller than the resolution limit of the optical system, making the AO correction pretty useless. In theory, the problem of a wide-

field AO can be solved by a multi-conjugate (volume) corrector with the refraction index volumetric distribution conjugated to that of the atmosphere, however at the present time, the authors have no information about the existence of such a corrector. Even if it exists, control of volumetric phase represents an enormous technical problem.

Since the efficiency of the AO for wide-field correction of the atmospheric turbulence is limited, and in some cases impossible, other methods of enhanced atmospheric imaging are of a great interest. An alternative way would be based on the computer processing of a number of images, obtained through uncorrelated turbulence realizations. The effect of turbulence can be mitigated by making difference between the unchanged object and changing turbulence. To achieve uncorrelated input data, the observation should be done through different realizations of the turbulent atmosphere, by introducing delays between frames, or by splitting the pupil of the optical system, to create multiple images through different turbulent paths.

OKO extends the capabilities of adaptive optics, by introducing StillI purely software-based system for real-time image stabilization, object tracking, frame integration and multi-frame deconvolution. The software can be used in combination with adaptive optics, and as a completely standalone solution. It offers an almost real time enhanced imaging through turbulent and wavy media. The system works with live video sequences fed via DirectShow (webcam) interface, or from a CMOS or CCD camera. Standard OKO plugins are used for interface, thus a number of applicable cameras is quite large.

OKO has developed custom systems for:

- Directing and focusing of high power laser beams through horizontal turbulence.
- Precise tracking of quickly randomly moving objects in turbulent conditions.
- Imaging through turbulence, using AO, blind deconvolution and aperture multiplexing.

Fig. 5.2 illustrates the enhanced horizontal imaging over a 2-km

turbulent path in the conditions of medium turbulence. Uncorrected (left) and corrected with a combination of StillI software with OKO AO system based on FrontSurfer.

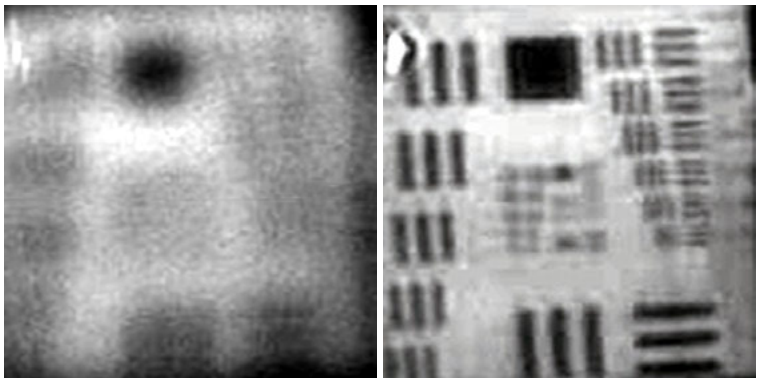

Figure 5.2: *Horizontal imaging through a 2-km path in the conditions of medium turbulence. Uncorrected (left) and corrected with a combination of OKO AO system based on FrontSurfer, with further enhancement with StillI software. Both images were registered in real time.*

5.2 StillI software package

The practical choice of the architecture of the imaging system and the processing algorithm is a function of many natural and engineering factors such as the range of turbulence strengths, observation distance, resolution, maximum aperture, number of frames, permitted temporal lag etc. We have chosen the following approach for the design of turbulent imager:

- The input pupil of the optical system follows r_0, remaining in the range $D \sim 1 \ldots 5r_0$. This range provides optimal resolution by limiting the pupil aberrations mainly to tip-tilt and some low-order aberrations.
- A number of uncorrelated frames of the object should be collected, to mitigate the turbulence effects. Either temporal or spatial multiplexing is used for obtaining of these images.

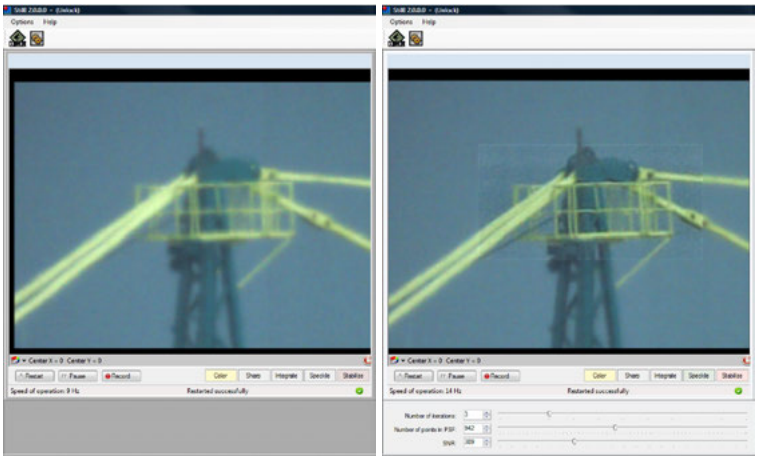

Figure 5.3: *Unprocessed (left) and processed (right) images, obtained with OKO StillI system for multiplexed imaging through turbulence. The object at 4.25 km is observed with a 13-cm F/7.6 telescope, the image is reconstructed from 10 frames registered with 100 ms temporal sampling, with total observation and processing lag not exceeding 1 s.*

- If (quasi) real-time imaging is required, spatial multiplexing by means of input pupil sampling [30] can be used, in combination with fast processing methods, such as iterative PSF resonstruction, based on convex projection [31, 32], combined with multiframe deconvolution [31].

- The problem can be considered as isoplanatic, because when we limit the aperture, we also limit not only the expected phase error in the aperture, but also the difference between any two wavefronts produced by independent sources of an extended object. Thus, for a given turbulence strength, it is always possible to find the aperture size at which the whole field is isoplanatic, simply because the aberrations are too small. However, in practice we chose apertures that are slightly bigger than this minimum, to achieve a compromise between the isoplanatic angle and the achievable resolution.

- The imaging system has fixed pixel size. This means that

in all cases when the system aperture scales with r_0, the focal length of the system should be changed too, to preserve the system F-number and the linear resolution in the image plane, while the image scale changes. A zoom-lens configuration in a temporally-multiplexed system can be used to implement this feature. Interchangeable microlens rasters with equal F-number and different pitch, can be used in the pupil image, to form multiple object images in a spatially multiplexed system.

First results obtained with the commercial realization of a quasi-real-time temporally multiplexed system "StillI", developed by us, are shown in Fig. 5.3. The images were obtained on 6 Oct 2011, with a 4.25 km observation path starting from Polakweg 10, in Rijswijk 2288GG, The Netherlands (the OKO office), with the observed object (top of a construction crane) situated near Kiekendiefstraat 25, The Hague 2496RP. The observation has been conducted during the day time, at overcast weather with relatively low ground layer heat exchange, with the wind speed ranging from 5 to 12 m/s.

The system allows to run the processing either in the whole frame, or in a chosen region of interest (foveated imaging). The proper choice of the region of interest makes the processing faster, and also increases the quality of reconstructed image, because of its better isoplanatic properties.

6

CONSULTING

Since 1997 we develop breakthrough products, create intellectual property and provide technical consulting in optical science and technology for customers world-wide.

Our experience include development of custom AO systems for education, industry, astronomy, medicine and military applications. These include adaptive microscopes, spectrographs, laser adaptive optics, compressors of femtosecond pulses, fine imaging systems, target tracking, and directed energy weapons.

Other activities include optical metrology, shop testing, imaging through atmospheric turbulence, optical systems for telescopes, microscopes and lasers, scanners, wavefront sensors, interferometry and custom optical sensors.

Key personnel:

Dr. Gleb Vdovin

received his masters degree in Optical Engineering in 1986 from the Leningrad Institute of Fine Mechanics and Optics (USSR), and his PhD in 1996 from Delft University of Technology in the Netherlands, with thesis “Adaptive mirror micromachined in silicon”. He is a founder of OKO Technologies. In 1997 he received Rudolph Kingslake Medal and Prize form SPIE. Some work published by Dr. G. Vdovin received citation index of higher than 100.

Dr. Oleg Soloviev

received his masters degree (cum laude) in Mathematics and Applied Mathematics in 1994 from Moscow State University (Russia), and his PhD in 2006 from Delft University of Technology in the Netherlands, with thesis "Methods and sensors for accurate wavefront measurements". Dr. Soloviev has more than 10 years experience in optical measurements, simulation and development of smart optical systems. From 2006, he is with Flexible Optical B.V.

Dr. Seva Patlan

received his masters degree in 1993 from Samara State University (Russia), and his PhD in 2002 from Kanazawa University (Japan) with thesis "Strain localization and fatigue of ultra-fine grained materials: acoustic emission analysis". From 2012, he is with Flexible Optical B.V. Dr. Patlan has more than twenty years of experience in building hardware and software for physical experiment automation, data acquisition and analysis.

For consulting services contact us at **oko@okotech.com**

7

DEFORMABLE MIRRORS, TECHNICAL DATA

7.1 DM model codes

The basic code for any OKO DM consists of 3 parts. The first part is either “MMDM” or “PDM”. The second part - mirror aperture in mm. The third part, separated by minus sign - the number of control channels. For example: “MMDM15-37” means membrane micromachined deformable mirror with a diameter of 15 mm and controlled by 37 actuators. PDM50-109 means piezoelectric deformable mirror with a diameter of 50 mm, controlled by 109 actuators. “PDM11x55-20-linear” corresponds to linear piezoelectric DM with 11x55 mm rectangular aperture, controlled by 20 actuators.

7.2 MMDM10-1-focus

The DM, shown in Fig. 7.1 designed for quick correction of the defocus aberration. The mirror can change its focal length from infinity to about 50 cm in less than one millisecond, allowing for changing the focus distance up to 1000 times per second. Because of very high speed, the mirror can be used for dynamic selection of focus in laser and imaging systems.

Defocus corrector is a 10 mm single-channel MMDM specially designed to correct the aberration of defocus. The mirror has better than 2 fringes P-V initial flatness over the whole aperture. The optical power of the mirror can be controlled continuously in the range of 0 . . . +2 dioptres, for Al-coated devices.

The DM capacitance is less than 200 pF and the current consumption is practically zero. These devices can be driven from a single voltage source with very high internal impedance of tens of MOhms since they consume no DC current. Driver voltage should be in a range 0 to Vmax (see Table 7.1). Available coatings: Al, gold. Available sizes: 10mm (stock). Devices with 5 mm and 15 mm aperture are available on a special order.

One channel of A4MEMS high-voltage amplifier - see section **??** can be used to drive the defocus correctors.

Table 7.1: *Technical parameters*

Parameter	Value
Focusator	
Aperture shape	approximately circular
Mirror coating	Al
Aperture dimensions	10 mm diameter
Control voltages V_c	0 . . . 192 V
Initial RMS deviation from plane	less than 0.1 μm
Frequency range	0 . . . 1kHz
Deflection of the mirror center at 192	9.4 μm

See Table 7.1 for the typical technical parameters of the focusator.

Small surface defects are possible. They do not influence the quality of the mirror.

Figure 7.1: *Typical view of single-channel micromachined deformable mirrors (aka defocus corrector or focusator)*

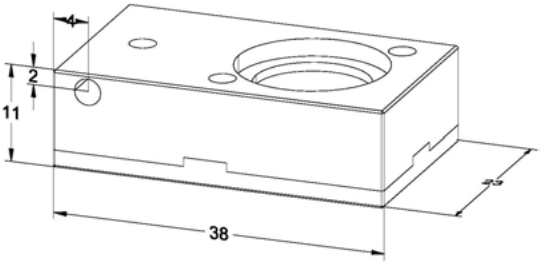

Figure 7.2: *Dimensions of the packaged defocus corrector, in mm*

Never apply voltage greater than Vmax to focusators. This will damage the membrane. To ensure the safe operation of the focusators, you can trim the maximum output voltage of A4MEMS by limiting the voltage of its power supply (e.g., set power supply to 13 V to trim the maximum output voltage to 300 V). The A4MEMS shipped with the focusator has been tuned already to the maximum safe voltage.

7.3 OKO MMDM15-37

15 mm 37-channel MMDM was introduced in 1997 and has been the most popular deformable mirror ever made.

The mirror, shown in Fig. 7.4, consists of a silicon chip mounted over a PCB holder. The chip contains silicon nitride (composite) membrane, which is coated to form a mirror. The PCB contains the control electrode structure, spacer and connector. It also serves as the mirror package. The shape of the reflective membrane is controlled by voltages applied to the control electrodes with the membrane grounded.

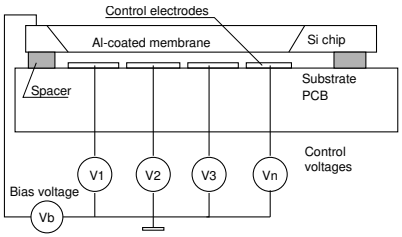

Figure 7.3: *Schematic section of the micromachined adaptive mirror.*

Figure 7.4: *Typical view of a 37-channel micromachined deformable mirror with and without package. Please note that these mirrors can be fabricated with different package designs, so the mirror you have may look differently.*

The device can be used for fast dynamic correction of low-order

optical aberrations such as defocus, astigmatism, coma, etc. in lasers, telescopes, ophthalmic devices, displays and imaging optics.

The scheme of the assembled mirror and the principle of control are illustrated in Fig. 7.3

Technical data

Table 7.2: *Technical parameters of 15mm 37-channel MMD mirror.*

Parameter	Value
Aperture shape	approximately circular
Mirror coating	Metal or Metal + dielectric
Aperture dimensions	15mm diameter
Number of electrodes	37 (19) (see Fig. 7.6)
Control voltages V_c	0 . . . 150 to 300 V, dependent on the mirror
Initial RMS deviation from plane	less than 0.45 μm
Main initial aberration	1.5 fringes at 630nm
Maximum deflection of the mirror center	10 μm
Package dimensions	see Fig. 7.7
Weight	140 g

See Table 7.2 for typical technical parameters of the mirror.

Small surface defects are possible. They do not influence the quality of the mirror.

Optical quality

Typical interferograms of the mirror are shown in Fig. 7.5.

Actuator structure

The membrane is mounted over the printed actuator structure shown in Fig. 7.6. The center-to-center distance between actuators is 1.8mm. The whole actuator structure is located within 12mm circle under the mirror membrane.

The first (close to the mirror) cable connector controls central 19 actuators of the hexagonal structure and provides connection to the ground. The second connector controls 18 peripheral electrodes (two pins are not connected). In principle the mirror can

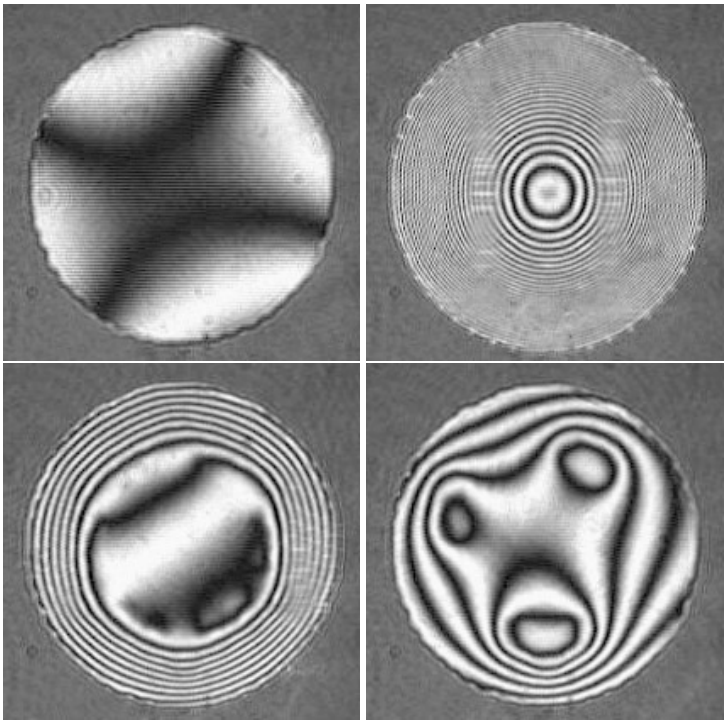

Figure 7.5: *Test of the mirror: zero voltage applied, control signal +1 applied to all actuators, control signal +1 applied to actuators 20 to 37, non-zero bytes applied to some actuators (left to right)*

be used with only one control board (19-channel variant) - ground the actuators 20...37 for reliable mirror operation.

19 amplifiers of the driver board connected to the first connector are used to drive the mirror actuators. The membrane is grounded (right jumper on the driver board in the upper position, no left jumper). The membrane can be connected to the amplifier number 20 (bias) by setting both jumpers on the amplifier board to the lower position - **this is not recommended**.

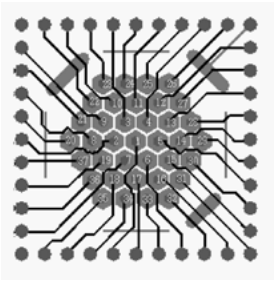

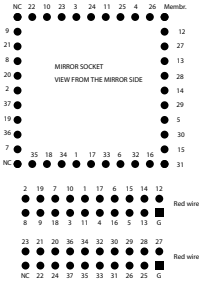

Figure 7.6: *The PCB actuator structure and the pinout (actuator numbers) of PGA connector, shown from the top (mirror surface) view. The cables should be connected from the back side with red-colored wire oriented to the "Ground" pin. See "Red wire" mark in the figure.*

Specific remarks

When operated with 19 channels, use shorting link for the second connector to prevent charging of floating electrodes.

See also general remarks on page 144.

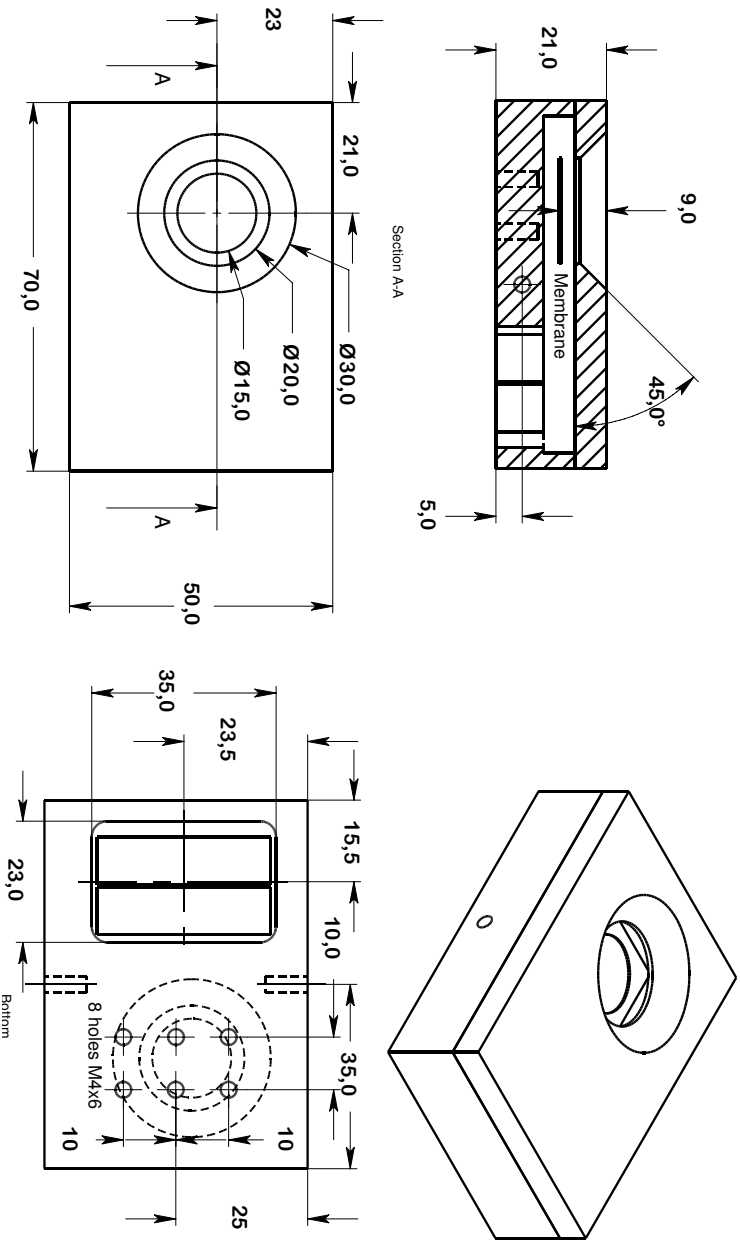

Figure 7.7: *Technical drawing of the package and mounting holes of the 15mm 37-channel MMDM*

7.4 MMDM15-17-TT

This DM is very special. It contains piezoelectric tip-tilt stage for the compensation of jitter. The DM is mounted on independent tip-tilt stage, integrated into the mirror package.

The mirror, shown in Fig. 7.8, consists of a silicon chip mounted over a PCB holder. The chip contains silicon nitride (composite) membrane, which is coated to form a mirror. The PCB contains the control electrode structure, spacer, connector, and a tip-tilt stage. The shape of the reflective membrane is controlled by voltages applied to the control electrodes with the membrane grounded. The tip-tilt stage is controlled by the voltages applied to two piezoelectrical actuators.

The device can be used for fast dynamic correction of low-order optical aberrations such as defocus, astigmatism, coma, etc in lasers, telescopes, ophthalmology, displays and general imaging optics.

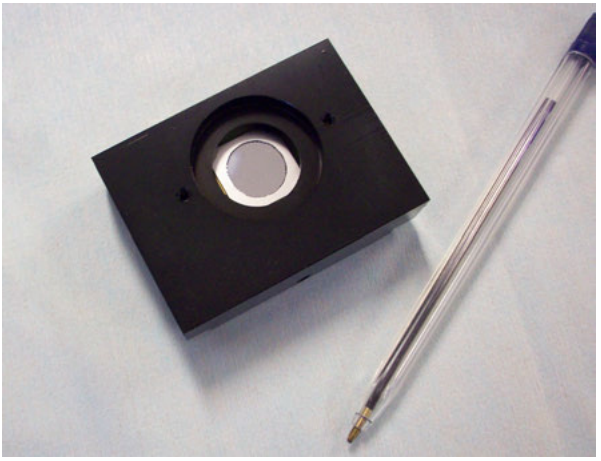

Figure 7.8: *Typical view of a 17-channel micromachined deformable mirror with the built-in tip-tilt stage. Please note that these mirrors can be fabricated with different package designs, so the mirror you have may look differently.*

Technical data

Table 7.3: *Technical parameters of the mirror.*

Parameter	Value
Aperture shape	approximately circular
Mirror coating	Metal or Metal + dielectric
Aperture dimensions	15mm diameter
Number of electrodes	17 (see Fig. 7.10)
Control voltages V_c	0 . . . 150 to 300 V, dependent on the mirror
Initial RMS deviation from plane	less than 0.45 μm
Main initial aberration	1.5 fringe at 630nm
Maximum deflection of the mirror center	10 μm
Tip/Tilt range	+/- 2 mrad in reflected beam

See Table 7.3 for typical technical parameters of the mirror.

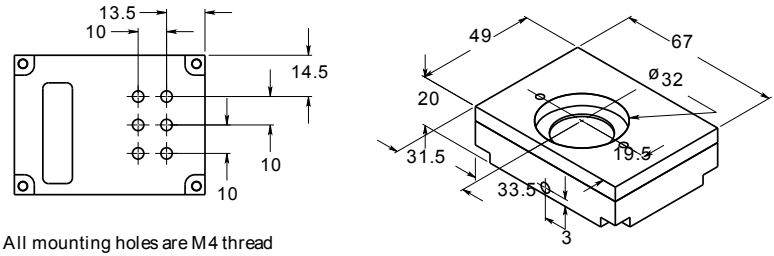

Figure 7.9: *Technical drawing of the package and mounting holes of the 15mm 37-channel MMDM*

Small surface defects are possible. They do not influence the quality of the mirror.

Actuator structure

The membrane is mounted over the printed actuator structure shown in Fig. 7.10. The actuator are arranged into three circles with radii $1.81902, 4.06745,$ and 7.5 mm.

19 amplifiers of the driver board connected to the first connector are used to drive the mirror actuators. The membrane is grounded (check the bottom of the HV unit for configuration or the HV board jumper description).

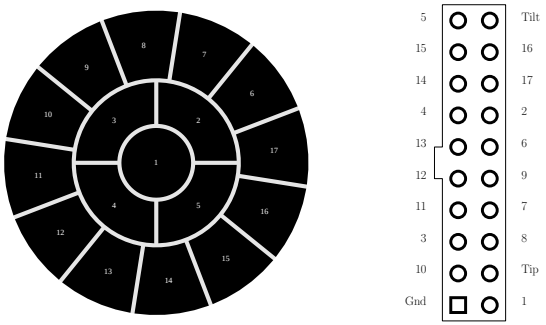

Figure 7.10: *The PCB actuator structure and the pinout (actuator numbers) of its connector, shown from the top (mirror surface) view. The cables should be connected from the back side with red-colored wire oriented to the "Ground" pin.*

Optical quality

The interferograms of the mirror obtained before shipping are shown in Fig. 7.11.

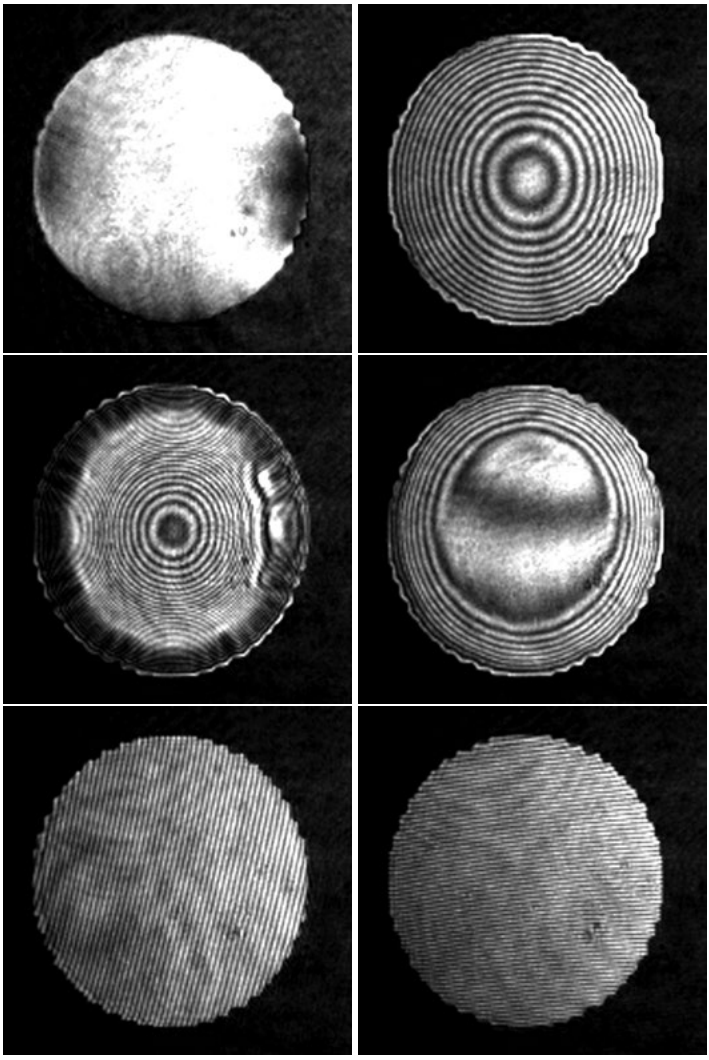

Figure 7.11: *Test of the mirror: zero voltage (control signal* -1*) applied, control signal* 0 *applied to all actuators, control signal* $+1$ *applied to all actuators, control signal* $+1$ *applied to external ring of actuators, control signal* $+1$ *applied to tip and tilt actuators (left to right, top to bottom)*

7.5 MMDM30-39/59/79

The mirror, shown in Fig. 7.12, consists of a silicon chip mounted over concentric electrostatic electrode structure. The chip contains multilayer silicon nitride membrane, which is coated to form the mirror. The PCB contains the control electrode structure, spacer and connectors. The initial shape of the reflective membrane can be adjusted using 8 adjustment micrometric screws on the back side of the mirror mount.

The device can be used for fast dynamic correction of low-order optical aberrations such as defocus, astigmatism, coma, etc. in lasers, telescopes, ophthalmic devices, displays and imaging optics.ed for fast dynamic correction of optical aberrations.

The scheme of the assembled mirror and the principle of biased control are illustrated in Fig. 7.3 on page 98

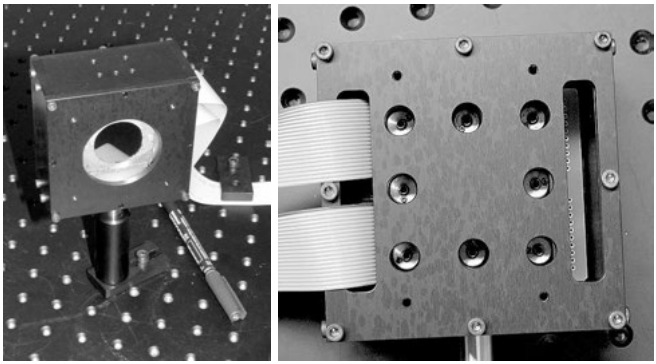

Figure 7.12: *Front and back view of the mirror.*

Technical data

See Table 7.4 for typical technical parameters of the mirror.

A number of surface and coating defects with total area not exceeding 2mm^2 can be present on the mirror surface. These defects do not influence the quality of the mirror.

Table 7.4: *Technical parameters of 30mm 39/59-channel MMD mirror.*

Parameter	Value
Aperture shape	approximately circular
Aperture dimensions	30mm diameter
Number of electrodes	39/59/79 (see Fig. 7.13-7.14)
Control voltages V_c	0 ... 150 to 300 V, dependent on the mirror
Initial RMS deviation from reference sphere	less than 0.9μm
Main initial aberration	astigmatism
Maximum deflection of the mirror center	9μm
Surface defects	up to 2 coating defects
Package dimensions	see Fig. 7.15
Weight	$\approx$500 g

Actuator structure

The membrane is mounted over the printed actuator structure (20mm in diameter for 39ch mirror and 30mm in diameter for 59- and 79-channel mirror) shown in Fig. 7.13.

Optical quality

The mirror was tested interferometrically before shipping. The interferometric patterns are shown in Fig. 7.16.

Specific remarks

See also general remarks on page 144.

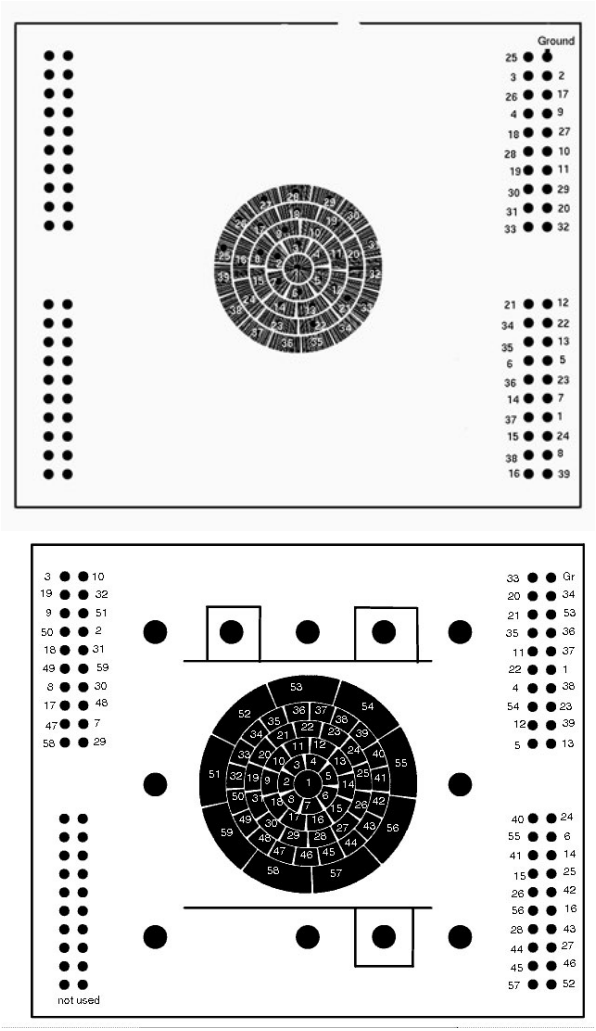

Figure 7.13: *The PCB actuator structure and pinout of MMDM30-39 and MMDM30-39, top (mirror surface) view.*

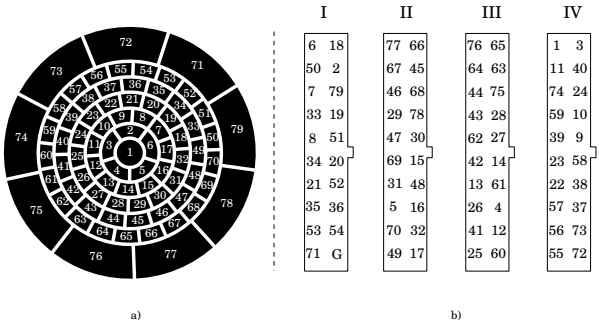

Figure 7.14: *a) The geometry and pinout of MMDM30-79 actuators.*

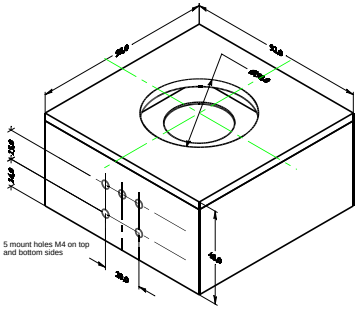

Figure 7.15: *Technical drawing of the package and mounting holes of the 30mm 39/59/79-channel MMDM*

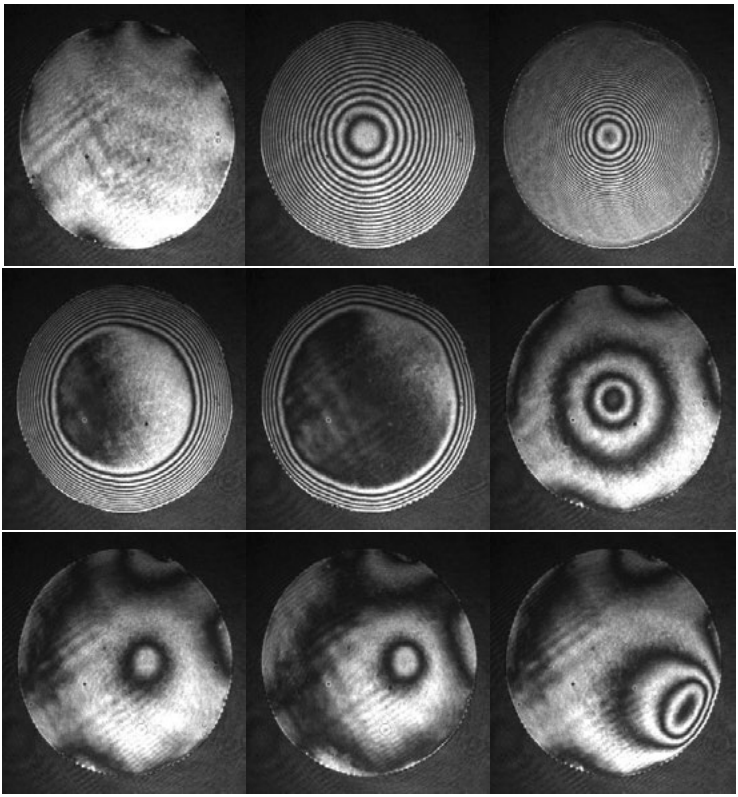

Figure 7.16: *The initial optical figure of the MMDM30-59, response to control signal 0 applied to all actuators, control signal +1 applied to all actuators and to edge alignment actuators, to the external rings of actuators and to some single actuators. Maximum deflection of the order of 40 fringes with all actuators at maximum voltage. Interferograms recorded at 633 nm wavelength.*

7.6 MMDM40-59/79

The mirror consists of a silicon chip mounted over concentric electrostatic electrode structure. The chip contains multilayer silicon nitride membrane, which is coated with a special coating to form the mirror. The PCB contains the control electrode structure, spacer and connector. The initial shape of the reflective membrane can be adjusted using 8 adjustment micrometric screws on the back side of the mirror mount.

The device can be used for fast dynamic correction of optical aberrations.

The scheme of the assembled mirror is illustrated in Fig. 7.3 on page 98.

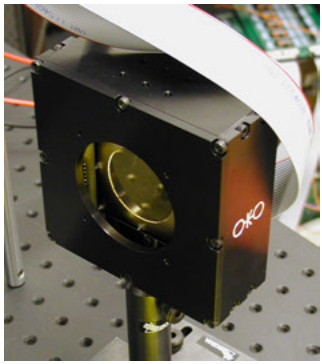

Figure 7.17: *Front view of the MMDM40.*

Technical data

See Table 7.5 for typical technical parameters of the mirror.

Small surface defects are possible. They do not influence the quality of the mirror.

Optical quality

Typical interferometric patterns of the mirror are shown in Fig. 7.19.

Table 7.5: *Technical parameters of 40mm 59 / 79-channel MMD mirror.*

Parameter	Value
Aperture shape	approximately circular
Aperture dimensions	40mm diameter
Number of electrodes	59 or 79 (see Fig. 7.20)
Control voltages V_c	0 . . . 150 to 300 V, dependent on the mirror
Initial RMS deviation from reference sphere	less than 0.9μm
Main initial aberration	coma
Maximum deflection of the mirror center	15μm
Reflectivity	better than 89% in visible
Surface defects	up to 2 coating defects
Package dimensions	see Fig. 7.18
Weight	≈600 g

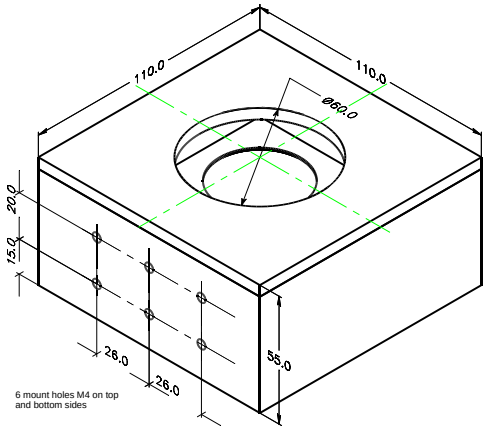

Figure 7.18: *Technical drawing of the package and mounting holes of the 40mm 59 / 79-channel MMDM*

Actuator structure

The printed actuator structure (40 mm in diameter for the59ch mirror) is shown in Fig. 7.20.

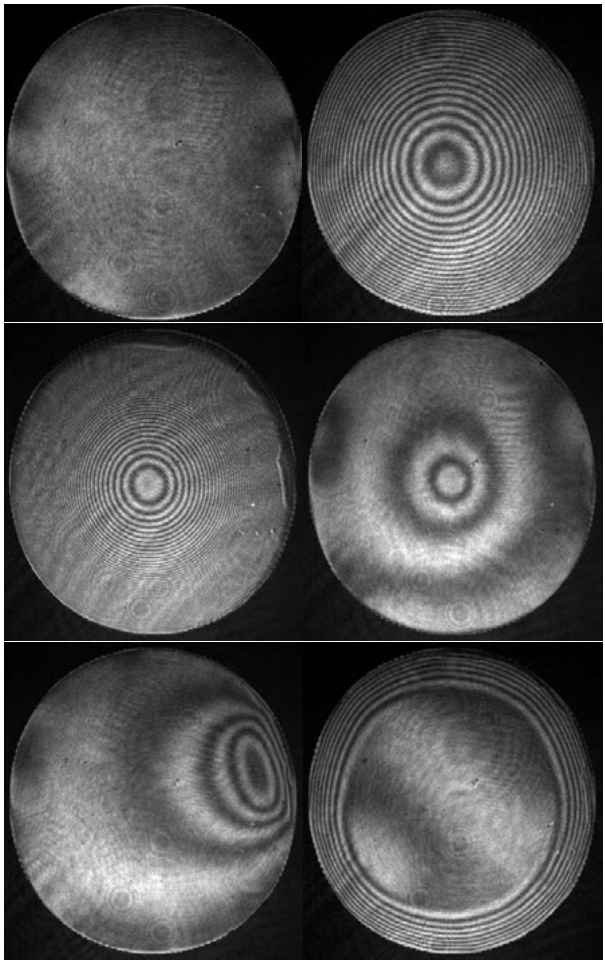

Figure 7.19: *The initial optical figure of the MMDM40-59, bias voltage (control signal 0) applied to all actuators (top), response to control signal +1 applied to all actuators, control signal +1 applied to the central actuator (middle), to a single external actuator,to the external rings of actuators (bottom). Maximum deflection is 45 fringes with control signal +1 applied to all actuators* ($\lambda = 633$ *nm).*

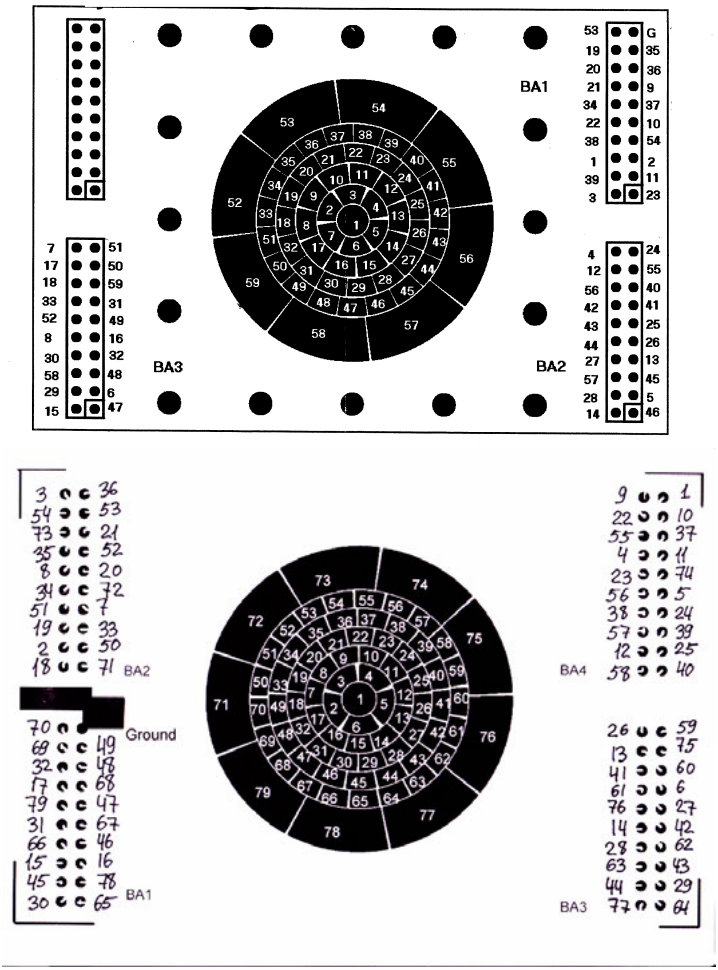

Figure 7.20: *The PCB actuator structure and pinout for MMDM40-59 and MMDM40-79, top (mirror surface) view.*

7.7 MMDM50-79

The mirror consists of a silicon chip mounted over concentric electrostatic electrode structure. The chip contains multilayer membrane, coated to form the mirror. The PCB contains the control electrode structure, spacer and connector. The initial shape of the reflective membrane can be adjusted using 8 adjustment micrometric screws on the back side of the mirror mount.

The device can be used for fast dynamic correction of optical aberrations.

The scheme of the assembled mirror is illustrated in Fig. 7.3 on page 98.

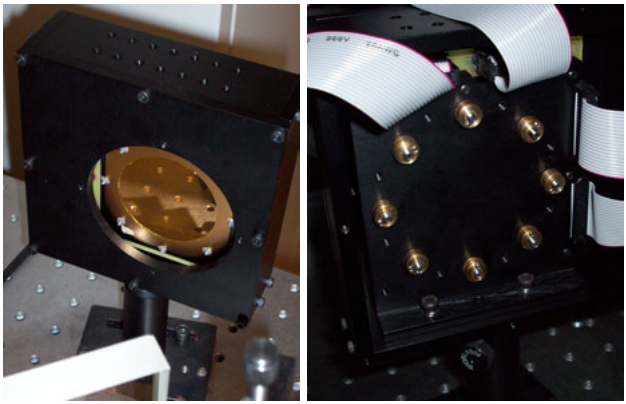

Figure 7.21: *Front and back view of the mirror. The 50-mm mirror does not have any adjustment holes in the back cover. The cover should be removed for mirror alignment.*

Technical data

See Table 7.6 for typical technical parameters of the mirror. For the mounting and package dimensions, contact us.

Optical quality

Typical interferometric patterns of the mirror are shown in Fig. 7.23.

Table 7.6: *Technical parameters of 50mm 79-channel MMD mirror.*

Parameter	Value
Aperture shape	approximately circular
Aperture dimensions	50mm diameter
Number of electrodes	79 (see Fig. 7.22)
Control voltages V_c	0 . . . 150 to 300 V, (depends on the DM alignment and range)
Initial RMS deviation from reference sphere	less than 0.9μm
Main initial aberration	coma
Maximum deflection of the mirror center	15. . . 30 μm
Reflectivity	better than 89% in visible
Surface defects	up to 2 coating defects
Weight	≈650 g

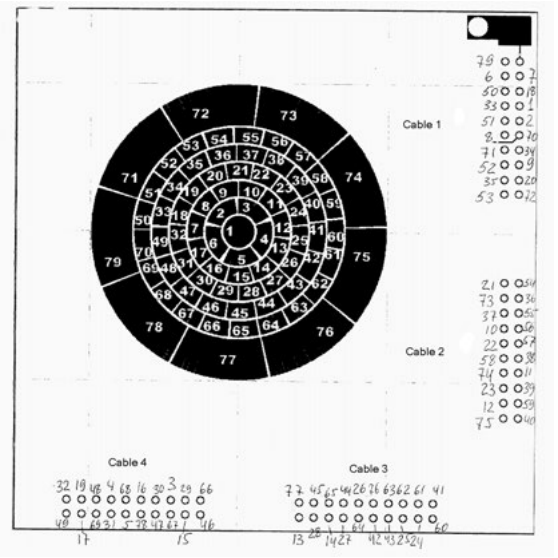

Figure 7.22: *The PCB actuator structure and pinout for79-channel MMDMs, top (mirror surface) view.*

Actuator structure

The membrane is mounted over the printed actuator structure (40mm in diameter for a 79ch mirror) shown in Fig. 7.22.

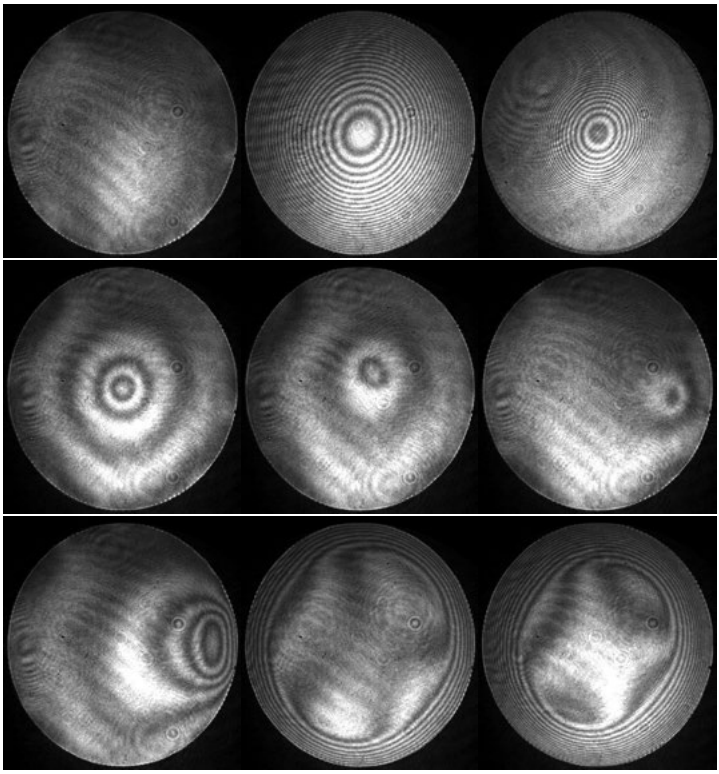

Figure 7.23: *The initial optical figure of the MMDM50-79, bias voltage (control signal 0) applied to all actuators, response to control signal +1 applied to all actuators (top row), control signal +1 applied to the central actuator, to some single actuators, to the external rings of actuators. Maximum deflection is 40 fringes with control signal +1 applied to all actuators* ($\lambda = 633$ *nm).*

7.8 MMDM11x39-19/38 linear

Silicon micromachined mirrors are fabricated by OKO Technologies using the technology of silicon bulk micromachining.

In the temporal domain, the device can be used to control the duration and the temporal shape of ultrafast pulses in femtosecond lasers and amplifiers. In the spatial domain, the device can be used as a normal deformable mirror to control the phase of extended in one dimension laser beams.

The mirror, shown in Fig. 7.24, consists of a silicon chip mounted over a PCB holder. The chip contains thin micromachined membrane, which is coated to form the mirror. The chip is mounted over 6 micrometric (see Fig. 7.24(b)) screws to adjust the mirror figure and the mirror-to-actuator distance.

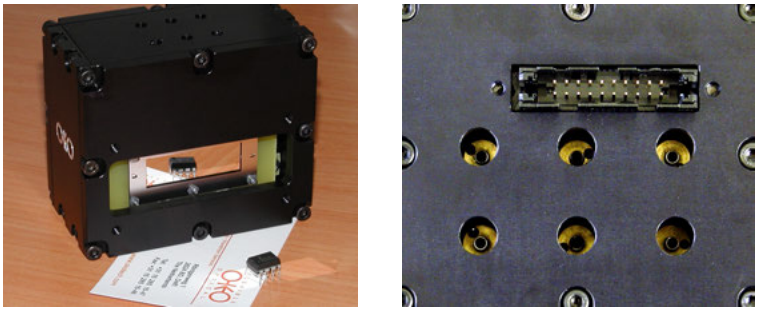

(a) **(b)**

Figure 7.24: *(a) Typical view of a linear 19-channel micromachined deformable mirror and (b) adjustment micrometric screws on the back side of the mirror. Please note that these mirrors can be fabricated with different package designs, so the mirror you have may look differently.*

The printed circuit board substrate contains the control electrode structure and connectors. It also serves as the mirror package.

The scheme of the assembled mirror and the principle of biased control are illustrated in Fig. 7.3 on page 98

Technical data

Table 7.7: *Technical parameters of 19 / 38 linear MMD mirror.*

Parameter	Value
Aperture shape	rectangle 11x39mm
Number of electrodes	19 or 38
Control voltages V_c	0 . . . 150 to 300 V, dependent on the mirror
Mirror coating	Metal or Metal + dielectric
Initial RMS deviation from plane/cylinder	less than 1μm
from plane/cylinder	
Main initial aberration	defocus/cylinder/adjustable
Maximum deflection of the mirror center	10μm (30 fringes)
Maximum optical load	not available
Package dimensions	see Fig. 7.25
Weight	≈500 g

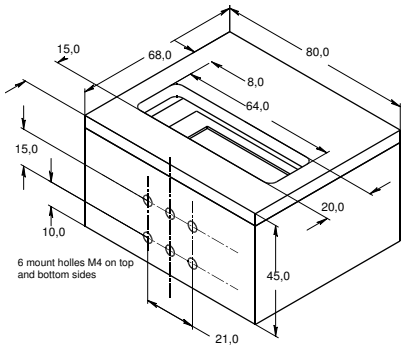

Figure 7.25: *Technical drawing of the package and mounting holes of the linear MMDM*

See Table 7.7 for technical parameters of the mirror before shipping.

Small surface defects are possible. They do not influence the quality of the mirror.

Actuator structure

The membrane is mounted over the printed actuator structure. On Fig. 7.26 addresses, with reference to the base address of PCI

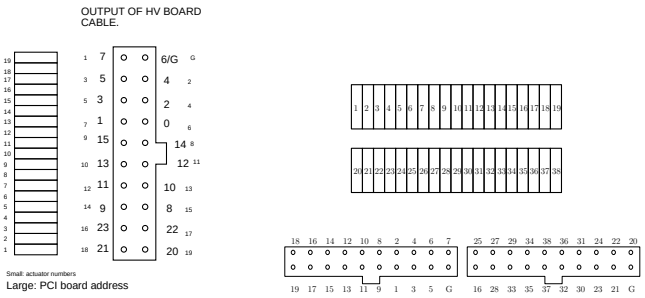

Figure 7.26: *Actuator connections for (a) 19- and (b) 38-ch mirrors.*

board are shown in large font, corresponding actuator numbers - in small font. The array of actuator addresses from one side of the 19-ch mirror to another – see Fig. 7.26(a):

```
7 4 5 2 3 0 1 14 15 13 12 11 10 9 8 23 22 21 20
```

In the case of a 38-ch mirror the actuators have the following addresses – see Fig. 7.26(b):

```
top row:    20 21 22 23 8 9 10 11 12 13 14 15 7 5 4 3 2 1 0

bottom row: 13 12 15 10 11 8 14 1 0 9 22 23 20 21 3 2 5 4 7
```

Optical quality

Typical interferometric patterns of the mirror are shown in Fig. 7.27.

Specific remarks

See also general remarks on page 144.

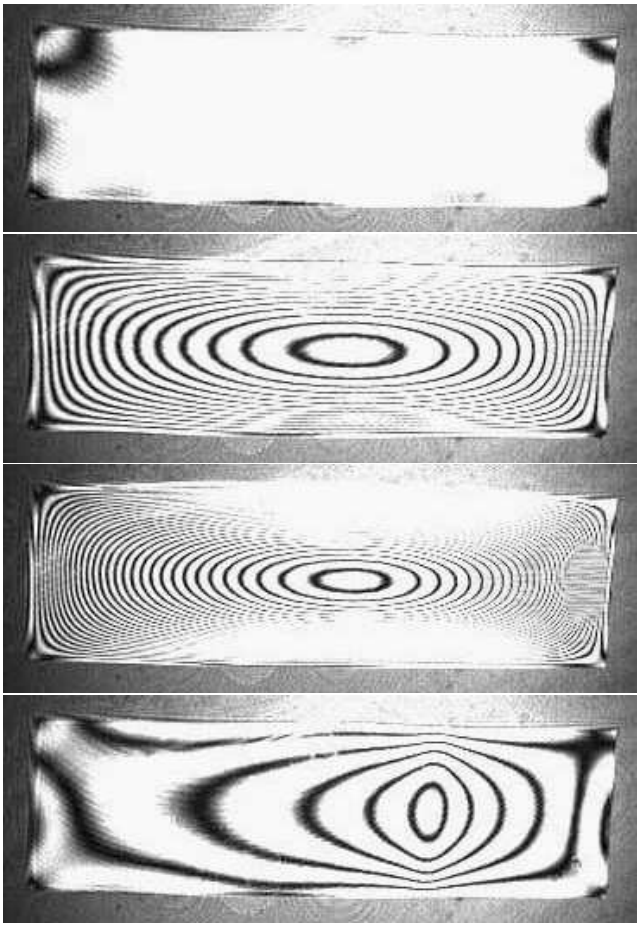

Figure 7.27: *The response to control byte 0, 180, 255 applied to all electrodes and 255 to a single electrode (left to right, top to bottom).*

7.9 PDM30-19

The mirror, shown in Fig. 7.28, consists of 19 piezoelectric column actuators bonded to the base holder. Reflective plate is bonded to the top of the actuator structure and coated to form the mirror. The shape of the faceplate is controlled by the voltages applied to the actuators.

The device can be used for fast dynamic correction of low-order optical aberrations such as defocus, astigmatism, coma, etc, in lasers, telescopes, ophthalmology, displays and general imaging optics.

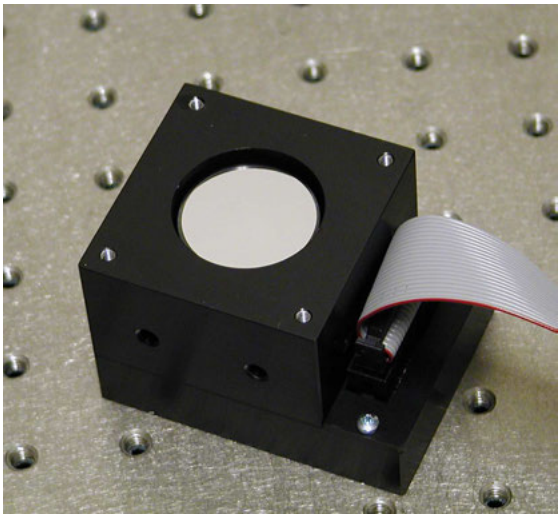

Figure 7.28: *Typical view of a 19-ch piezoelectric deformable mirror. Please note that these mirrors can be fabricated with different package designs, so the mirror you have may look differently.*

Technical data

See Table 7.9 for typical technical parameters of the mirror.

The mirror can be supplied with initially slightly curved spherical surface. This sphericity is caused by the stress in the mirror coating. It does not influence the parameters of the mirror, but

Table 7.8: *Technical parameters of 30mm 19-channel PD mirror.*

Parameter	Value
Aperture shape	circular 30 mm in diameter
Mirror coating	Metal or Metal + dielectric
Actuator voltages	$0 \ldots + 300$V (with respect to the ground electrode)
Number of electrodes	19 (see Fig. 7.30)
Actuator capacitance C_a	5 nF
Main initial aberration	sphere
Initial RMS deviation from reference sphere	less than 1μm
Maximum stroke	8μm at $+400V$
Actuator pitch	7 mm
Package dimensions	see Fig. 7.29
Weight	320 g

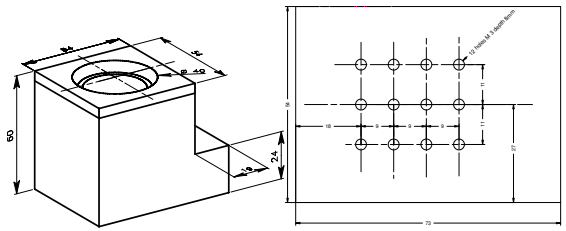

Figure 7.29: *Technical drawing of the package and mounting holes of the 30mm 19-channel PDM*

should be taken into account when the mirror is incorporated into the optical setup.

Due to hysteresis of actuators, the initial aberration may change during the mirror usage and deviate more from the reference sphere. This deviation is a superposition of actuator response functions and is irrelevant in active setups with closed-loop control, though it may slightly reduce the correction range.

The PDM can be also fabricated with design optimized for low-order pritthrough - free operation. In this case 18 actuators are positioned in two rings for edge actuation, and one optional actuator is positioned in the center. 18-actuator design corrects all 3rd order Zernike terms except spherical aberration, addition of

the central actuator facilitates correction of all 3rd order Zernike terms.

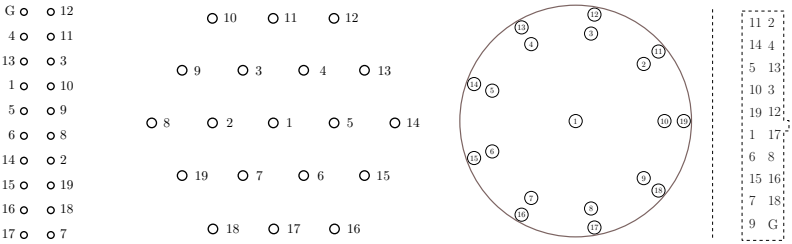

Figure 7.30: *The connector pinout and the geometry of mirror actuators for the 19-ch mirror (left — standard mirror, right — optimized for low-order aberration correction), view from the mirror side.*

Optical quality

Typical interferograms of the mirror are shown in Fig. 7.31.

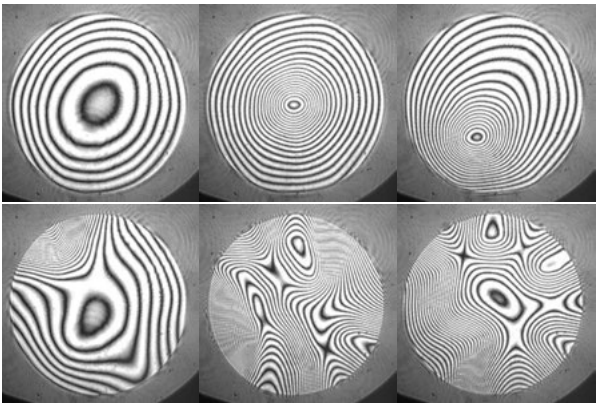

Figure 7.31: *Test of PDM19-30: zero voltage applied, 300V applied to the central, internal and edge actuators, random voltages to all actuators.*

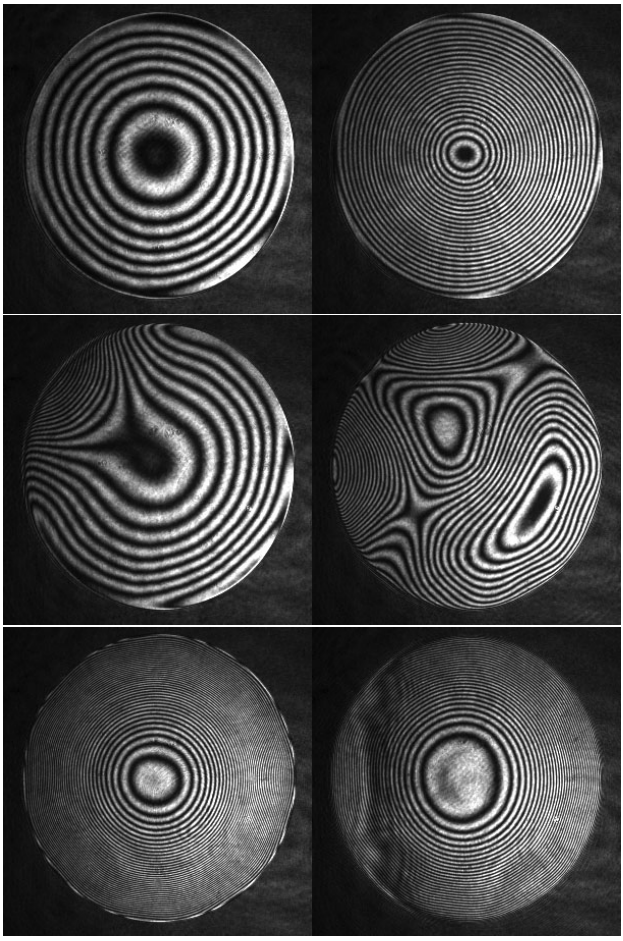

Figure 7.32: *Test of PDM30-19 with low-order-optimized geometry: zero voltage applied, 300V applied to the central, internal and edge actuators, random voltages to all actuators, 300 V applied to external ring of actuators, 300 V applied to center actuator and internal ring of actuators.*

Specific remarks

The mirror can be fabricated in the same package as the 30 mm 37ch PDM.

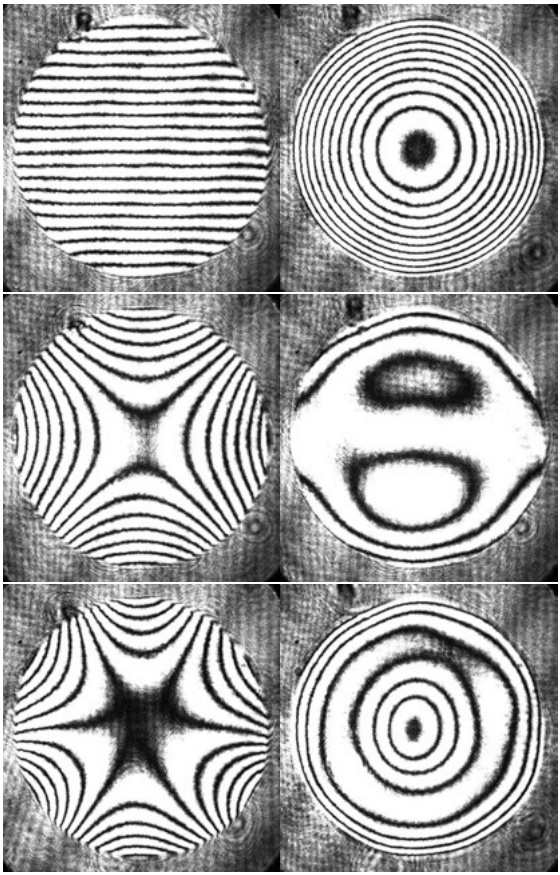

Figure 7.33: *Generation of Zernike polynomials with PDM30-19 with low-order-optimized geometry (left to right, top to bottom): shape of the mirror after active flattening; defocus (Zernike term Z[2,0], amplitude 3 μm); astigmatism (Zernike term Z[2,-2], amplitude 4 μm); coma (Zernike term Z[3,1], amplitude 1 μm); trifoil (Zernike term Z[3,3], amplitude 3 μm); spherical aberration (Zernike term Z[4,0], amplitude 1 μm).*

See also general remarks on page 144.

7.10 PDM30-37

The mirror, shown in Fig. 7.34, consists of 37 piezoelectric column actuators bonded to the base holder. Reflective plate is bonded to the top of the actuator structure and coated to form the mirror. The shape of the faceplate is controlled by the voltages applied to the actuators.

The device can be used for fast dynamic correction of low-order optical aberrations such as defocus, astigmatism, coma, etc, in lasers, telescopes, ophthalmology, displays and general imaging optics.

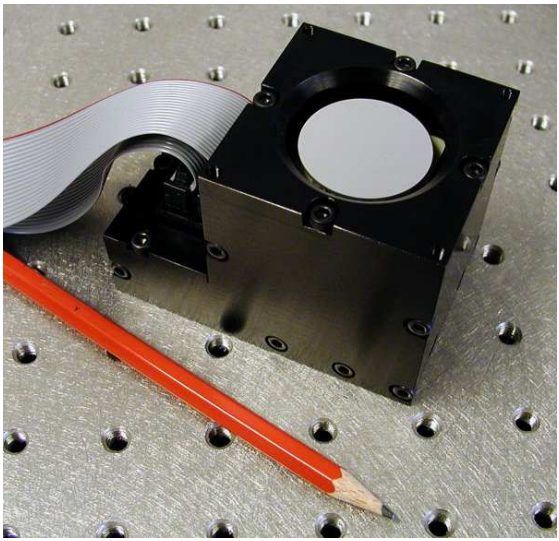

Figure 7.34: *Typical view of a 37-ch piezoelectric deformable mirror. Please note that these mirrors can be fabricated with different package designs, so the mirror you have may look differently.*

Technical data

See Table 7.9 for typical technical parameters of the mirror.

The mirror can be supplied with initially slightly curved spherical surface. This sphericity is caused by the stress in the mirror

Table 7.9: *Technical parameters of the mirror.*

Parameter	Value
Aperture shape	circular 30 mm in diameter
Mirror coating	Metal or Metal + dielectric
Actuator voltages	$0 \ldots +300$V (with respect to the ground electrode)
Number of electrodes	37 (see Fig. 7.36)
Actuator capacitance C_a	5 nF
Main initial aberration	sphere
Initial RMS deviation from reference sphere	less than 1μm
Maximum stroke	8μm at $+400V$
Actuator pitch	4.3 mm
Package dimensions	see Fig. 7.35
Weight	370 g

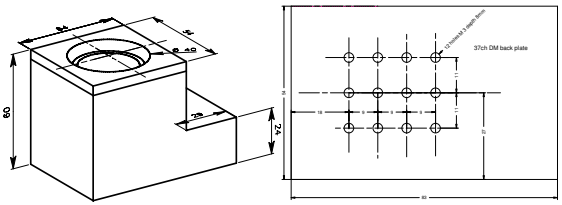

Figure 7.35: *Technical drawing of the package and mounting holes of the 30mm 37-channel PDM*

coating. It does not influence the parameters of the mirror, but should be taken into account when the mirror is incorporated into the optical setup.

Due to hysteresis of actuators, the initial aberration may change during the mirror usage and deviate more from the reference sphere. This deviation is a superposition of actuator response functions and is irrelevant in active setups with closed-loop control, though it may slightly reduce the correction range.

Optical quality

Typical interferograms of the mirror obtained before shipping are shown in Fig. 7.37.

NC	o	o	13	10	o	o	22
28	o	o	4	11	o	o	21
36	o	o	12	23	o	o	9
29	o	o	27	24	o	o	3
14	o	o	26	25	o	o	1
5	o	o	34	35	o	o	20
30	o	o	33	17	o	o	8
15	o	o	32	18	o	o	2
6	o	o	16	7	o	o	37
G	o	o	31	G	o	o	19

o 23 o 24 o 25 o 26

o 22 o 10 o 11 o 12 o 27

o 21 o 9 o 3 o 4 o 13 o 28

o 20 o 8 o 2 o 1 o 5 o 14 o 29

o 37 o 19 o 7 o 6 o 15 o 30

o 36 o 18 o 17 o 16 o 31

o 35 o 34 o 33 o 32

Figure 7.36: *The connector pinout and the geometry of mirror actuators for the 37-ch mirror (view from the back side of the mirror).*

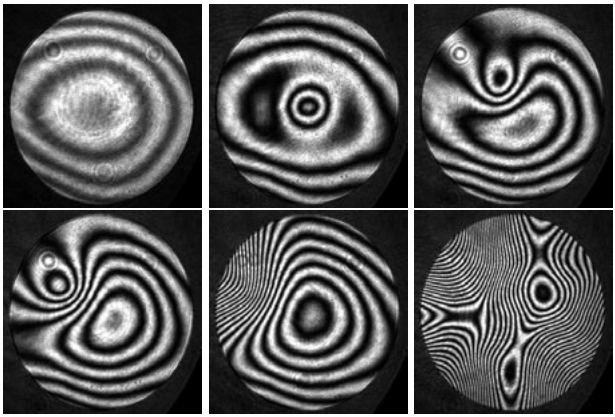

Figure 7.37: *Test of the mirror: zero voltage applied, 300V applied to the central, internals and edge actuators, random voltages to all actuators.*

Typical interferograms of actively flattened mirror are shown in Fig. 7.38 (see Chapter 4 on page 67 for details).

Specific remarks

See also general remarks on page 144.

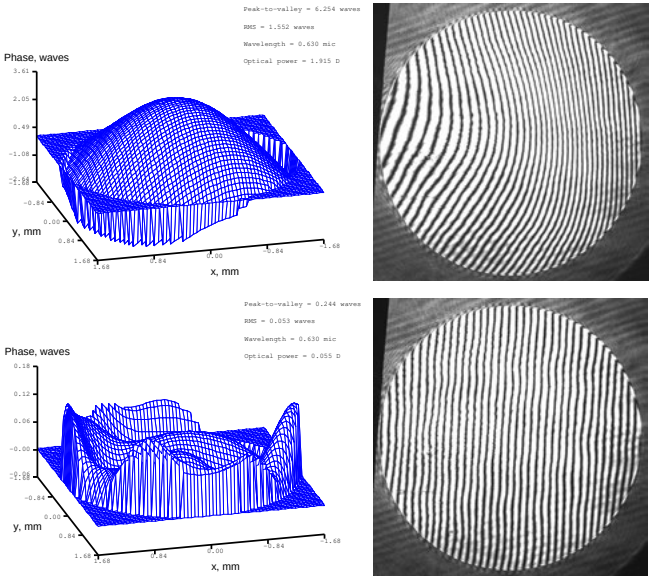

Figure 7.38: *Initial shape of the mirror, which was produced by setting all mirror values to zero, and shape of the mirror after active flattening.*

7.11 PDM50-19/37/79/109

The mirror, shown in Fig. 7.39, consists of 19, 37, 69, 79, or 109 piezoelectric column actuators bonded to the base holder. Reflective plate is bonded to the top of the actuator structure and coated to form the mirror. The shape of the faceplate is controlled by the voltages applied to the actuators.

The 19/37/69/79/109-ch 50 mm piezoelectric OKO mirror is suitable for fast dynamic correction of large high-order optical aberrations such as defocus, astigmatism, coma, etc, in lasers, telescopes, ophthalmology, displays and general imaging optics. **The mirror can be supplied with HR coating and cooling fan, specially for high-power applications, with power handling ability of up to tens of kW.**

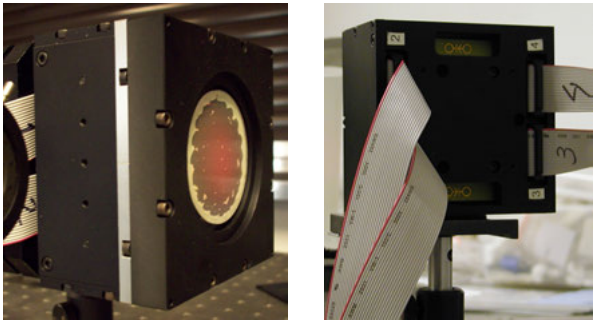

Figure 7.39: *Typical front and back view of a 19/37/69/79/109-ch 50mm piezoelectric deformable mirror. Please note that these mirrors can be fabricated with different package designs, so the mirror you have may look differently.*

Technical data

See Table 7.10 for typical technical parameters of the mirror.

The mirror can be supplied with initially slightly curved spherical surface. This sphericity is caused by the stress in the mirror coating. It does not influence the parameters of the mirror, but should be taken into account when the mirror is incorporated into the optical setup.

Table 7.10: *Technical parameters of the mirror.*

Parameter	Value
Aperture shape	circular 50mm in diameter
Mirror coating	Metal or Metal + dielectric
Maximum actuator voltages	$0 \ldots +400$V (with respect to the ground electrode)
Recommended actuator voltages	$0 \ldots +300$V
Number of electrodes	19/37/69/79/109 (see Fig. 7.41 – 7.45)
Actuator capacitance C_a	~ 5nF
Main initial aberration	defocus
Initial RMS deviation from reference sphere	less than 2μm
Maximum stroke	8μm at $+400V$ 6μm at $+300V$
Interactuator stroke	$\approx 1.5\mu$m[1]
Actuator pitch (37/69/79/109)	$6.83, 4.75, 4.72, 4.3$mm
Package dimensions	see Fig. 7.40
Weight	650 g

Due to hysteresis of actuators, the initial aberration may change during the mirror usage and deviate more from the reference sphere. This deviation is a superposition of actuator response functions and is irrelevant in active setups with closed-loop control, though it may slightly reduce the correction range.

Optical quality

Typical interferograms of the mirror are shown in Fig. 7.47.

Specific remarks

"High-power" version of the case (optional) incorporates a fan and a 2.5mm socket for the fan external 5V power supply.

See also general remarks on page 144.

[1] depends on the actuator pitch and position and on the faceplate thickness. See also Fig. 7.46

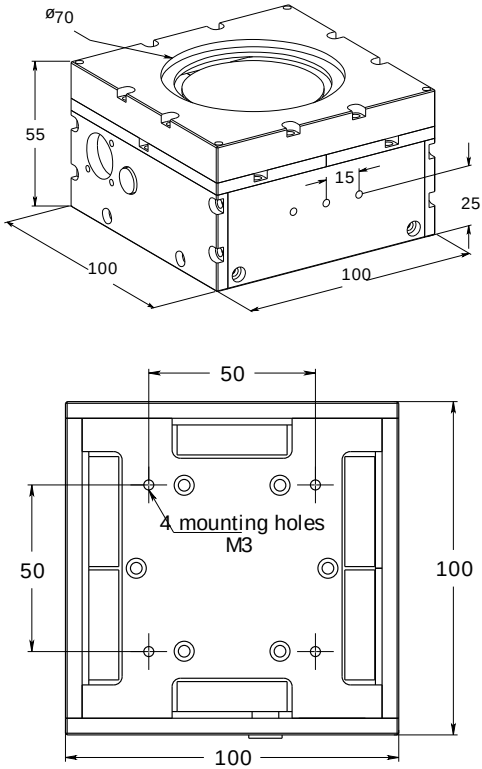

Figure 7.40: *Technical drawing of the mirror case. Three mounting holes on the case bottom and side walls have M3 threading. "High-power" version of the case with a fan and a 2.5mm socket for the fan external 5V power supply is shown.*

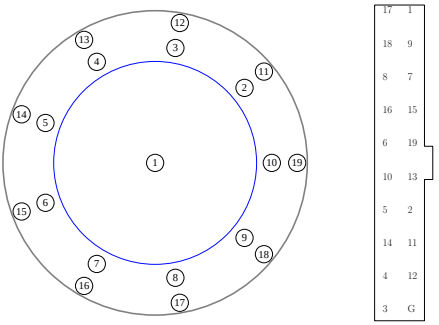

Figure 7.41: *The geometry of the mirror actuators (for 19- and 18- channel version; 18-channel version doesn't have the central actuator).*

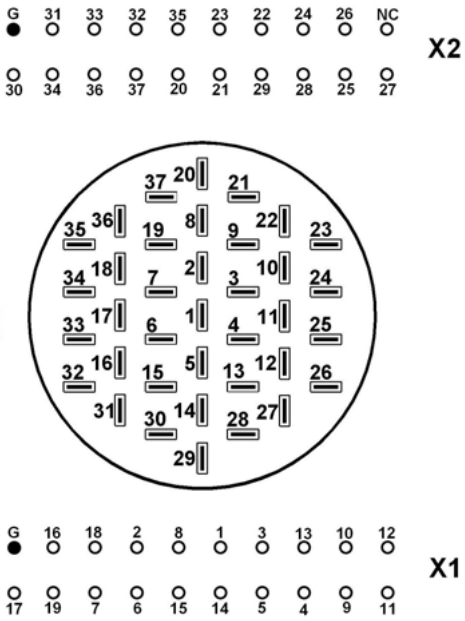

Figure 7.42: *The geometry of the 37-ch mirror actuators and its correspondence to the mirror connectors pinout (view from the mirror side).*

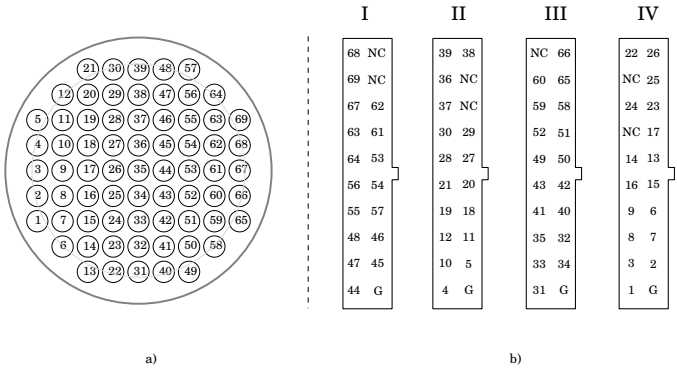

Figure 7.43: *The geometry of the 69-ch mirror actuators and its correspondence to the mirror connectors pinout (view from the mirror side).*

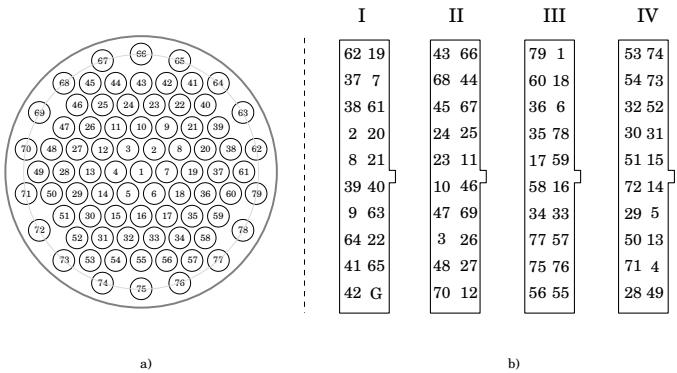

Figure 7.44: *The geometry of the 79-ch mirror actuators and its correspondence to the mirror connectors pinout (view from the mirror side).*

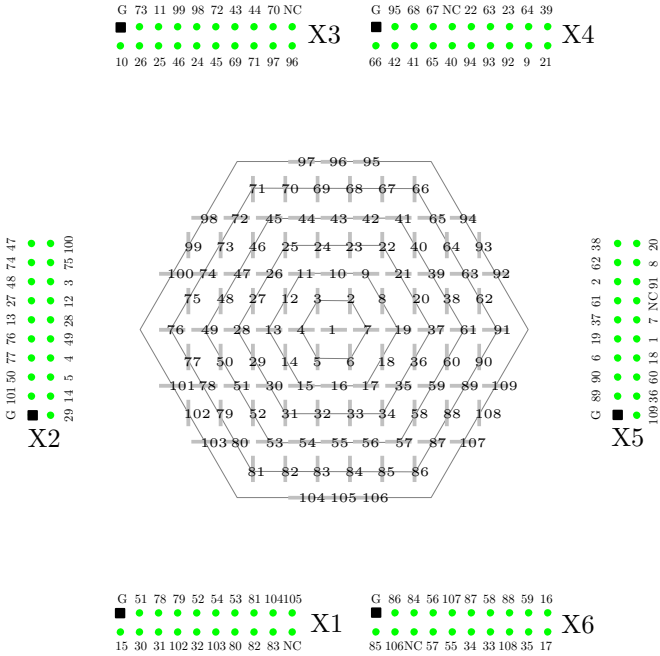

Figure 7.45: *The geometry of the 109-ch mirror actuators and its correspondence to the mirror connectors pinout (view from the mirror side)*

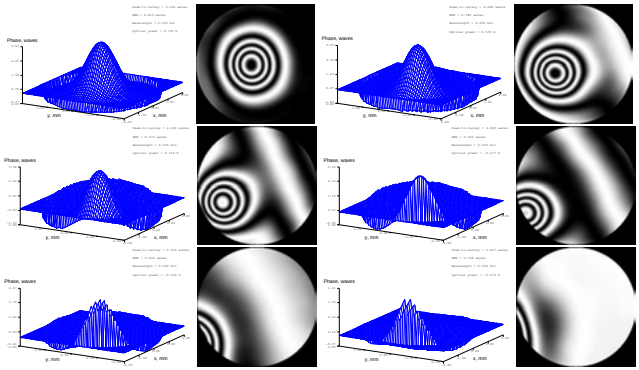

Figure 7.46: *Results of Shack-Hartmann measurement of the response functions of the 79-ch mirror in 30mm aperture: wavefront reconstruction and simulated interferogram. Left to right, top to bottom: actuators 1, 3; 11, 25; 45, 67.*

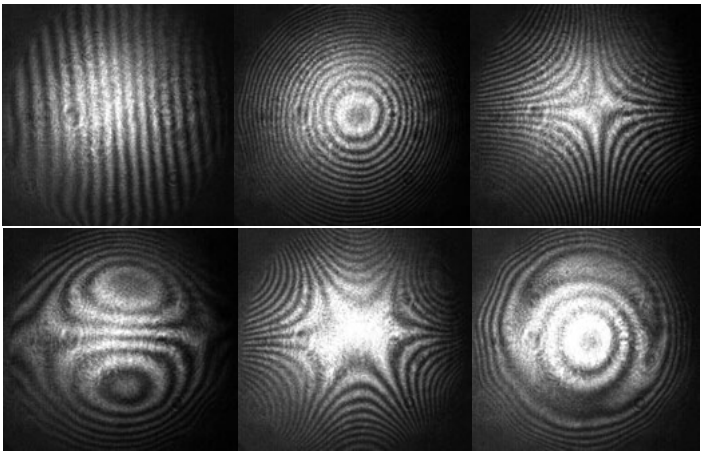

Figure 7.47: *Test of the 109-ch mirror. Mirror flattening (initial aberration corrected), shown with a tilt introduced, generated aberrations: defocus, astigmatism (top),coma, trefoil, and spherical aberration.*

7.12 PDM11x55-20

The mirror, shown in Fig. 7.48, consists of 20 piezoelectric column actuators bonded to the base holder. Reflective plate is bonded to the top of the actuator structure and coated to form the mirror. The shape of the faceplate is controlled by the voltages applied to the actuators.

In the temporal domain, the device can be used to control the duration and the temporal shape of ultrafast pulses in femtosecond lasers and amplifiers. In the spatial domain, the device can be used as a normal deformable mirror to control the phase of extended in one dimension laser beams.

Figure 7.48: *Typical view of a 20-ch linear piezoelectric deformable mirror. Please note that these mirrors can be fabricated with different package designs, so the mirror you have may look differently.*

Technical data

See Table 7.11 for typical technical parameters of the mirror.

The mirror can be supplied with initially slightly curved spherical surface. This sphericity is caused by the stress in the mirror coating. It does not influence the parameters of the mirror, but should be taken into account when the mirror is incorporated into the optical setup.

Table 7.11: *Technical parameters of the mirror.*

Parameter	Value
Aperture shape	rectangular 10×50 mm^2
Mirror coating	Metal or Metal + dielectric
Actuator voltages	$0 \ldots + 400$V (with respect to the ground electrode)
Number of electrodes	20 (see Fig. 7.50)
Actuator capacitance C_a	6 nF
Main initial aberration	sphere
Initial RMS deviation from the reference sphere	less than 1 μm
Maximum stroke	8μm at $+400V$
Actuator pitch	5 mm
Package dimensions	see Fig. 7.49
Weight	300 g

Due to hysteresis of actuators, the initial aberration may change during the mirror usage and deviate more from the reference sphere. This deviation is a superposition of actuator response functions and is irrelevant in active setups with closed-loop control, though it may slightly reduce the correction range.

Optical quality

A result of the active flattening using FrontSurfer wavefront sensor is shown in Fig. 7.51. Typical correction performance is illustrated in Fig. 7.52.

Connection to the control electronics

For a 20-channel mirror, you need a USB unit with a ground connector on its back panel. This USB unit is configured to provide 20-channel output in the signal corrector and a separate ground connector. Do not change the jumper setting of the USB unit.

Specific remarks

See also general remarks on page 144.

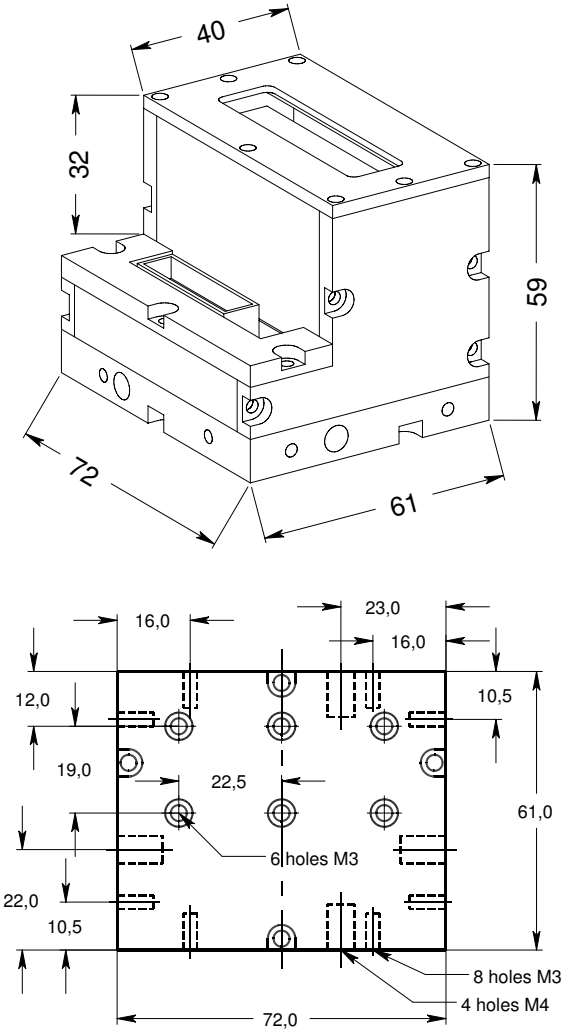

Figure 7.49: *Technical drawing of the package and mounting holes of the 30mm 37-channel PDM*

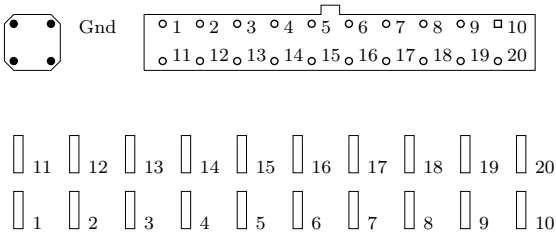

Figure 7.50: *The connector pinout and the geometry of mirror actuators for the 20-ch linear piezoelectric mirror (view from the front side).*

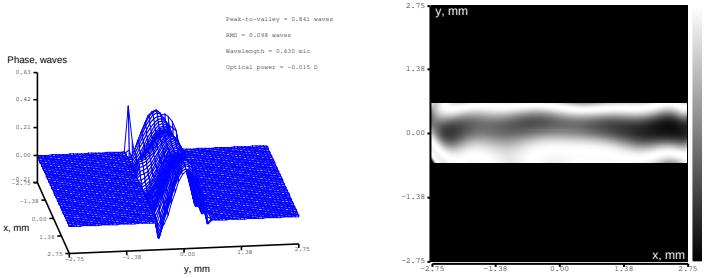

Figure 7.51: *The mirror shape after active flattening; tested using Front-Surfer wavefront sensor*

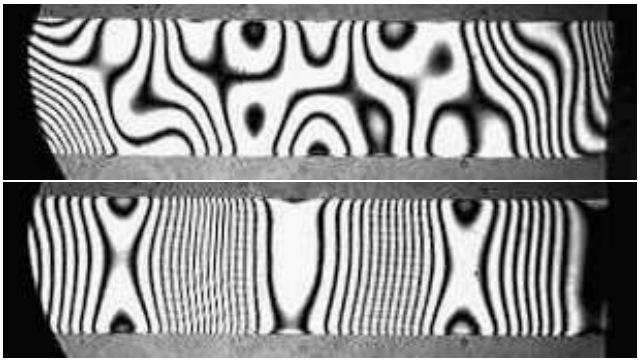

Figure 7.52: *Test of the mirror: non-zero values applied to some actuators*

7.13 PDM-2-TT fast steering platform

The fast steering platform, shown in Fig. 7.53, is controlled by 3 piezoelectric actuators.

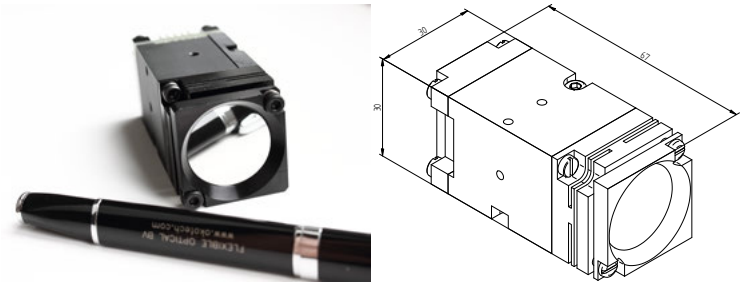

Figure 7.53: *Piezoelectric fast steering mirror*

Technical data

Table 7.12: *Technical parameters of the fast steering mirror.*

Parameter	Value
Aperture	up to 50 mm
Actuator voltages	$0 \ldots +350$V (with respect to the ground electrode)
Hysteresis	7-12%, typical
Number of electrodes	3
Actuator capacitance C_a	15 nF
response time	3 ms with a 25mm mirror mounted
dimensions	35x35x65 mm

See Table 7.12 for the typical technical parameters of the platform.

The device is supplied without optical part. Any front surface mirror with diameter from 10 to 25 mm can be mounted on the fast steering platform.

The typical frequency range with a round 25 mm mirror is 300 Hz, the optical tip-tilt range is +/- 1 mrad.

Connection to the control electronics

The unit can be controlled by a single A4MEMS high-voltage amplifier - see section **??**.

The computer interface is provided by either EDAC40, USB DAC40, or special 4-channel USB DAC (technical data on request).

7.14 General remarks

The maximum voltage for the DM should never exceed the specified maximum control voltage.

Do not trim the resistors in the DAC modules. These resistors were set before shipping to match the DM voltage range.

The jumpers on the amplifier board or in the amplifier unit, in the DAC USB control unit or ethernet controller, are preset before shipping; this configuration should not be changed. **The system and jumper configuration were tested before shipping.**

Do not touch or clean the mirror. We are not responsible for any damage to the mirror due to a cleaning attempt. If you need to clean the mirror, please contact us; we can clean it for you.

8

HV AMPLIFIERS AND INTERFACE

8.1 High-voltage amplifier units

8.1.1 Unipolar HV amplifiers for OKO DM

OKO produces a range of high-voltage amplifiers, to drive MEMS and piezoelectric actuators.

Unipolar DC HV amplifiers have 40 (20) independent channels, each producing output in the range 0 to +300V. These amplifiers are specially designed to drive MEMS devices and deformable mirrors. Each unit has 40 (20) identical indepndent amplifiers with gain of 55 (80). The module features compact 40x200x280mm size, weight of 1,2 kg, 20W energy consumption and works in any country with AC power supply in the range from 85 to 250 V. Full signal response is linear from DC to 700 Hz on loads of up to 10 nF. The frequency response of the amplifier is shown in Fig. 8.4. Other technical data is listed in Table 8.1. Loads up to 10 uF can be driven with a lower cutoff frequency. A number of units can be combined (stacked) to drive more than 40 (20) channels. Units with a bandwidth of 5 kHz and/or bi-polar output are available on a special order.

To use the unit, you must connect it to the mirror, to a DAC

Table 8.1: *Technical parameters of HV unit*

Parameter	Value
Number of channels	40 (20)
DC gain	79
Output impedance, kΩ	5
Short circuit protection	yes
Frequency range, kHz, at 1 nF load	see Fig. 8.4
Input voltage, V	0...12
Input voltage, V	0...100...350 trimmable
Maximum capacitive load, nF	up to 4 μF, slower response

USB unit (or PCI boards) and to the wall outlet (85 to 250V AC, 50 to 60 Hz). Connect the mirror with a supplied flat ribbon cables to the 20-pin output connectors on the front side of the unit. Connect the driver boards, or the USB unit to the 26-pin input connectors. When using two or more HV units, connect them together using the ground sockets on the back panels, to provide the common ground.

Every unit shipped with any OKO adaptive mirror is pre-configured for this specific mirror eliminating the need of any further configuration by the user. The pre-configuration includes jumper and output voltage range settings. The maximum output voltage can be set in the range 100 ... 350 V (400 V on a special order).

For 20-channel linear PDM Connect the ground pin of the mirror with the ground connector of the amplifier unit located on the back panel using the supplied cable, and to the ground connector of the USB unit (or to the metal case of the PC, if PCI board is used to drive the mirror).

8.1.2 Bipolar HV amplifiers

Bipolar DC HV amplifiers have 8 independent channels with a gain of 50, each producing output in the range of -300 to +300 V. These amplifiers are designed to drive tube actuators and tip-tilt stages. Application include adaptive optics, beam control, and

Figure 8.1: *40-channel high-voltage amplifier*

scanning microscopes. The module features compact $40 \times 200 \times 280$ mm size, weight of 1,2 kg, 30 W energy consumption, and works in any country with AC power supply in the range from 85 to 250 V. Full signal response is linear from DC to 3 kHz on a 5 nF load. Custom amplifiers with a wider voltage range (up to ± 500 V) and/or wider bandwidth are available on special order.

8.1.3 A4MEMS prototyping HV amplifier

A4MEMS is a 3-channel high-voltage amplifier specially designed as a quick low-cost solution for prototyping of multichannel high-voltage MEMS circuits. It is a convenient tool for driving a wide variety of electrostatic and piezoelectric actuators.

The frequency response of the gain for various loads is presented on figure 8.4.

A4MEMS measures $110 \times 60 \times 30$ mm. It provides $0 \ldots 300$ V output in 3 independent channels, as well as optional high voltage output from the HV converter. Devices with extended up to $0 \ldots 400$ V voltage range are available on special order. The unit does not require any external high voltage supply and can be powered from any 16 to 25 V 200 mA laboratory supply. See Table 8.2 for the technical parameters.

A4MEMS features a complete short circuit protection – the unit can continuously operate with all 3 outputs connected to the

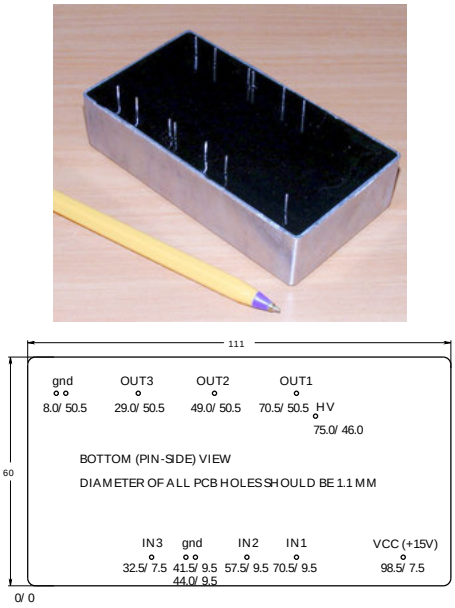

Figure 8.2: *Typical view and pin-out of A4MEMS*

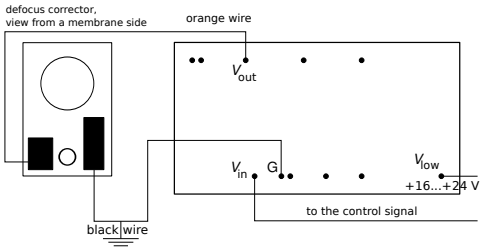

Figure 8.3: *Example of connection scheme for the defocus corrector and A4MEMS*

ground, regardless of the state of its inputs. Several units can be combined for quick prototyping of multi-channel high-voltage drivers in telecom applications and adaptive optics. The device have single common ground for all inputs, outputs, and the power supply. The metal case of the device is connected to the zero

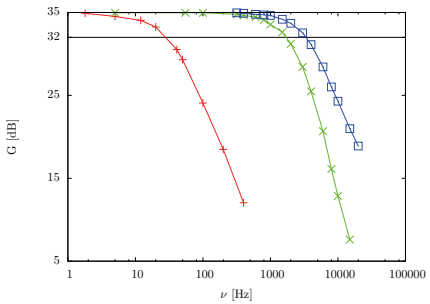

Figure 8.4: *DC gain* ($20\log_{10}(U_{out}/U_{in})$) *as a function of input signal frequency for the loads of* $0.47\ \mu F$ (+), $4\ nF$ (×), *and no load* (□)

output and can be grounded.

Table 8.2: *Technical parameters*

Parameter	Value
Number of channels	3
DC Gain	≈ 56
Output impedance	$10\,k\Omega$
Short circuit protection	yes
Frequency range at 1 nF load	$0 \ldots 1$ kHz
Input voltage	$0 \ldots 12$ V
Low voltage power supply	$14 \ldots 24$ V
Output voltage	$0.5 \ldots 300$ V
Maximum capacitive load	30 nF
Power dissipation	3.4 W
Size	$110 \times 60 \times 30$ mm^3
Weight	330 g

8.2 20-ch HV amplifier board

OKO produces OEM version of HV amplifier boards - see Fig. 8.5. Each board includes 20 non-inverting DC amplifiers with gain of 79 (85 as an option). The board needs a high-voltage power supply

Table 8.3: *Technical parameters of HV amplifier board*

Parameter	Value
Number of channels	20
DC gain	79
Output impedance, kΩ	5
Short circuit protection	yes
Frequency range, kHz, at 1 nF load	see Fig. 8.4
Input voltage, V	0...12
Low voltage DC power supply, V	+10 ...+24
High voltage Dc power supply, `V_high`, V	0 ...350
Maximum capacitive load, nF	up to 4 μF, slower response
Steady dissipation, W	3
Size, mm^2	100×160

(100 ...350 V) and a stabilized DC supply of 10 ...24 V. The connection pins are clearly marked on the board. The parateters are listed in Table 8.3. Please contact OKO for the specs of older boards, marked “1997”, “2004” and “2005”.

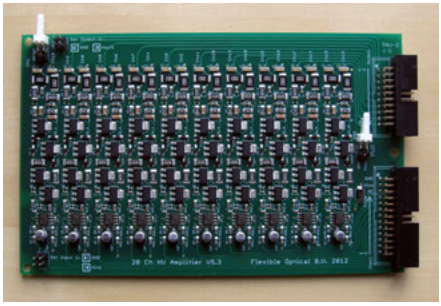

Figure 8.5: *The latest version of the 20-channel DC amplifier board*

8.3 EDAC-40 driver module

8.3.1 Specifications

The EDAC-40 unit is a network-enabled device providing 40-ch 16-bit voltage output remotely controlled by computer via network. Technical data are listed in Table 8.4.

Figure 8.6: *EDAC40 Ethernet control unit*

Table 8.4: *EDAC-40 technical specifications*

Parameter	Value
Analog outputs	40
Output resolution	16 bits (65536 levels)
Maximum output span	12 V (adjustable)
Minimum output level	-12 V (adjustable)
Maximum output level	+12 V (adjustable)
Output mode	synchronous for all channels
Short-circuit current, each channel	15 mA
Capacitive load, each channel	$\leq$2200 pF
Network protocols for data	UDP, TCP (port 1234)
Minimal data packet size	8 bytes
Maximum data packet size	86 bytes
Network service protocols	DHCP client, ICMP
Automatic device recognition	Microchip *discover* protocol (UDP port 30303)
Method of range adjustment	software, stored in nonvolatile memory (NVRAM)
Supply power	+5 V DC
Frame (40ch) refresh TCP	100 . . . 300 Hz
Frame (40ch) refresh UDP	2.5 kHz

8.3.2 General design and principle of operation

The unit is designed as single PCB mounted in compact plastic enclosure. Its layout is shown schematically in Fig 8.7. The board carries two double-row angle 20-pin male connectors for analog outputs (J4: channels 1-20, J5:channels 21-40), network RJ-45 connector J1, power connector J3. Channel numbers are market on the rear panel of the device. A set of header jumpers JP1–JP4 provides the possibility to modify assignments of selected outputs. To get access to external controls one should disengage lower and upper parts of the housing by simultaneously depressing of their side surfaces.

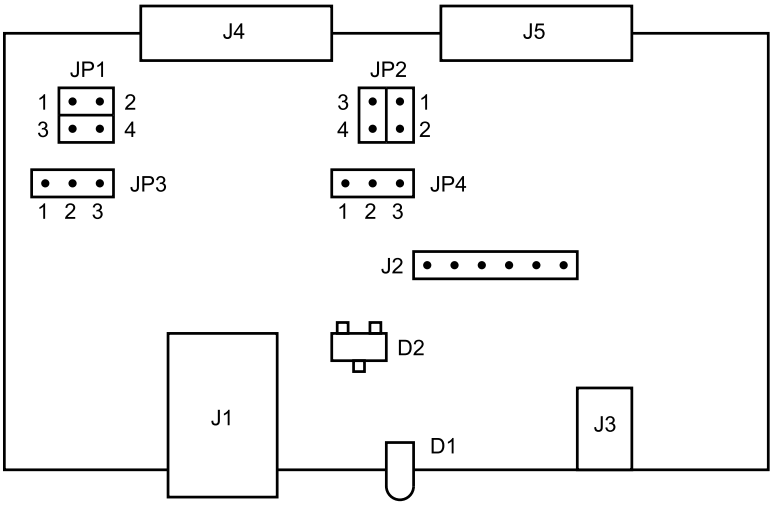

Figure 8.7: *EDAC40 external connections and indication*

Please refer to the device manual for the detailed description of the communication protocol, and the programming interface. The manual is available from OKO Tech.

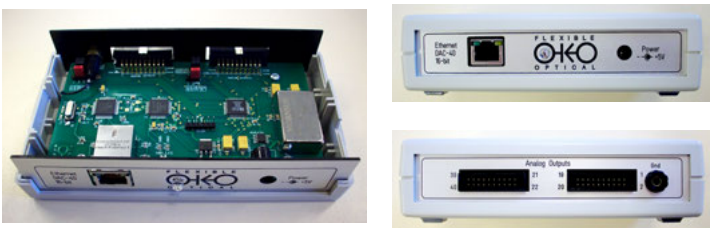

Figure 8.8: *EDAC40 board view (left), front and rear panels (right)*

Figure 8.9: *DAC-40-USB driver module.*

8.4 DAC-40-USB driver module

Digital-to-analog converter unit “DAC-40-USB” (see Figure 8.9) is intended to provide multi-channel voltage output controlled from a personal computer via a USB port. Its primary purpose is to drive deformable mirrors produced by OKO Technologies.

Technical data are shown in Table 8.5 on the following page.

8.4.1 General design

“DAC-40-USB” is designed as a PCB with two double-row angle connectors BH-20R (male) and a B-type USB connector; it is mounted in a compact housing. Pins of the output connectors are labeled according to the numbering order of the output channels. The maximum output voltage value can be adjusted (all channels simultaneously) by a variable resistor, whose slot is sunk in a hole on the front side of the unit (Figure 8.10). To provide access to the PCB, one should disconnect upper and lower decks of the housing

Table 8.5: *40-channel DAC USB unit*

Parameter	Value
Analog outputs	40
Output range	0...5.5 V
Output resolution	12 bits (4096 levels)
Output mode	synchronous for all channels
Range of adjustment of the maximum control voltage	2.5...5.5 V
Ohmic load, each channel	$\geq$ 100 kΩ
Load capacitance, each channel	$\leq$ 500 pF
Power	provided via the USB port

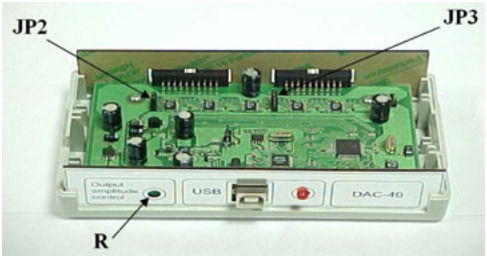

Figure 8.10: *DAC-40-USB; view from the output connectors' side*

by simultaneous depression of their side surfaces. To close the housing, the decks must be pushed vertically one to another till latched.

8.4.2 Programming interface

Data transfer between PC and DAC via USB bus is managed by the interface chip FT245BM. To provide necessary speed of data transfer between PC and DAC it is necessary to use FDTI Direct Driver. The corresponding program interface is implemented in the library **FTD2XX.DLL**.

Please read the technical description supplied with the USB DAC unit, for more information about the SDK and programming interface.

8.5 24-channel PCI DAC board

OKO digital PCI boards[1] provide 8-bit voltage control for 24 output channels. The output voltage range can be trimmed continuously in the range 2.5... 10 V for all channels. Setting time per channel is about 1 microsecond, each channel is controlled by a separate DAC. Several boards can be used simultaneously with a single PC. These boards are applicable to a range of environments when a simultaneous independent control of a large number of analog output channels is required.

Figure 8.11: *24-channel 8-bit PCI DAC board.*

The pinout of the board and the pinouts of the board cable and the cable coming from the high voltage board are shown in Fig. 8.12. The board connector pinout is given for the board make connector. The cable pinouts are given for the cable female connectors viewed from the front side.

8.5.1 Programming interface

The output voltage of the channel N [N=0...23] of the 24-channel DAC board is controlled by sending control byte V [0...255] to the

[1]Available till stock is exhausted

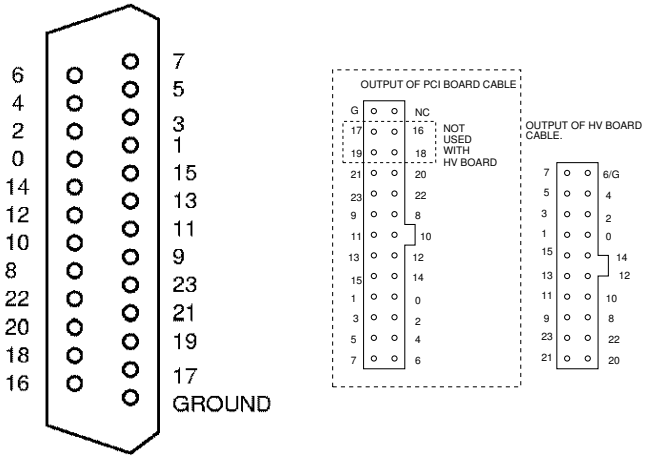

Figure 8.12: *Pinouts of the digital board and cables. The numbers correspond to the addresses of the pin with respect to the base address of the board.*

output port BA+N*4, where BA is the base address of the board. The most simple way to do it is to use direct access to the output ports corresponding to the control channels of the digital boards. In a Linux program written in C (GCC compiler), addressing to I/O ports is implemented using "write_port" function, and in Windows using "DlPortWritePortUchar" function of "DlPortIO" library (Scientific Software Tools, Inc.), which is freely available. The installer of DlPortIO (`port95nt.exe`) and programming example (`am_set_pci.cpp`) are supplied on a CD enclosed with the boards (directory `\Drivers\PortDriver\deformable_mirror`).

To obtain the base I/O address of the board, go to "Control Panel → System → Hardware → Device manager". The boards are listed in the section "Multifunction adapters". Double-click on the device named "PROTO-3/PCI" and check the section "Resources" for its base I/O address.

8.6 Four-channel USB DAC

This small digital-to-analog converter module designed to drive adaptive optics devices with small number of actuators, for example tip-tilt correctors. Its architecture mostly follows one of DAC40USB module with scaled down number of channels, so programming interface is also very similar. Parameters are listed in the Table 8.6. Analog output range of the device is adjustable by trimming potentiometer and the jumper (5V/adjustable voltage) visible on the photo (Fig. 8.13). Power and control are provided by PC through USB type B connector. Analog output (IDC 10-pin connector) is typically serves as an input for high-voltage amplifier.

Table 8.6: *40-channel DAC USB unit*

Parameter	Value
Analog outputs	4
Output range	0...5.5 V
Output resolution	16 bits
Output mode	synchronous for all channels
Settle time	$\leq 10\mu$s
Range of adjustment of the maximum control voltage	2.5...5.5 V
Maximum ohmic load, each channel	≥ 100 kΩ
Load capacitance, each channel	≤ 500 pF
Power	provided via the USB port

8.7 Four-channel high voltage driver

The device shown in the Fig. 8.14 features four-channel digital-to-analog converter with USB interface, A4MEMS high-voltage amplifier and mains power supply assembled in single housing box. For detailed specifications of those components please refer to corresponding sections of this guide. Primary purpose of the unit is for driving tip-tilt correctors.

Figure 8.13: *Four-channel digital-to-analog converter with USB interface.*

Figure 8.14: *Tip-tilt driver unit (includes four-channel DAC, high-voltage amplifier and mains power supply).*

9

FREQUENTLY ASKED QUESTIONS

9.1 Deformable mirrors

- ***What is MMDM?***

  MMDM stands for "Micromachined Membrane Deformable Mirror".

  MMDMs with 37, 39, 59, and 79 control channels are fabricated by

  > Flexible Optical BV (Okotech),
  > http://www.okotech.com,
  > Polakweg 10-11, 2288 GG Rijswijk ZH, The Netherlands,
  > fax: +31-70 262 94-20, email: oko@okotech.com.

  MMDM consists of a thin (500 to 10000 nm thick) membrane made of silicon nitride or a nitride - poly - nitride sandwich. The membrane is coated by a thin layer of aluminum or gold to produce a highly reflective surface. The membrane is fixed to silicon frame and suspended over a number of planar electrodes. When the membrane is electrically grounded and a voltage is applied to one or a number of the electrodes, the

membrane is deformed locally changing its shape. Different combinations of voltages applied to different electrodes form different shapes.

- ***What is PDM?***

  PDM stands for "Piezoelectric Deformable Mirror". PDMs with 18, 19, 37, 79, and 109 control channels are fabricated by

  Flexible Optical BV (Okotech),
  http://www.okotech.com,
  Polakweg 10-11, 2288 GG Rijswijk ZH, The Netherlands,
  fax: +31-70 262 94-20, email: oko@okotech.com.

- ***What is "biased operation"?***

  The MMDM membrane can be deflected only in the direction of the electrode structure because the electrostatic force can be only attractive. The deflected membrane can produce only concave optical shapes. To achieve a bi-directional operation the membrane should be initially deflected towards the actuators and made perfectly spherical by adjusting the actuator voltages. From this state the membrane can be moved to both positive (from the electrode structure) and negative (to the actuator structure) directions by controlling the actuators voltage.

- ***How to bias the MMDM?***

  In the simplest case biasing can be achieved by applying a constant voltage to all actuators of the MMDM. Theoretically under the constant bias the MMDM should take a parabolic shape. In practice, MMDM biased with a constant voltage has a figure error of up to 300nm RMS from the nearest perfect parabola. The bias voltages should be adjusted to make the biased surface perfect. The theoretical value of the bias voltage equals to:

  $0.71 \cdot V_{max}$

  where V_{max} is the maximum voltage that can be applied to the mirror. This value provides for equal mirror strokes in

positive and negative direction from the biased position. For example, with 8-bit digital control (one byte, 0 to 255 per channel) all electrodes should be set to 180. These values should be adjusted to obtain a perfect spherical figure.

- ***Is it possible to use MMDM for tilt correction (scanner mode)?***

  The device can be specially calibrated to correct for tilts, preserving the diffraction-limited quality of the reflected beam in the range of about $25\lambda/D$ where Λ is the wavelength and D is the mirror diameter. Using the device in scanner mode will reduce its correction performance for higher order aberrations.

  OKO manufactures a special MMDM with 2 tip-tilt channels and 17 deformable mirror channels. This device uses special piezoelectric tip-tilt stage. The MMDM is mounted to this stage inside the DM package.

- ***How good the mirrors will correct our aberrations?***

  Information about the spatial and temporal spectra of the aberrated wavefronts is required for a good answer to this question. Membrane mirrors in general are good in correcting smooth continuous aberrations. 37-ch MMDM provides high-quality correction of all 3-rd order aberrations and is reasonably good in correcting the 5-th order aberrations. 79-ch MMDM will correct aberrations up to 5th order. PDM with 19 and 37 channels will correct low order aberrations with relatively large amplitude. OKO mirrors can be flattened to produce better than $\lambda/20$ *rms* reflected wavefronts. Contact OKO with specific questions on the correction performance.

- ***How large can be the amplitude of the corrected aberrations?***

  Standard 37-ch 15-mm DM provides about 20000nm of wavefront deformation for defocus. Third and fifth order aberrations with wavefront amplitudes of up to 3000 nm can be corrected. In general the dynamic range is higher for low spatial frequencies.

The maximum profile difference between the adjacent actuators reaches 800 nm for MMDM and can be as large as 2 μm for a PDM.

- ***How linear is the MMDM response?***

  The displacement of the MMDM surface is approximately proportional to the square of the applied voltage. The mirror response can be linearized using the operation of square root. For 8-bit biased digital control the following expression can be used to convert the control signal CS (in the range -1...1) into the control byte CB applied directly to the digital board controlling the mirror actuator:

  ```
  CB=(int)sqrt(0.5*(CS+1))*255.;
  ```

  This formula provides linear correspondence between the control signal CS and the mirror displacement and sets the mirror into theoretical biased position when CS=0. **MMDM features negligible hysteresis**.

- ***How linear is the PDM response?***

  OKO piezoelectric mirrors have linear response and feature 7 to 10% hysteresis and up to 1% creep. Application of special control procedures to the PDM can reduce the hysteresis by a factor of 5.

- ***What is the size of MMDM?***

  As in 2013, OKO Tech fabricates membrane mirrors with diameters of 10, 15, 30, 40 and 50 mm with 1 to 79 channels and linear membrane mirrors with 11x39mm membrane.

- ***What is the size of PDM?***

  As in 2013, OKO Tech fabricates 30 mm piezoelectric mirrors with 19 and 37 actuators and 50 mm mirrors with 37, 79, and 109 actuators. Linear configuration with 10x55mm aperture and 20 (2x10) actuators is also available.

- ***How good is the initial figure of OKO deformable mirrors?***

  The standard scratch/dig is 20/10. Scratch/dig 10/5 is available on special request.

The initial figure of MMDM is flat with RMS deviation from the nearest reference plane better than 400nm. OKO mirror with 37 channels and a diameter of 15 mm will have less than 1 fringe of astigmatism in a 10mm aperture, averaged over a number of devices. Larger MMDM have 8 adjustment screws that allow to set the initial figure of the mirror. The initial optical quality is very good.

The initial figure of PDM is flat with RMS deviation from the nearest sphere better than 500 nm. The initial surface may have some irregularity due to random hysteresis state of different actuators. These irregularities are always formed as combinations of the mirror influence functions, thus they are completely correctable by the mirror.

- ***What is the power handling ability of OKO DM?***

  Standard 15mm Al-coated MMDM can handle up to 3 W optical load in the visible range. On a special order MMDM can be coated with a special HR metal-dielectric coatings, making them suitable for optical loads of up to 500 W and even 1 kW in some cases.

  Piezoelectric mirrors can be coated with high-power HR coatings, making them suitable for optical load of up to 15 kW and higher - on a special order.

9.2 Wavefront sensors

- ***What is FrontSurfer?***

  FrontSurfer is a wavefront analysis and control system based on Shack-Hartmann wavefront sensors and deformable mirrors from OKO Technologies.

- ***What the FrontSurfer system can be applied for?***

  Applications include optical shop testing of transmissive and reflective optics, alignment of optical systems, real-time monitoring and compensation of optical aberrations with adaptive optics.

- ***What is included in the FrontSurfer wavefront sensor package?***

  The wavefront sensor package includes FrontSurfer software and a measurement head - Hartmann or Shack-Hartmann wavefront sensor. The Hartmann wavefront sensor consist of a precision Hartmann mask and a CMOS (or CCD) camera. In the Shack-Hartmann sensor, the mask is replaced by a microlens array.

- ***Which modifications of FrontSurfer software are available?***

  FrontSurfer is available in two modifications - with and without support for adaptive optics feedback.

- ***How many measurements are required for FrontSurfer to reconstruct a wavefront?***

  One in the absolute measurement mode and two in the reference mode.

- ***What is the absolute measurement mode of FrontSurfer?***

  In this mode, the wavefront is reconstructed from one intensity pattern captured by the wavefront sensor. Geometric parameters of the Hartmann mask or microlens array are used for the reference. This mode can only be used with a precision Hartmann mask (or microlens array) having complete hexagonal or square structure of subapertures (for example, see Figure 3.5).

- ***What is the reference measurement mode of FrontSurfer?***

  In this mode, the wavefront is reconstructed from two intensity patterns captured by the wavefront sensor. The first one (*main* pattern) is measured in presence of the the aberration to be reconstructed, and the second one (*reference* pattern) is measured for calibration purposes, i.e., with the aberration removed. In this mode, the microlens array (Hartmann mask) can be neither complete nor regular; one can even use an array with random positioning of sub-apertures.

- ***What is the sensitivity of FrontSurfer wavefront sensor?***

  Typical configuration of the FrontSurfer wavefront sensor (see parameters in Table 3.1) has a noise-limited sensitivity of about $\lambda/100$ PV (for λ=0.63 μm). The sensitivity can be improved by averaging over multiple frames to about $\lambda/500$ *rms*.

- ***What is the precision of FrontSurfer wavefront sensor?***

  Typical configuration of the FrontSurfer wavefront sensor (see parameters in Table 3.1) has a precision of about $\lambda/60$ PV (for λ=0.63 μm) in the reference mode and about $\lambda/10$ PV in the absolute measurement mode.

  In the reference mode, the precision is mainly limited by the sensor noise and can be improved by averaging over multiple frames and using a microlens array with larger focal distance. In the absolute measurement mode, the precision is limited by fabrication errors of the microlens array (or Hartmann mask).

  Please note that the precision is specified for low-order aberrations, when the sampling error can be neglected. It is important that the microlens array (or Hartmann mask) provides sufficient sampling for the aberration.

- ***Which mask or microlens array can be used with FrontSurfer?***

  In the reference mode, any mask or microlens array with up to several hundred subapertures over the image sensor area can be used. For the absolute measurement mode, a precision array with complete hexagonal or square structure of sub-apertures is required.

- ***Which camera can be used with FrontSurfer?***

  FrontSurfer can be interfaced with any camera or frame grabber, but it requires a special video plugin for FrontSurfer. Plugins for a number of popular cameras are included in the distribution. FrontSurfer manual contains description of the

functions that should be included in the plugin. The user can develop his own plugin following these instructions.

- ***How to use FrontSurfer wavefront sensor for optical shop testing?***

  Setup for testing of optical components should provide optical conjugation between the component under test and the wavefront sensor with proper scaling. See the section 3.4 for general recommendations and typical measurement schemes.

9.3 Adaptive optical systems

- ***What is included in a typical FrontSurfer adaptive optics package?***

  FrontSurfer adaptive optics package includes a deformable mirror with a full set of control electronics and the FrontSurfer wavefront sensor package including FrontSurfer software with adaptive optics enabled.

- ***Which deformable mirror can be used with FrontSurfer?***

  FrontSurfer have embedded support of OKO's deformable mirror controllers, including 24-channel ISA and PCI boards and 40-channel USB and ethernet driver modules. With these features, FrontSurfer can control any mirror from OKO Technologies - MMDM with up to 79 channels and PDM with up to 109 channels - or any custom mirror using the same controllers. Custom controllers can be interfaced to FrontSurfer using external libraries - plugins. FrontSurfer manual contains instructions on development of a custom mirror plugin.

- ***How to integrate FrontSurfer adaptive optics package into your application?***

  FrontSurfer adaptive optics package can be used for building an adaptive optical system for correction of aberrations. Optical design of the system is dependent on the application and should be made by a specialist. In general, the system

should provide optical conjugation between the optical aberrations, deformable mirror and the wavefront sensor with proper scaling.

- ***What is the closed-loop correction speed in FrontSurfer?***

  The average correction rate is dependent on the camera, the computer and the available light in the system. OKO has demonstrated working AO systems with frame rates from 1 to 1500 frames per second.

- ***What is included in a complete adaptive optical system from OKO Technologies?***

  On demand, OKO Technologies can supply a complete closed-loop adaptive optical system (AOS), which includes all necessary optical and mechanical components in addition to the FrontSurfer adaptive optics package. It has a numerical aperture of 1:10 and can be applied for real-time correction of optical aberrations and generation of precision wavefronts. The system is shown in Figure 4.2.

- ***How to improve the stability of AO operation?***

  1. Ensure the DM, the tip-tilt correector, the WF pupil are correctly conjugated to the aberration source (pupil).
  2. Make sure the image in the WFS has all spots clearly visible, good S/N ratio and no oversaturation.
  3. Make sure all other parameters are correctly set in the software and the calibration results are sound. Check SVD values and modes.

10

WARRANTY AND EXPORT DISCLAIMERS

10.1 Warranty

The equipment is covered by a one-year factory-defect warranty.

We offer separate shipping insurance. The price of the shipping insurance is 2% of the total value of the insured item. Insured items damaged during shipping will be replaced by a similar device within two months. A photo of the damaged device followed by a damage report should be sent to Flexible Optical B.V. (OKO® Technologies) within 5 working days after the damaged device is received.

EXCEPT WHEN OTHERWISE STATED IN WRITING FLEXIBLE OPTICAL B.V. (OKO® TECHNOLOGIES) AND/OR OTHER PARTIES PROVIDE THE EQUIPMENT AND SERVICES "AS IS" WITHOUT WARRANTY OF ANY MERCHANTABILITY AND/OR FITNESS FOR ANY PARTICULAR PURPOSE. THE ENTIRE RISK AS TO THE QUALITY AND PERFORMANCE OF THE EQUIPMENT IS WITH YOU.

IN NO EVENT UNLESS REQUIRED BY APPLICABLE LAW OR AGREED TO IN WRITING WILL FLEXIBLE OPTICAL B.V. (OKO® TECHNOLOGIES) BE LIABLE TO YOU FOR DAMAGES, INCLUDING ANY GENERAL, SPECIAL, INCIDENTAL OR CONSEQUENTIAL DAMAGES ARISING OUT OF THE USE OR INABILITY TO USE THE

HARDWARE SOFTWARE AND SERVICES DESCRIBED IN THIS DOCUMENT AND/OR SUPPLIED BY FLEXIBLE OPTICAL BV.

10.2 Export

According to the European export law, a license to export outside the EU should be obtained for any product that matches the definition:

"Deformable mirrors having either continuous or multi-element surfaces, and specially designed components therefor, capable of dynamically repositioning portions of the surface of the mirror at rates exceeding 100 Hz."

Export inside the EU is free from this restriction. Export to some selected destinations can be or can not be free from this restriction.

Bibliography

[1] R. K. Tyson. *Principles of adaptive optics, second edition*. Academic Press, 1998.

[2] Gleb Vdovin and P Sarro. Flexible mirror micromachined in silicon. *Applied Optics*, 34:2968, 1996.

[3] G.V. Vdovin, Simon Middelhoek, and Pasqualina M. Sarro. Technology and applications of micromachined silicon adaptive mirrors. *Optical Engineering*, 36:1382, 1997.

[4] C. Schwartz, E. Ribak, and S. G. Lipson. Bimorph adaptive mirrors and curvature sensing. *JOSA A*, 11(2):895, 1994.

[5] Gleb Vdovin. Closed-loop adaptive optical system with a liquid mirror. *Opt. Lett.*, 34(4):524–526, Feb 2009.

[6] M. C. Roggemann and B. Welsh. *Imaging through turbulence*. CRC Press, 1996.

[7] G. D. Love, editor. *Adaptive optics in industry and medicine*. World Scientific, 2000.

[8] U. Wittrock, editor. *Adaptive optics for industry and medicine*, volume 102 of *Springer Proceedings in Physics*. Springer, 2005.

[9] E. J. Fernandez, I. Iglesias, and P. Artal. Closed-loop adaptive optics in the human eye. *Optics Letters*, 26:746–748, 2001.

[10] O. Albert, L. Sherman, G. Mourou, T. B. Norris, and G. Vdovin. Smart microscope: an adaptive optics learning system for aberration correction in multiphoton confocal microscopy. *Optics Letters*, 25:52–54, 2000.

[11] R. Bartels, S. Backus, E. Zeek, L. Misoguti, G. Vdovin, I. P. Christov, M. M. Murnane, and H. C. Kapteyn. Shaped-pulse optimization of coherent emission of high-harmonic soft x-rays. *Nature*, 406:164–166, 2000.

[12] S. Timoshenko and S. Woinowsky-Krieger. *Theory of plates and shells*. McGraw-Hill, 1953.

[13] A. I. Lourye. Some problems of bending of a thin plate. *Prikladnaja matematika i mehanika (in Russian)*, 4:93–102, 1940.

[14] M. Born and E. Wolf. *Principles of optics*. Pergamon Press, 1993.

[15] Gleb Vdovin, Oleg Soloviev, Alexander Samokhin, and Mikhail Loktev. Correction of low order aberrations using continuous deformable mirrors. *Opt. Express*, 16(5):2859–2866, 2008.

[16] A. Kolmogorov. Dissipation of energy in locally isotropic turbulence. In S. Friedlander and E. Topper, editors, *Turbulence, Classic Papers on Statistical Theory*. Wiley-Interscience, 1961.

[17] J. Y. Wang and J. K. Markey. Modal compensation of atmospheric turbulence phase distortion. *J. Opt. Soc. Am. A*, 68:78–87, 1978.

[18] M. Loktev, D. W. De Lima Monteiro, and G. Vdovin. Comparison study of the performance of piston, thin plate and membrane mirrors for correction of turbulence-induced phase distortions. *Optics Communications*, 192:91–99, 2001.

[19] G. V. Vdovin, N. Kugler, and M. Schacht. Membrane deformable mirrors under cw laser load. *Proceedings of SPIE*, 3762:58–66, 1999.

[20] G. V. Vdovin. Optimization-based operation of micromachined deformable mirrors. *Proceedings of SPIE*, 3353:902–909, 1998.

[21] Gleb Vdovin and Vadim Kijko. Intracavity control of a 200-w continuous-wave nd:yag laser by a micromachined deformable mirror. *Optics Letters*, 26(11):798, 2001.

[22] Harold Dyson, Ray Sharples, N. Dipper, and Gleb Vdovin. Cryogenic wavefront correction using membrane deformable mirrors. *Opt. Express*, 8(1):17–26, Jan 2001.

[23] O. Soloviev and G. Vdovin. Hartmann-shack test with random masks for modal wavefront reconstruction. *Optics Express*, 13:9570–9584, 2005.

[24] L. Baker. *C tools for scientists and engineers*. McGraw-Hill, 1989.

[25] C. Paterson, I. Munro, and C. Dainty. A low cost adaptive optics system using a membrane mirror. *Optics Express*, 6:175–185, 2000.

[26] R. Bartels, S. Backus, E. Zeek, L. Misoguti, G. Vdovin, I.P. Christov, M.M. Murnane, and H.C. Kapteyn. Shaped-pulse optimization of coherent emission of high-harmonic soft x-rays. *NATURE*, 406 (6792):164–166, 2000.

[27] O. Albert, L. Sherman, G. Mourou, T. B. Norris, and G. Vdovin. Smart microscope: an adaptive optics learning system for aberration correction in multiphoton confocal microscopy. *Opt. Lett.*, 25(1):52–54, Jan 2000.

[28] H. Song, R. Fraanje, G. Schitter, H. Kroese, G. Vdovin, and M. Verhaegen. Model-based aberration correction in a closed-loop wavefront-sensor-less adaptive optics system. *Opt. Express*, 18(23):24070–24084, Nov 2010.

[29] H. Song, G. Vdovin, R. Fraanje, G. Schitter, and M. Verhaegen. Extracting hysteresis from nonlinear measurement of wavefront-sensorless adaptive optics system. *Opt. Lett.*, 34(1):61–63, Jan 2009.

[30] Svyatoslav Savenko Mikhail Loktev, Oleg Soloviev and Gleb Vdovin. Speckle imaging through turbulent atmosphere based on adaptable pupil segmentation. *Optics Letters*, 36:2656, 2011.

[31] A.A. Pakhomov and K.R. Losin. Processing of short sets of bright speckle images distorted by the turbulent earth's athmosphere. *Optics Communications*, 125:5 – 12, 1996.

[32] W. H. Press, S. A. Teukolsky, W. T. Vetterling, and B. P. Flannery. *Numerical recipes in C*. Cambridge University Press, 1997.